

**UCSF**

**UC San Francisco Electronic Theses and Dissertations**

**Title**

Endocavity Ultrasound Thermal Therapy of Pelvic Malignancies: Modeling and Device Development

**Permalink**

<https://escholarship.org/uc/item/7xw0n2j8>

**Author**

Wootton, Jeffery Howard

**Publication Date**

2010

Peer reviewed|Thesis/dissertation

Endocavity Ultrasound Thermal Therapy of Pelvic Malignancies:

Modeling and Device Development

by

Jeffery Howard Wootton

DISSERTATION

Submitted in partial satisfaction of the requirements for the degree of

DOCTOR OF PHILOSOPHY

in

Bioengineering

in the

GRADUATE DIVISION

of the

UNIVERSITY OF CALIFORNIA, SAN FRANCISCO

AND

The dissertation of Jeffery Howard Wootton is approved:

Chris D. Tisdell 12/15/10  
Research Director and Chair Date

David H. H. 12/16/10  
Date

P. Chow 12/16/10  
Date

University of California, San Francisco

University of California, Berkeley

Fall 2010

**Endocavity Ultrasound Thermal Therapy of Pelvic Malignancies:  
Modeling and Device Development**

Copyright 2010

by

Jeffery Howard Wootton



## **Abstract**

Endocavity Ultrasound Thermal Therapy of Pelvic Malignancies:

Modeling and Device Development

by

Jeffery Howard Wootton

Doctor of Philosophy in Bioengineering

University of California, San Francisco and Berkeley

Chris Diederich, Ph.D., Dissertation Research Director and Chair

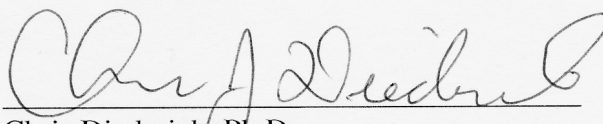
Catheter-based ultrasound technology has demonstrated locally targeted heating for ablation or hyperthermia treatment of cancerous tissue with minimal heating of organs at risk. Site-specific selection of device parameters and treatment strategies is necessary for achieving thermal goals. This dissertation investigates the influences of applicator parameters and treatment strategies on heating patterns in the prostate and cervix using biothermal simulation, which translates into the design of an intrauterine ultrasound applicator that is experimentally characterized and implemented in clinical treatment.

Thermal therapy offers potential for prostate cancer/BPH treatment with reduced morbidity. Ultrasound absorption by pelvic bones can cause pain and damage to adjacent nerves. Guidelines for device properties and treatment regimens in relation to prostate size and pelvic bone distance are developed by analyzing their impact on bone heating

and treatment time during transurethral prostate ablation. A sectored tubular design is superior to planar and curvilinear designs in reducing bone heating and treatment time with bone <3 cm from the gland.

The feasibility of the endocavity ultrasound device, consisting of an array of multi-sectored tubular transducers, to heat tumor targets in the cervix is explored with extensive theoretical analysis. Coverage of 4-5cm targets with therapeutic temperature ( $>41^{\circ}\text{C}$ ) is possible, using sector orientation for preferential avoidance of rectum and bladder. Hyperthermia delivery in conjunction with interstitial devices is investigated using treatment planning software for 14 patient cases. Temperatures  $>41^{\circ}\text{C}$  throughout targets are achieved in most cases using sectoring and aiming to limit  $T_{\text{max}} <47^{\circ}\text{C}$  and rectum and bladder  $<41.5\text{-}42.5^{\circ}\text{C}$ .

Devices were characterized for acoustic emission, imaging compatibility, radiation attenuation, and thermal output using implanted thermometry and MR temperature imaging. Collimated acoustic output with independent power control to sectors and transducers is demonstrated and used to produce tailored heating along the device length and in angle with temperatures of  $41^{\circ}\text{C} >2\text{cm}$  in tissue. Thermal delivery is more penetrating than implantable RF devices and more controllable than deep heating technology. The applicator was implemented in two clinical treatments, demonstrating facile integration with HDR brachytherapy, delivery of temperatures  $>41^{\circ}\text{C}$  throughout the target, and resulting in disease remission without adverse side effects in one patient.



---

Chris Diederich, Ph.D.  
Dissertation Research Director and Chair

To you, mom  
An inspiration, always

# Contents

<b>List of Figures</b>	vi
------------------------	----

<b>List of Tables</b>	xi
-----------------------	----

<b>1 Introduction</b>	<b>1</b>
1.1 Thermal therapy .....	1
1.1.1 Thermal ablation .....	1
1.1.2 Hyperthermia .....	4
1.2 Pelvic malignancies .....	6
1.2.1 Prostate cancer .....	6
1.2.2 Cervical cancer .....	7
1.3 Heating modalities .....	9
1.4 Catheter-based ultrasound .....	10
1.5 Research goals .....	10
1.5.1 Thesis content .....	12

<b>I Biothermal Modeling and Patient-Specific Treatment Planning: Theoretical Studies Towards Device Design and Performance</b>	<b>16</b>
---	-----------

<b>2 Prostate Thermal Therapy with High Intensity Transurethral Ultrasound: The Impact of Pelvic Bone Heating on Treatment Delivery</b>	<b>17</b>
2.1 Abstract .....	17
2.2 Introduction .....	18
2.3 Methods .....	23
2.3.1 Acoustic and biothermal solver .....	23
2.3.2 Model geometry and properties .....	25
2.3.3 Ultrasound interaction with bone .....	27
2.3.4 Treatment simulations .....	28
2.4 Results .....	30
2.4.1 Temperature and thermal dose distributions .....	30
2.4.2 Power and frequency effects .....	31
2.4.3 Other parameters .....	39
2.4.4 Full absorption and partial transmission models .....	40
2.5 Discussion .....	41

2.6	Conclusions .....	46
<b>3</b>	<b>Endocavity hyperthermia in the cervix</b>	<b>48</b>
3.1	Abstract .....	48
3.2	Introduction .....	49
3.3	Methods .....	50
3.3.1	Anatomical inspection .....	50
3.3.2	Biothermal model .....	51
3.3.3	Catheter material .....	54
3.3.4	Transducer sectoring .....	55
3.3.5	Patient treatment simulations .....	56
3.4	Results .....	57
3.4.1	Anatomical inspection .....	57
3.4.2	Catheter material .....	58
3.4.3	Transducer sectoring .....	61
3.4.4	Patient treatment simulations .....	62
3.5	Discussion .....	64
3.6	Conclusions .....	67
<b>4</b>	<b>Implant strategies for catheter-based ultrasound hyperthermia adjunct to HDR brachytherapy in the uterine cervix</b>	<b>67</b>
4.1	Abstract .....	68
4.2	Introduction .....	69
4.3	Methods .....	71
4.3.1	Regular implant spacing .....	73
4.3.2	Patient-specific optimization .....	76
4.4	Results .....	77
4.3.1	Regular implant spacing .....	77
4.3.2	Patient-specific optimization .....	84
4.5	Discussion .....	90
4.6	Conclusions .....	95
<b>II</b>	<b>Experimental Device Design, Performance Characterization and Clinical Feasibility</b>	<b>97</b>

<b>5</b>	<b>An endocervical ultrasound applicator for integrated hyperthermia and HDR brachytherapy in the treatment of locally advanced cervical carcinoma</b>	<b>98</b>
5.1	Abstract .....	98
5.2	Introduction .....	100
5.3	Methods .....	102
5.3.1	Applicator fabrication .....	101
5.3.2	Acoustic characterization .....	104
5.3.3	Thermal characterization .....	106
5.3.4	Imaging characterization .....	107
5.3.5	Radiation attenuation .....	108
5.4	Results .....	109

5.4.1	Acoustic output .....	109
5.4.2	Thermal characterization .....	111
5.4.3	Imaging characterization .....	115
5.4.4	Radiation attenuation .....	115
5.5	Discussion .....	116
5.6	Conclusions .....	122
<b>6</b>	<b>Clinical feasibility of endocavity ultrasound therapy</b>	<b>123</b>
6.1	Abstract .....	123
6.2	Introduction .....	124
6.3	Methods .....	125
6.3.1	Clinical protocol .....	125
6.3.2	Thermal treatment planning .....	125
6.3.3	Catheter-based ultrasound devices .....	126
6.4	Results .....	128
6.5	Discussion/Conclusions .....	134
<b>7</b>	<b>Conclusions and Future Directions</b>	<b>136</b>
7.1	Research Summary .....	136
7.2	Future directions .....	141
	<b>Bibliography</b>	<b>146</b>



## List of Figures

2.1	Generalized schematic of the catheter-based transurethral ultrasound applicator with planar, curvilinear, and sectored tubular transducers .....	19
2.2	Transverse CT sections of 3 cm and 5 cm prostate cases with pubic bones in close proximity .....	22
2.3	Geometry of the biothermal simulation model with the transurethral ultrasound applicator .....	25
2.4	Temperature contour profiles for the curvilinear, planar, and tubular applicators at 6.5 – 10 MHz .....	33
2.5	Peak temperature and maximum thermal dose at the bone surface for a 3 cm prostate at 4 – 8 W and 8.5 – 10 MHz .....	35
2.6	Peak temperature and maximum thermal dose at the bone surface for a 4 cm prostate at 4 – 10 W and 6.5 – 10 MHz .....	36
2.7	Peak temperature and maximum thermal dose at the bone surface for a 5 cm prostate at 6 – 10 W and 5 – 7.5 MHz .....	37
3.1	Schematic of catheter-cooled endocavity applicator .....	51
3.2	Axial MR section with clinical target volume, gross tumor volume, rectum, bladder, endocervical tandem and interstitial catheters .....	52
3.3	Therapeutic thermal penetration assessed at 15 minutes with parametric changes in ultrasound transducer, catheter, and tissue properties .....	60
3.4	Temperature and thermal dose distributions after 60 min hyperthermia in uterine tissue .....	63
4.1	Implant geometries tested for heating volume characterization in homogeneous uterine tissue .....	74
4.2	Extent of 41°C contour shown for select implant geometries with directional interstitial and endocavity devices .....	78
4.3	Power values $P_{per1}$ and $P_{per3}$ used to produce maximal tissue volume > 41°C for the regular implant geometries in Table 4.1 .....	81
4.4	Patient-specific optimization results demonstrating thermal coverage of clinical target volumes .....	85
4.5	$T_{90}$ values for all patient cases .....	87
4.6	Power values to create optimal treatment plans for the patients in Table 4.3 ....	89
4.7	Difficulties in the ability to heat throughout clinical target volumes .....	94

5.1	Drawing of endocervical ultrasound applicator with MR image of brachytherapy implant .....	102
5.2	Endocervical ultrasound device integrated within HDR brachytherapy delivery applicators .....	105
5.3	Rotational acoustic pressure-squared distributions .....	111
5.4	Demonstration of electronic isolation of transducer sectors .....	112
5.5	Comparison of rotational acoustic intensity plot to optical displacement .....	113
5.6	Comparison of normalized temperature elevation in phantom to rotation acoustic intensity distributions and optical displacement in water .....	114
5.7	Artifact characterization with standard CT or MRI .....	116
5.8	MR temperature imaging demonstrating power control in length and angle ...	117
5.9	Experimental setup for and results of radiation attenuation measurements .....	118
6.1	Interstitial and endocavity applicators used in clinical hyperthermia .....	127
6.2	Hyperthermia implant in cervix .....	129
6.3	3-D reconstruction of patient anatomy and temperature profiles .....	131
6.4	Acoustic power values used in the first hyperthermia implant .....	132
6.5	Acoustic power values used in the second hyperthermia implant in Fig. 6.3 ..	133

## List of Tables

2.1 Thermal and acoustic parameters used in simulations .....	27
2.2 Simulation results comparing the effects of power, frequency, and absorption model on bone temperature, dose, and treatment time .....	33
3.1 Thermal and acoustic properties of cervix and catheter materials .....	54
3.2 Summary of CTV and GTV dimensions and distances of organs at risk .....	57
3.3 The effects of catheter parameters on thermal penetration and thermal dead zone with the 2×180° applicator .....	61
4.1 Thermal and acoustic properties of cervix and catheter .....	72
4.2 Tissue volumes >41°C (cm <sup>3</sup> ) with regular implant spacing .....	83
4.3 Thermal descriptors for the 8 patients with the same implant configuration at 1 and 3 kg m <sup>-3</sup> s <sup>-1</sup> perfusion .....	88
5.1 Acoustic characterization of fabricated devices .....	110

## **Acknowledgements**

I would like to express my utmost gratitude to my research mentor and Ph.D. advisor, Dr. Chris Diederich, whose constant counsel and guidance fully enriched my graduate experience and made the full extent of this project possible. I would also like to thank Dr. I-Chow Joe Hsu, whose clinical expertise and insight was essential to the practical application of this research. I would like to acknowledge the aid of Dr. Jean Pouliot at UCSF, Dr. Viola Rieke at Stanford University, the UC Berkeley / UCSF Joint Graduate Group, the present and former members of the Thermal Therapy Research Group, and funding from NIH R01CA122276.

I am enduringly grateful for the love and support of my family, my greatest gift. To my mother Teresa, my father Barry, my brother Jon, my sister Christina, and to grandparents, aunts and uncles, and cousins, thank you for all of your encouragement throughout the years. To my wife Sharon, thank you for everything you have given me and all that our life will become.

# **Chapter 1**

## **Introduction**

### **1.1 Thermal Therapy**

The elevation of temperature in bodily tissues above normothermia (37°C) can be used for the targeted destruction of tumors. Thermal therapy is divided into two realms based on temperatures achieved: 1) thermal ablation, where tissue temperature is elevated greater than 50 – 60°C, and 2) hyperthermia, where tissue temperature is raised to 40 – 45°C. Whereas thermal ablation is typically a standalone treatment causing direct tissue destruction, hyperthermia is typically an adjunct therapy that sensitizes tissue to the effects of standard cancer treatment involving radiotherapy and chemotherapy.

#### **1.1.1 Thermal Ablation**

Exposure of tissue to temperatures >60°C causes thermal fixation, tissue coagulation, cellular destruction and vascular disruption within seconds. At temperatures of 45 – 60°C, changes in tumor physiology and cellular biology lead to necrotic cell death over the course of minutes and hours. Cell membrane poration, mitochondrial

degeneration, and release of lysosomal enzymes causes widespread cellular destruction. Vascular degeneration exacerbates hypoxia and acidosis within the tumor enhancing necrosis [1, 2].

The extent of thermal damage to tissue can be characterized by the temperature achieved coupled with the duration of treatment. Thermal damage can be expressed by an Arrhenius model derived from a series of skin burn experiments [3-6] which can be used to express the % probability of damaged proteins after thermal exposure [7]. The more commonly used thermal dose parameter described by Sapareto and Dewey [8, 9]

$$EM_{43^{\circ}C} = tR^{43-T} \quad \text{where} \quad R = \begin{cases} 0.25, & T < 43^{\circ}C \\ 0.5, & T > 43^{\circ}C \end{cases} \quad (1.1)$$

defines a time-temperature relationship using a unit for equivalent minutes at 43°C ( $EM_{43^{\circ}C}$ ) for inducing cellular damage, and is based on the analysis of a vast amount of *in vitro* and *in vivo* cell survival data. This expression is useful in a temperature range from ~40 – 60°C. Physically, this equation relates to the inactivation rate of enzymes. Below 43°C, cells are able to adapt to cope with thermal stresses, and thermotolerance from the heat shock response is thought to lead to the lower  $R$  value below this cutoff point [7, 10]. Practically, the thermal dose definition means that for every degree below 43°C, the duration of heating must be increased by a factor of 4 to achieve the same cell kill, while above 43°C, every degree increase means that the cell survival will decrease by a factor of 2 for the same heating duration. Thresholds for thermal destruction based on the Sapareto-Dewey relationship are tissue dependent, which is particularly important when considering thermal effects on non-targeted organs at risk; while complete thermal destruction might be achieved in the prostate at 50 – 52°C and 240  $EM_{43^{\circ}C}$  [11-13], significant thermal damage might occur in the rectum and bladder at much lower thermal



dose thresholds [10]. Particular care must be taken when treatment is delivered close to tissues that experience preferential heating by the treatment method, such as absorption of ultrasound by bone [14] or absorption of electromagnetic energy by fat [15, 16].

The ability to monitor thermal therapy delivery is crucial both to ensuring that adequate temperature and thermal dose are achieved in order to assure tumor destruction, and that toxicity is avoided by minimizing temperature and thermal dose accumulation in non-targeted structures. The most basic and straightforward method for treatment monitoring is implantation of thermometry catheters, but this requires additional intervention that may increase morbidity. Methods have been developed using MRI for thermometry, based on the temperature-dependent proton resonance frequency shift of water molecules, with  $<1^{\circ}\text{C}$  temperature accuracy and update times of seconds [17, 18]. Although costly, MR temperature imaging provides real-time, 3-D temperature information in a completely non-invasive manner. MR thermometry has been used to guide numerous ablation treatments such as during *in vivo* experiments in prostate [12, 19] or clinical treatments in breast, brain, or uterine fibroids [20-22]. Due to the physical changes in tissue induced by thermal ablation therapy, lesion volumes can also be visualized directly with imaging, with thermometry as a secondary verification. MRI or contrast-enhanced CT or ultrasound can be used for monitoring of the ablation volume during or post-treatment [23].

The appeal of thermal ablative therapies is the potential for non-invasive or minimally invasive tumor destruction that yields efficacy rates similar to or better than standard treatments with decreased morbidity. Ablation treatments are generally less costly, can be performed as outpatient procedures, are repeatable, and can be combined

with other treatments. Thermal ablation is particularly attractive in cases where disease is refractory to other therapies or surgery may be contraindicated [24]. Treatment monitoring and verification is highly important to ensuring effective treatment with minimal side effects, and is possible with implanted thermometry or imaging methods. Thermal ablation treatment can be augmented at the border, where temperatures in the hyperthermic range of 40 – 43°C are obtained, with radiation [25] or thermally-sensitive liposomes containing chemotherapeutic drugs [26].

### **1.1.2 Hyperthermia**

Hyperthermia involves the use of mild heating to sensitize cancerous tissue to conventional treatments such as radiotherapy or chemotherapy. Temperatures in the 40 – 45°C range cause a number of changes in cell physiology that enhance the cytotoxicity of radiation or chemotherapeutic drugs [27, 28]. Increased tumor oxygenation due to increased blood flow increases radiation- and drug-induced damage to DNA from oxygen free radicals, while impairing the DNA repair machinery to prevent successful recovery [29-32]. Mild heating increases the action of chemotherapeutic drugs along with increasing their local and intracellular concentration [33, 34]. Exposure to 40 – 45°C is also directly cytotoxic to cells in a hypoxic, low pH, nutrient-deprived environment typical of tumors [27, 35-37]. Although cells are sensitive to both heat and radiation in the mitotic phase, due to the precise nature by which chromosome alignment and separation must occur, cells are resistant to radiation in the S phase because DNA is protected from oxidative damage by the replication machinery. They are, however, sensitive to heating, which denatures proteins involved in replication, thus exposing cells to oxidative damage in their most radioresistant phase [7, 38]. Since tumor cells are

primarily in S phase due to their rapid growth, this contributes to the tumor-selective effect of hyperthermia. Increased oxygen tension is an important result of heat exposure; marked hypoxia in tumor is linked with poor outcome after radiotherapy due to radiation resistance of hypoxic cells [39]. Hypoxia increases radioresistivity but also increases thermosensitivity, and thus the adjunct of hyperthermia to radiotherapy will enhance cell kill both by direct cytotoxicity to hypoxic cells and increased efficacy of radiotherapy due to increased tumor oxygenation.

The success of clinical hyperthermia is dependent on sufficient heat delivery. A number of trials have demonstrated dramatic improvements in tumor control and overall survival when hyperthermia is added to radiation or chemotherapy treatments [40-46]. There are studies that have failed to demonstrate a clinical benefit of hyperthermia, but this has been linked to the use of inadequate heating techniques for the treatment site or inadequate thermal monitoring and treatment standardization [47-49]. Heat delivery can be quantified by the Sapareto-Dewey relationship for thermal dose, with the overall thermal dose value taken as the cumulative thermal dose delivery over all hyperthermia treatments. Cumulative thermal dose thresholds of 6 – 10 EM<sub>43°C</sub> have been identified for thermal enhancement of radiotherapy [50-52]. Jones et al. [52] identified a particularly dramatic improvement in complete response to hyperthermia (adjunct to radiotherapy) in previously irradiated patients with superficial tumors, from 24% with <1 EM<sub>43°C</sub> delivered and 68% with >10 EM<sub>43°C</sub> delivered.

The efficacy of hyperthermia also depends on the timing of delivery. *In vitro* and *in vivo* data suggest that the thermal enhancement of cell kill by hyperthermia when combined with radiotherapy is greatest when the modalities are delivered simultaneously

[53-56], and has led to device development and clinical investigations for sites such as deep pelvis [57] and recurrent chest wall [58-60]. Any device which minimizes the delay between delivery of heat and radiation will make the combined treatment more effective.

While adequate thermal dose delivery to the tumor is necessary for therapeutic response, thermal dose delivery to sensitive organs must be limited to avoid thermal damage. Maximizing efficacy of thermal treatment while minimizing toxicity requires precise delivery of thermal energy confined to the treatment site. While the goal of thermal therapy is to maximize thermal dose accumulation in the tumor, non-targeted organs must receive limited thermal dose. Examples of thresholds for gross thermal damage are 20 – 40  $EM_{43^{\circ}C}$  for the rectum and 80  $EM_{43^{\circ}C}$  for the bladder [7, 10, 61].

## **1.2 Pelvic Malignancies**

### **1.2.1 Prostate Cancer**

Prostate cancer is the most commonly diagnosed cancer in men in the United States, with 200,000 new cases reported annually and 35,000 deaths [62]. Worldwide, prostate cancer causes over 220,000 deaths [63]. Although no causal relationship has been proven, there are pathologic links between the development of benign prostatic hyperplasia (BPH) and prostate cancer [64]. BPH is highly prevalent in older men, with histologic evidence of disease observed in 50% of men age 51 – 60 and 90% of men age 81 – 90. Moderate to severe lower urinary tract symptoms are observed in 33% of men age 51 – 60 and 46% of men age 70 and older [65], leading to 117,000 emergency room visits and 90,000 prostatectomies annually [66, 67].

Thermal therapy is becoming more acceptable as a minimally invasive alternative to surgery or transurethral resection of the prostate (TURP) for treating prostate cancer or BPH [68-70]. Prominent technologies for delivering heat to the prostate include laser, thermal conduction or hot source devices, microwave, radiofrequency, and high-intensity focused ultrasound (HIFU) [2, 68]. The clinical safety and efficacy of transurethral, interstitial, and transrectal approaches with these technologies have been demonstrated [71-76]. Their success depends on achieving complete thermal coagulation of target zones within the prostate while avoiding damage to non-targeted tissue. Transrectal HIFU offers precise control over thermal coagulation, has been effective in treating recurrent or advanced prostate cancer [77, 78], and can be integrated with MRI for treatment guidance by temperature measurement and lesion verification [79]. Long treatment times may be required for larger prostate volumes [78, 80, 81], however, and the anterior portion of the gland may remain untreated due to limitations in accessibility [82].

### **1.2.2 Cervical Cancer**

Cervical cancer causes more than 250,000 deaths per year worldwide [63]. Although stage I (FIGO) disease can generally be well managed, treatment of more advanced tumors is often unsuccessful; 5-year survival for stage II disease is 70%, dropping to 40% for stage III and 15% for stage IV [83]. The standard of care for cervical cancer has traditionally been surgical excision for early disease (stage I – IIA) and for locally advanced disease (stage IIB – IVA), administration of a radiotherapy regimen consisting of external beam irradiation and high-dose-rate (HDR) brachytherapy [84]. The efficacy of radiotherapy can be limited, however, by extensive hypoxia

characteristic of cervical cancers, with the degree of hypoxia correlated with poor prognosis due to radiation resistance of hypoxic cells [39, 85, 86]. This is particularly pronounced in more advanced cervical cancers, with radiotherapy failure rates up to 75% for stage III (FIGO) disease [87].

Multi-modality therapy can potentially overcome limitations in efficacy due to development of resistance to a single form of treatment. In the 1990s, a series of studies were conducted showing that concurrent administration of chemotherapy with the standard radiotherapy regimen significantly improved tumor control and patient survival [88-92]. Unfortunately, the toxicity was also greatly increased, with grade 3 toxicities of 98% vs. 10 – 15% for the combined treatment vs. radiotherapy alone, and grade 4 toxicities of 22% vs. 2% for the combined treatment compared to radiotherapy alone. Toxicity included leucopenia, thrombocytopenia, gastrointestinal damage, nausea, and diarrhea.

Hyperthermia, when combined with radiotherapy, has shown particularly dramatic improvements in tumor control and overall survival compared to radiotherapy alone in the treatment of cervical cancer, but with toxicity comparable to radiotherapy alone [43, 46, 93, 94]. The large, multicenter, phase III trial by van der Zee et al. [46] exhibited improvements in complete response from 57% to 83% and in 3-year overall survival from 27% to 51% with the addition of hyperthermia to radiotherapy. For the more advanced cancers, further improvements in efficacy may be obtained by tri-modality therapy; a Phase II study employing the combined delivery of radiotherapy, chemotherapy, and hyperthermia has demonstrated promising initial results [95], and a multicenter Phase III trial is underway [96].



Although the results of the van der Zee trial are promising, hyperthermia was performed with a deep regional heating technique which requires bulky equipment and elevates temperature throughout the entire pelvic region. This results in low temperature and thermal dose delivery to the cervix ( $T_{90} < 40^{\circ}\text{C}$ ,  $<1.5 \text{ EM}_{43^{\circ}\text{C}}$ ), with temperatures in the rectum and bladder at or above tumor temperature [95, 97]. Hot spots created by microwave arrays due to the differing electrical properties of muscle, fat, and bone can occur outside the cervix and result in thermal toxicity [98, 99]. The production of these hot spots and the ability to treat deep-seated tumors are dependent on patient weight and position [100, 101]. Endocavity devices for localized hyperthermia in the cervix have been developed based on radiofrequency or microwave sources, but these devices have limited thermal penetration or limited control over temperature distributions [102-104].

### 1.3 Heating Modalities

There are a number of energy sources available for administering thermal therapies, including radiofrequency, microwave, thermal conduction sources, laser, and ultrasound. Radiofrequency applicators deliver alternating current between implanted electrodes at 375 – 500 kHz and the movement of ions creates frictional heating. Microwave applicators deliver electromagnetic waves at 60 – 3000 MHz, which causes frictional heating by water molecules rapidly rotating to align with the field. Laser fibers deliver light at 800 – 100 nm wavelength, which is absorbed by tissue-specific chromophores and transferred to heat [1, 24]. Ultrasound is propagated mechanically through tissue in the form of pressure waves typically at 1 – 10 MHz with sub-millimeter wavelength in soft tissue. Frictional heating and mechanical losses occurs from tissue

particles oscillating in the acoustic field [105]. Due to the small wavelength of ultrasound and the ability to create transducer arrays of any shape, ultrasound is more highly controllable than other heating modalities yet still has good penetration in tissue compared to implantable RF devices because of more energy propagation [106]. This allows for more accurate targeting of heating in order to maximize temperature elevation in the tumor while minimizing heating of organs at risk.

## 1.4 Catheter-Based Ultrasound

Catheter-based ultrasound devices have been developed for interstitial and transurethral implantation and treatment delivery [107]. The transurethral device offers increased access to the entire prostate gland, more extensive penetration and spatial control than microwave and RF transurethral technology, and potentially decreased treatment times with respect to transrectal HIFU techniques. The ability of transurethral ultrasound devices to produce precise coagulation zones *in vivo* under guidance from MR temperature imaging has been demonstrated [12, 108-111]. The pattern of energy deposition from these applicators can be controlled by selecting the shape, size, and frequency of the transducer arrays. Applicators based on planar, curvilinear, and tubular transducers have all shown success in conformal thermal therapy of the prostate tissue *in vivo* [12, 109, 111-113]. Smaller interstitial devices implanted directly in tissue have been used alone or in conjunction with the transurethral device to augment thermal ablation treatment in the prostate [112, 114]. Single-sectored and multi-sectored devices have been used for highly controllable energy deposition confined to the prostate boundary [115, 116].

In the cervix, an implantable intrauterine ultrasound applicator could be used to further improve upon positive results in the treatment of cervical carcinoma with deep regional heating techniques by creating conformable heating zones in close proximity to cervical lesions. This would maximize thermal dose coverage of the tumor and minimize damage to non-targeted structures. The applicator would be more easily disseminated, heat treatment easier to deliver than with regional heating devices. Interstitial devices could be implanted along with an intrauterine device to create larger heating volumes.

## **1.5 Research Goals**

Adequate thermal dose delivery to a target tumor volume with minimal dose to non-targeted tissue is crucial to the clinical efficacy of thermal treatments and the reduction of side effects. Catheter-based ultrasound offers the ability to create highly conformable heating patterns in order to satisfy these thermal goals, for both thermal ablation and hyperthermia. The effects of parametric changes in ultrasound device and catheter parameters are explored in their effects on heating of pelvic tumors using biothermal modeling. Specifically, the influence of pelvic bone heating and thermal damage on the ability to treat the prostate with transurethral ultrasound devices is explored, along with the ability to heat the cervix using an endocavity device. This implantable intrauterine ultrasound applicator is proposed as a means of obtaining improved heating localization over deep regional techniques in tumors of the cervix. By incorporating HDR radiation sources, this device could create highly conformable and controllable heating patterns monitored with non-invasive MR temperature imaging and aligned with conformal radiation to improve the clinical success of cervical hyperthermia.

The development of this device, from theoretical analysis to experimental characterization and eventual implementation in clinical treatments, is detailed in this report. The specific goals of the research project are summarized as follows:

- 1) Analyze the influence of transducer parameters on treatment time and pelvic bone toxicity during transurethral thermal ablation, and determine new designs and delivery strategies to improve use of this technology
- 2) Perform a theoretical, parametric study to determine optimal design parameters and treatment delivery strategies for heating clinically relevant cervical tumor volumes
- 3) Develop an implantable intrauterine ultrasound hyperthermia applicator, capable of incorporation with HDR brachytherapy delivery, with preferential targeting of tumor volumes
- 4) Characterize applicator performance based on acoustic output and temperature distributions during *ex vivo* experiments and clinical delivery

### **1.5.1 Thesis Content**

In this dissertation, extensive theoretical analysis is presented on the effects of a number of different applicator parameters and treatment delivery strategies on temperature distributions produced by catheter-based endocavity devices in the prostate and cervix. These include ultrasound transducer parameters such as shape, frequency, length, and angular sector distribution on tubular devices; catheter parameters such as thickness, attenuation, cooling flow rate, and cooling flow temperature; and the influences of tissue parameters such as attenuation and blood perfusion, which change with temperature. A thorough analysis of thermal profiles produced by planar,

curvilinear, and tubular applicators during transurethral ablation of the prostate and the influences of device properties and aspects of treatment delivery by mechanical rotation on treatment times and bone heating. The feasibility of hyperthermia in the cervix by a catheter-based endocavity device is assessed by comparing temperature distributions produced using a wide variety of applicator parameters to clinical target volumes for radiotherapy. The ability of the endocavity device to deliver therapeutic heating levels to targets in the cervix with minimal temperature elevation in the rectum and bladder, alone or in conjunction with interstitial ultrasound devices, is directly investigated using thermal treatment planning software with actual patient cases. Implant and treatment delivery strategies are devised for achieving thermal goals of sufficient temperature elevation throughout tumor targets in the cervix without excessive maximum temperature or thermal dose delivery to the rectum and bladder. Theoretical work is translated into the production of devices that are integrated within an HDR brachytherapy delivery applicator, and that use linear arrays of multi-sectored tubular transducers for production of heating profiles tailored in length and angle. Experimental characterization of these devices is conducted, including assessment of acoustic output using two detection methods and measurement of temperature distributions on the benchtop or with MR temperature imaging. The feasibility of clinical hyperthermia delivery using this newly designed device is explored during implementation in two clinical treatments as part of a pilot trial underway at UCSF.

The text consists of 7 chapters that are divided into two sections. In Section I, the results of studies using biothermal modeling and patient-specific treatment planning of heating with transurethral, endocavity, and interstitial ultrasound devices are presented.

These studies employ extensive parametric analysis of a variety of ultrasound applicator parameters in their effects on thermal delivery by transurethral and intrauterine ultrasound devices for ablation and hyperthermia. This leads to insight on site-specific parameter selection, treatment delivery strategies appropriate for each site and thermal goals, and establishes feasibility of clinical hyperthermia delivery with endocervical ultrasound device. Section II describes the experimental methods used to characterize the newly developed endocervical hyperthermia device and inform its design, along with the results of initial clinical implementation of the device.

Chapter 1 provides an overview of thermal therapy, prostate and cervical cancer along with their treatment, heating modalities, and catheter-based ultrasound technology.

Chapter 2 describes a thorough parametric study of the effects of transurethral ultrasound device parameters on pelvic bone heating and treatment time for thermal ablation of the prostate. Thermal delivery by planar, curvilinear, and tubular devices are modeled with variations in maximum power, frequency, and device rotation rate during sweeping treatment of prostate glands with varied dimension and bone at varied distance. Full acoustic field calculations are performed, changing tissue properties are considered, and two models of acoustic absorption by bone are used. The work in this chapter was published in the International Journal of Hyperthermia [117].

Chapter 3 analyzes the effects of transducer and catheter parameters on heating profiles for the endocavity ultrasound hyperthermia device. Clinical feasibility of the device is assessed by comparing heating profiles to radiotherapy clinical target volume dimensions and location of organs at risk. The work in this chapter is part of a paper accepted for publication in Medical Physics [118].



Chapter 4 uses treatment planning and optimization software to analyze heating patterns by endocavity and interstitial ultrasound devices in a number of patient cases to explore potential clinical feasibility and devise strategies for implant geometry and delivery of clinical hyperthermia.

Chapter 5 presents the endocavity ultrasound applicator along with experimental characterization methods to evaluate imaging compatibility, radiation attenuation, acoustic output, and thermal output in phantom and *ex vivo* tissue. The work in this chapter is part of a paper accepted for publication in Medical Physics [118] and presented at SPIE [119].

Chapter 6 describes the first clinical treatments using the endocavity ultrasound applicator as part of a pilot trial at UCSF. The feasibility of clinical hyperthermia delivery at therapeutic levels is investigated. The work in this chapter was presented at ISTU [120].

Chapter 7 summarizes the catheter-based ultrasound device development work and discusses future directions for related research.

## **Part I**

# **Biothermal Modeling and Patient-Specific Treatment Planning: Theoretical Studies Towards Device Design and Performance**

## **Chapter 2**

# **Prostate Thermal Therapy with High Intensity Transurethral Ultrasound: The Impact of Pelvic Bone Heating on Treatment Delivery**

### **2.1 Abstract**

This study was designed to assess pelvic bone temperature during typical treatment regimens of transurethral ultrasound thermal ablation of the prostate to establish guidelines for limiting bone heating. Treatment with transurethral planar, curvilinear, and sectorized tubular applicators was simulated using an acoustic and biothermal pelvic model that accommodates applicator sweeping, boundary temperature control, and changes in perfusion and attenuation with thermal dose to more accurately

model ultrasound energy penetration. The effects of various parameters including power and frequency (5 – 10 MHz) on bone heating were assessed for a range of prostate cross-section (3 – 5 cm) and bone distance (1 – 3 cm). All devices can produce significant bone heating (temperatures  $>50^{\circ}\text{C}$ , thermal dose  $>240 \text{ EM}_{43^{\circ}\text{C}}$ ) without optimization of applied frequency or power for bone  $<3$  cm from the prostate boundary. In small glands ( $\sim 3$  cm) increasing operating frequency of curvilinear and planar devices can increase bone temperatures, whereas the tubular applicator can be used at 10 MHz to avoid likely bone damage. In larger prostates (4 – 5 cm wide) increasing frequency reduces bone heating but can substantially increase treatment time. Lowering power can reduce bone temperature but may increase thermal dose by increasing treatment duration. All applicators can be used to treat glands 4 – 5 cm or larger with limited bone heating by selecting appropriate power and frequency. Pubic bone heating during ultrasound thermal therapy of the prostate can be substantial in certain situations. Successful realization of this therapy will require patient specific treatment planning to optimally determine power and frequency in order to minimize bone heating.

This chapter represents published work (J. H. Wootton, A. B. Ross, C. J. Diederich. Prostate thermal therapy with high intensity transurethral ultrasound: the impact of pelvic bone heating on treatment delivery. *Int J Hyperthermia*, 23(8), 609-22, 2007).

## 2.2 Introduction

Thermal therapy is an alternative to prostatectomy or can be an adjunct to radiotherapy in the treatment of prostate cancer, or an alternative to TURP or

pharmaceutical approaches to alleviating BPH. Transrectal HIFU has been used effectively for targeted thermal coagulation of the prostate or for hyperthermia as an adjunct to radiotherapy. Long treatment times and the inability to properly access the anterior portion of the prostate gland may limit the use of this technology. Transurethral ultrasound applicators have been developed to address these limitations by offering the ability to rapidly coagulate the entire prostate gland with targeted thermal delivery, which has been demonstrated during *in vivo* experiments using MR temperature imaging for feedback power control [121].

A general schematic of transurethral devices with three transducer configurations as being developed by our group is shown in Fig. 2.1. Transducers used in experimental prostate treatments by this group and others have typically been 3.5 – 4 mm wide, 6 – 20 mm in length and have operated at a frequency between 4.7 and 10 MHz [109-111, 113, 116, 121]. Transurethral cooling is implemented for thermal protection of the urethra. Planar and curvilinear devices each produce narrow heating zones and utilize mechanical sweeping to treat a large portion of the prostate. Directional tubular transducers, designed with 90- to 270-degree active sectors [12, 110, 112, 122] can be used either without rotation to coagulate sector zones or rotated to treat larger prostate regions. The transducer shape and frequency affect the penetration of ultrasound energy; the planar transducer has a narrow, penetrating unfocused beam, the curvilinear transducer lightly focuses ultrasound energy, producing a narrower beam compared to the planar transducer, and the tubular transducer exhibits a radial decay ( $1/r$ ) of energy emitted over a pre-defined sector with distance. Recent efforts by Chopra et al.[109, 123] have developed a planar transducer configuration that allows frequency modulation between

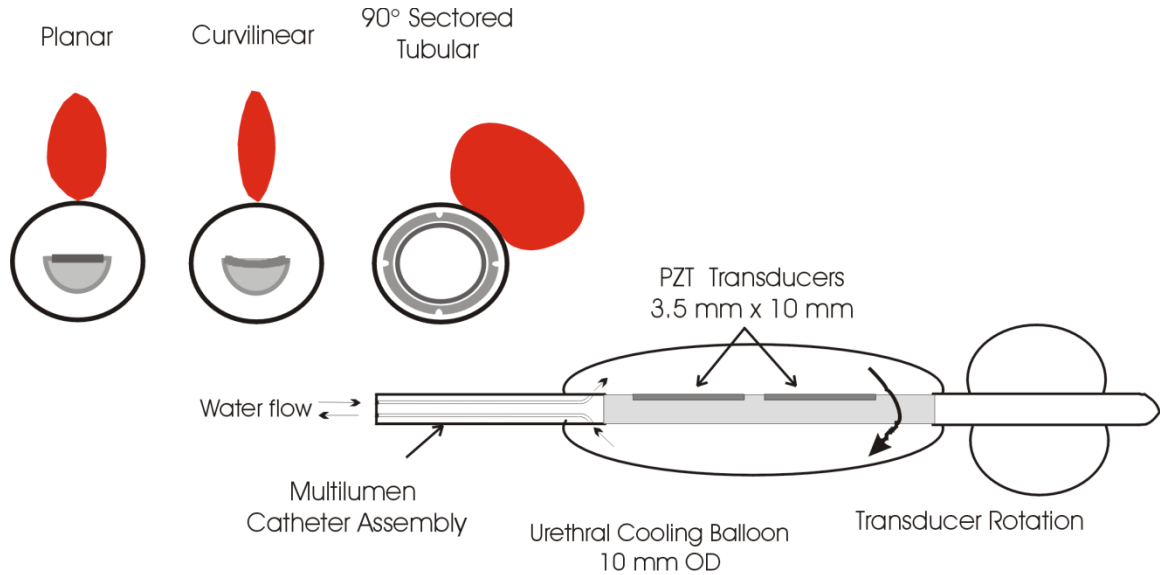


FIG. 2.1: Generalized schematic of the catheter-based transurethral ultrasound applicator capable of mechanical rotation within an inflatable urethral cooling balloon, with cross-sections of planar, curvilinear, and sector tubular transducers (single active 90° sector). Heating profiles for the three transducer types taken from temperature contours during simulated treatments are shown.

4.7 MHz and 10 MHz to adjust the radial depth of average energy deposition. The specific applicator configuration and corresponding energy penetration must be carefully considered in order to properly target specific treatment zones, reduce treatment duration, and avoid the accumulation of thermal dose in sensitive structures beyond the prostate.

The thermal treatment of soft tissue by ultrasound can be complicated by the presence of bone, causing unwanted heating. High temperature rises at the soft tissue/bone interface can be produced by ultrasound, primarily due to preferential energy absorption [14] resulting from a 20 – 30 fold greater attenuation in bone than in soft tissue [124]. This can cause patient pain [125], soft tissue necrosis in regions adjacent to bone, and possibly compromise long term bone integrity by inducing osteocyte necrosis

[126]. Ultrasound treatments in sites such as the chest wall, brain, and neck necessitate treatment planning and carefully considered applicator design to achieve therapeutic temperature rises in the target tissue while avoiding excessive temperature rises in adjacent bone [127-130]. In contrast, HIFU can be used to specifically target bone for palliation of pain in patients with bone metastases, taking advantage of high bone attenuation to preferentially localize treatment to nerves at the cortical shell of the bone [131]. In addition, there is anecdotal evidence of preferential heating ( $\sim 50^{\circ}\text{C}$  or greater) of bone interfaces, located within 1 cm proximity of the canine prostate, occurring during some *in vivo* evaluations of transurethral planar ultrasound devices under rotation control, as noted from inspection of previously reported temperature distributions [132, 133].

An inspection of pelvic anatomy reveals that the pubic bones are often in close proximity to the prostate, as seen in Fig. 2., and they should therefore be considered when planning transurethral ultrasound treatments. The position of the pubic bones varies widely among patients, but they can be less than 1 cm from portions of the gland [134-137]. Treatment limiting pain has been documented in ultrasound hyperthermia of the prostate [138] and chest wall [139], highlighting a need to identify and implement strategies to avoid bone temperature rises that may either prevent successful treatment delivery or produce unanticipated tissue damage outside targeted regions.

The objective of this study is to investigate the potential impact that pelvic bone may have on applicator design and treatment strategies specific for the three general configurations of transurethral ultrasound devices currently under development. An acoustic and biothermal model of these devices in prostate [111] that incorporates pubic bone was used for this analysis. Ranges of prostate diameter (3 – 5 cm) and pubic

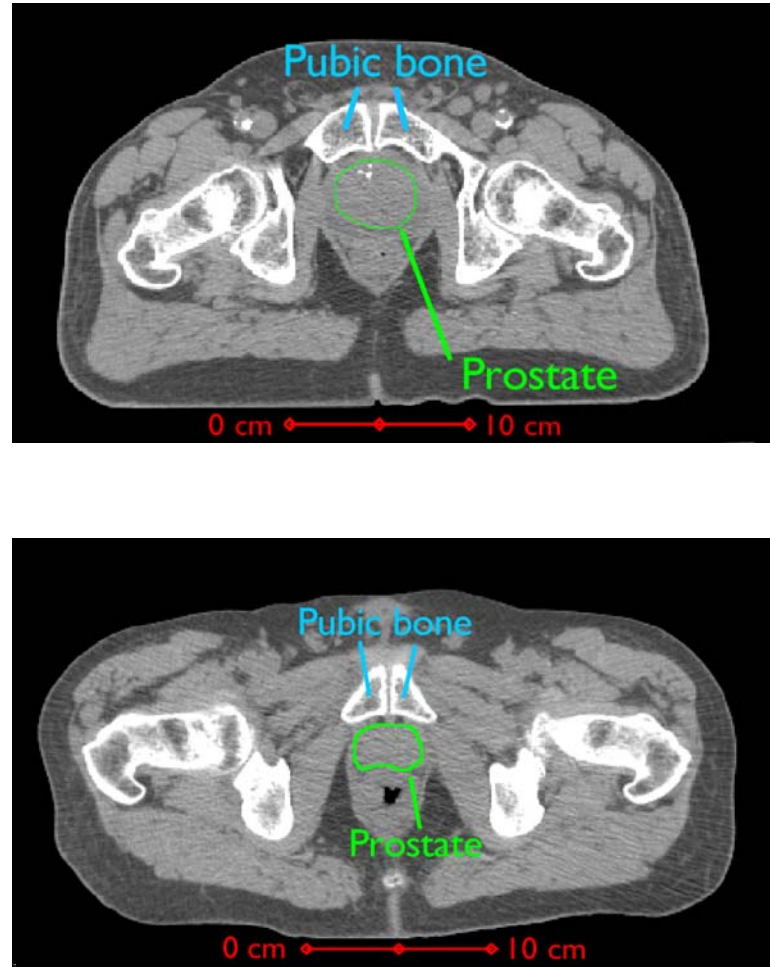


FIG. 2.2: Transverse CT sections depicting example cases of two separate patients, one with a 5 cm gland (top) and the other with a 3 cm gland (bottom), that show the pubic bones in close proximity to the prostate.

bone distance from the prostate (1 – 3 cm) were considered in order to model natural patient variation. Bone temperature rises were assessed during simulated treatment of a portion of the prostate with planar, curvilinear, and tubular applicators for various operating parameters: power, frequency, transducer size, radius of curvature (curvilinear), and sweeping rate (planar and curvilinear). The results of this study were used to identify applicator and treatment parameters that dominantly affect bone heating, determine



criteria to establish when treatment planning around bone may be necessary, and provide recommendations for applicator design and treatment strategies to limit bone heating during transurethral ultrasound thermal therapy. The intent is to provide general guidelines for the various applicator types, and not to provide a critical assessment of any one approach for applying transurethral ultrasound to the prostate.

## 2.3 Methods

### 2.3.1 Acoustic and Biothermal Solver

Theoretical simulations of prostate ablation with transurethral ultrasound devices were performed using a transient acoustic and biothermal model [111, 133, 140] modified to include pelvic bone. The model employs finite difference methods to solve for temperature distributions using the Pennes bioheat transfer equation [141]:

$$\rho_t c_t \frac{\partial T_t}{\partial t} = \nabla k_t \nabla T_t + \dot{\omega}_b c_b (T_b - T_t) + \dot{q} \quad (2.1)$$

where  $\rho_t$  is the tissue density ( $\text{kg m}^{-3}$ ),  $c_t$  is the tissue heat capacity ( $\text{J kg}^{-1} \text{ } ^\circ\text{C}^{-1}$ ),  $T_t$  is the tissue temperature ( $^\circ\text{C}$ ),  $t$  is time (s),  $k_t$  is the conductive heat transfer coefficient ( $\text{W m}^{-1} \text{ } ^\circ\text{C}^{-1}$ ) in the tissue,  $T_b$  is the blood temperature ( $^\circ\text{C}$ ),  $\dot{\omega}_b$  is the mass flow rate of the blood ( $\text{kg m}^{-3} \text{ s}^{-1}$ ), and  $\dot{q}$  is the power deposition ( $\text{W m}^{-3}$ ). At time  $t = 0$ ,  $T_b = T_t = 37^\circ\text{C}$ . The tissues within the model are assumed to be isotropic, which reduces the  $\nabla k_t$  term in Equation 1 to  $k_t$ . The ultrasound power deposition in the tissue was calculated by:

$$\dot{q}(x, y, z) = \frac{\alpha p_o^2(x, y, z)}{\rho v} \quad (2.2)$$

where  $\alpha$  is the acoustic absorption coefficient ( $\text{Np m}^{-1} \text{ MHz}^{-1}$ ) and  $v$  is the ultrasound propagation velocity ( $\text{m s}^{-1}$ ). The acoustic pressure distribution  $p_o^2(x, y, z)$  was calculated by the Rayleigh-Sommerfield diffraction integral for the planar and curvilinear transducers using the rectangular radiator method that accounts for wave interactions [142]. The acoustic pressure distribution for the tubular transducer is calculated by a proven geometric method that accounts for transducer shape and tissue attenuation [133, 140]. The Crank-Nicholson method involving mixed implicit and explicit integration is used to improve numerical stability in time with fine grid spacing [140].

In order to accurately model the large change in attenuation between soft tissue and bone, and to achieve stable solutions at tissue interfaces, a radial spacing of 0.05 mm, an angular spacing of  $1^\circ$ , and a temporal spacing of 0.2 s were applied. The large discrete increase in attenuation between bone and periprostatic soft tissue was modeled as a linear increase over 0.5 mm as a means of improving the numerical stability of the finite difference solver. For increased spatial and temporal resolution to achieve higher accuracy with decreased simulation time, a 2D model was considered appropriate. This model is expected to provide a reasonable approximation for determining the extent of potential bone heating and evaluating the impact on applicator design and treatment delivery strategies.

The biothermal model uses cumulative thermal dose thresholds to dynamically change perfusion and acoustic attenuation within soft tissue during heating. Thermal dose is calculated by the method of Sapareto and Dewey [7, 143]. The perfusion is reset from its baseline normothermic value to zero above a thermal dose of 300 equivalent minutes at  $43^\circ\text{C}$  ( $\text{EM}_{43^\circ\text{C}}$ ), with this threshold substantiated by *in vivo* measurements of

blood flow and vessel damage obtained in rodents and human tumors during thermal exposures [144, 145]. Tissue attenuation is increased linearly to twice its original value as the cumulative thermal dose increases logarithmically from  $10^2$  to  $10^7$   $\text{EM}_{43}^\circ\text{C}$ , above which the attenuation no longer increases. This relationship between thermal dose and attenuation is substantiated directly by the *in vivo* studies of Damianou et al. within perfused muscle, liver, and kidney tissue [146], and also supported by numerous *in vitro* studies which demonstrated a 1.5 – 2 fold or more increase of attenuation due to heating [147-150]. These changes in perfusion and attenuation with thermal dose, observed during *in vivo* experiments as a result of tissue necrosis and coagulation, are incorporated to improve the accuracy of the model, particularly in terms of energy penetration and time required to coagulate tissue out to the prostate boundary. Simulations incorporating these changes have been performed by our group and lesion sizes matched to *in vivo* and *ex vivo* studies [111, 133, 140, 150]. The threshold for complete soft tissue necrosis is considered in this study to be  $240 \text{ EM}_{43}^\circ\text{C}$  [11, 13], although tissue damage can still occur at lower values [7].

### 2.3.2 Model Geometry and Properties

The model consists of a tranverse section through the midgland of the prostate including the rectum and pubic bones (Fig. 2.1). The shape of the prostate was approximated by a cardioid function with the cusp at the posterior margin of the gland, and was varied from 3 – 5 cm wide at midgland to effectively bracket dimensions anticipated in the clinic. The urethra is placed at the center of the cardioid. The cooling balloon contiguous with the ultrasound applicator is located within the urethra and

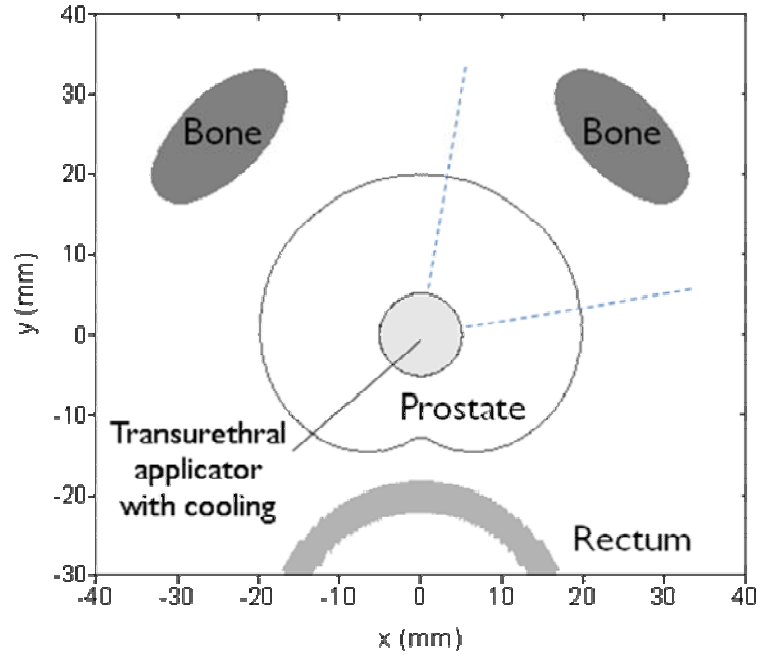


FIG. 2.1: Geometry of the biothermal simulation model with a transurethral ultrasound applicator within the prostatic urethra, the prostate of variable dimensions, the rectum with endorectal cooling, and a simplified representation of pubic bones at variable distance from the prostate capsule. The intended target zone for the simulations is demarcated by a  $\sim 90^\circ$  sector or quadrant of the prostate centered on a pelvic bone.

surrounded by an inflated urethral wall for coupling and protection of the urethral mucosa. The diameter of the balloon is 10 mm and cooling flow is applied at  $23^\circ\text{C}$  with a convective heat transfer coefficient ( $h$ ) =  $1000 \text{ W m}^{-2} \text{ }^\circ\text{C}^{-1}$ . The rectal wall is displaced about 5 mm from the posterior margin of the prostate and is 4 mm thick. An endorectal balloon provides convective cooling flow for rectal protection within the rectum (diameter = 18.5 mm,  $h = 1000 \text{ W m}^{-2} \text{ }^\circ\text{C}^{-1}$ ,  $23^\circ\text{C}$ ). Periprostatic tissue is modeled as a mixture of adipose, muscle, and connective tissue. For purposes of this study, two pubic bones were modeled as ovoids with a short axis of 1 cm and a long axis of 2 cm orthogonal to a radial line extending from the center of the urethra. They are placed

TABLE 2.1: Thermal and acoustic parameters used for different tissue types in the simulations.

Parameter	Prostate <sup>f</sup>	Periprostatic tissue <sup>c</sup>	Bone <sup>c</sup>	Rectum <sup>c</sup>
Thermal conductivity (W m <sup>-1</sup> °C <sup>-1</sup> )	0.56	0.5	0.3 <sup>g,h,i</sup>	0.55
Density (kg m <sup>-3</sup> )	1050	1000	1700	1044
Specific heat (J kg <sup>-1</sup> °C <sup>-1</sup> )	3639	3600	1250	3639
Attenuation coefficient (Np m <sup>-1</sup> MHz <sup>-1</sup> )	5.3 - 10.6 <sup>a,d</sup>	5 - 10 <sup>a,d</sup>	250 <sup>e</sup>	6.0
Perfusion (kg m <sup>-3</sup> s <sup>-1</sup> )	5.0 <sup>b,c</sup>	4.0 <sup>b</sup>	0 <sup>g,j,k</sup>	5.0 <sup>b</sup>

<sup>a</sup>Increases with thermal dose

<sup>b</sup>Reduces to 0 kg m<sup>-3</sup> s<sup>-1</sup> at 300 EM<sub>43</sub> °C

<sup>c</sup>Duck 1990

<sup>d</sup>Worthington 2002 and Damianou 1997

<sup>e</sup>Hynynen 1990

<sup>f</sup>Diederich 1996

<sup>g</sup>Fujii 1999; <sup>h</sup>Biyikli 1986; <sup>i</sup>Liu 2005

<sup>j</sup>Moros 2000; <sup>k</sup>Lin 2000

anteriolateral to the prostate at a distance of 1, 2, or 3 cm from the gland. The size and shape of the bone in cross-section will vary greatly, and the ovoid shape used in the model is intended solely as a simple approximation to assess bone temperature elevation in a straightforward manner as a sweeping ultrasound applicator rotates from soft tissue and aims directly at bone. The pubic bones have acoustic and thermal properties similar to cortical bone, but unlike soft-tissue, the attenuation and perfusion of bone remain unchanged during heating. The acoustic and thermal properties used for the prostate, bone, rectum, and periprostatic tissue within this model are shown in Table 2.1 [14, 105, 122, 124, 146, 149, 151-154].

### 2.3.3 Ultrasound Interaction with Bone

The absorption, reflection, and transmission of ultrasound energy at a soft-tissue/bone interface is complex [14, 127, 128, 153, 155-157]. When ultrasound is aimed directly at bone, ~65% of the incident energy is transmitted into the bone in the form of longitudinal waves [14, 153]. As the incident angle of ultrasound on bone increases, the transmission of longitudinal waves decreases but shear waves with a higher attenuation coefficient than longitudinal waves are generated [157]. The generation of shear waves depends strongly on angle; at an incident angle near 40°, the absorption of shear waves can cause temperature rises nearly twice as great as when the angle of incidence is 0° [14]. Marked ultrasound energy absorption in bone results from an extremely high attenuation of 150 – 350 Np m<sup>-1</sup> MHz<sup>-1</sup> compared to 5 – 10 Np m<sup>-1</sup> MHz<sup>-1</sup> typical of soft tissues [105, 158]. For this effort, the propagation of ultrasound energy at the soft-tissue/bone interface was approximated using two different absorption models to effectively bracket temperature rises that may occur at the pubic bone: (1) a full transmission model where all energy is transmitted and absorbed into the bone independent of incidence angle, thus approximating the complex absorption of longitudinal and shear waves over all angles; and (2) a partial absorption model where 65% of the energy is transmitted assuming normal incidence and no shear waves. Both of these models assume that the reflected absorbed energy in soft tissue local to the bone interface has a small contribution to the local temperature elevation in bone, indicated by the extreme differences in reported attenuation and absorption [105, 158]. By Equation 2, using values of  $\alpha$ ,  $\rho$ , and  $v$  typical of bone and soft tissue, the energy absorbed by the periprostatic tissue is only about 6% of that absorbed by the pubic bone.

### 2.3.4 Treatment Simulations

The targeted treatment zone for all simulations was defined as a 90° sector portion or quadrant of the prostate gland, centered on a pubic bone. The thermal goal of the treatment is to achieve a temperature of 52°C at the outer prostate boundary, which is sufficient to deliver a lethal thermal dose and coagulation over the target zone [159-161]. Applied power levels were controlled from preset initial values using a bang-bang power controller that reduces applied power as necessary to maintain temperatures within the prostate target below a preset maximum threshold. The maximum temperature threshold was set at 85 °C for the 3 cm and 4 cm gland, but increased to 90 °C in the 5 cm gland in order to lower treatment time. Pilot-point treatment control was implemented at the target boundary [162]. For the planar and curvilinear applicators, power is applied and regulated as above to treat a narrow zone of the prostate, and successively rotated to the next scan position when the outer target boundary reaches the 52°C threshold. The 90° sector tubular applicator is centered on the target zone and power is applied as above until 52°C is achieved at the outer boundary – rotation is not required. For each treatment, the maximum temperature and cumulative thermal dose reached in the bone is recorded along with the time required to treat the target zone.

During this simulation study a number of parameters were investigated to determine their influence on temperature elevation at the bone produced with each of the transurethral applicator configurations: prostate width was varied between 3, 4, and 5 cm; separation distance of bone from the prostate was varied between 1, 2, and 3 cm; applied maximum power levels were varied from 3 W to 20 W (with 50% transducer efficiency); frequency was varied between 5, 6.5, 7, 7.5, 8.5, and 10 MHz; transducer width ranged between 3.5 – 5.0 mm (default width is 3.5 mm, length is 10 mm); radius of curvature for

the curvilinear transducers varied from 15 – 22 mm (default is 15 mm); and sequential rotation step size varied between 2 and 20°, with a default step of 10°.

## **2.4 Results**

### **2.4.1 Temperature and Thermal Dose Distributions**

Temperature and cumulative thermal dose distributions resulting from the three different applicator test configurations in the prostate/bone model were calculated for the various applicator design and prostate treatment parameters under consideration. The heating profiles associated with the planar, curvilinear, and tubular applicators are demonstrated for typical cases in Fig. 2.. Snapshots of temperature contours during the thermal ablation sequence are shown for a 4 cm wide prostate, with bone at 1 and 2 cm distance (Power = 10 W). In Fig. 2.a-b, the curvilinear applicator (6.5 MHz, radius of curvature = 15 mm) generates a narrow heating zone that quickly penetrates to the outer capsule of the prostate and is sequentially rotated (10° increments) under temperature feedback control (52°C at boundary) to closely contour the treatment to the target zone boundary. Maximum temperatures calculated from the full absorption model at the bone surface during scanning were 57°C and 54°C for 1 cm and 2 cm bone cases, respectively. The zone of preferential bone heating tracks the applicator sweeping pattern over the bone surface. As shown in Fig. 2.c, increasing the operating frequency to 10 MHz reduces peak bone temperature to 45°C for the 1 cm case but increases the relative treatment duration from 14 min to 55 min.



Similarly, a planar applicator (6.5 MHz) contours a selective heating zone for thermal treatment to the outer target boundary, and generates maximum temperatures along the bone surface of 54° for 1 cm bone separation and 50°C for 2 cm separation (Fig. 2.d-e). Increasing the frequency to 10 MHz decreases bone heating to 44°C (Fig. 2.f), while increasing treatment time from 9 min to 24 min.. Fig. 2.g-i depicts the typical heating patterns of a stationary sectored tubular applicator (90° sector). A sectored ablation zone extending to the target boundary is produced without applicator rotation. The maximum temperatures obtained along the bone surface in the full absorption model with the 6.5 MHz applicator were 50°C for the 1 cm bone and 42°C for 2 cm bone. Increasing the frequency to 8.5 MHz for the 1 cm case reduces peak bone temperature to 44°C (Fig. 2.i) and only slightly increases treatment time from 4.7 min to 6.4 min. In contrast to rotating or sweeping devices, the preferential heating in bone extends along the entire exposed surface over the course of treatment.

#### **2.4.2 Power and Frequency Effects**

The maximum bone temperature and cumulative thermal dose delivered to the pelvic bone during the simulated treatment for the parametric studies is summarized in Fig. 2.5 – 2.7 and Table 2.2. Temperature and thermal dose values plotted in Fig. 2.5 – 2.7 are from the full absorption model, while corresponding values from the 65% absorption model are given in Table 2.2. The results are stratified according to prostate dimension and distance of adjacent pelvic bone. Results for each applicator configuration within the 3 cm prostate are shown in Fig. 2.. When bone is 1 cm from the prostate, large temperature rises at the bone interface can occur, particularly when the

gland is treated with the planar or curvilinear applicator. At 8 W and 8.5 MHz deleterious bone temperatures of nearly 70°C and necrotic thermal doses of  $10^6$  EM<sub>43°C</sub> are predicted for the planar and curvilinear devices, while for the tubular device peak bone temperature is 49°C and accrued thermal dose at the bone is only slightly above 100 EM<sub>43°C</sub>. In the 3 cm prostate model, increasing the frequency from 8.5 to 10 MHz for the planar and curvilinear devices causes an increase in bone temperature and thermal dose, but for the tubular device bone temperature decrease and dose decrease (46°C, 10 EM<sub>43°C</sub>). Power has notable effects in the small 3 cm gland. The influence of power on thermal dose accrued at the bone is shown in Fig. 2.b. When the power is reduced from 8 W to 4 W, bone temperature is reduced for all transducer types and thermal dose in the bone is also reduced for the planar and curvilinear applicators. For the tubular applicator, this reduction in power pushes the bone dose above the threshold for necrosis (102 to 320 EM<sub>43°C</sub>) as required treatment time is increased from 2 min to 11 min. With bone 2 cm away, bone temperatures of 47 – 51°C and 45 – 48°C occur with the planar and curvilinear applicators, respectively, but thermal doses are <20 EM<sub>43°C</sub> due to short treatment duration (<12 min). Bone heating is negligible for the tubular applicator when bone is 2 cm away and for all applicator types when bone is 3 cm away.

As depicted in Fig. 2., for the 4 cm prostate with bone 1 cm away, all applicator configurations may produce deleterious heating or necrosis. At 6.5 MHz and 10 W, bone temperatures for the planar, curvilinear, and tubular applicators reach 57°C, 53°C, and 50°C, respectively, with respective accompanying thermal doses of 6297 EM<sub>43°C</sub>, 976 EM<sub>43°C</sub>, and 370 EM<sub>43°C</sub>. In the 4 cm prostate, increasing the applicator frequency can

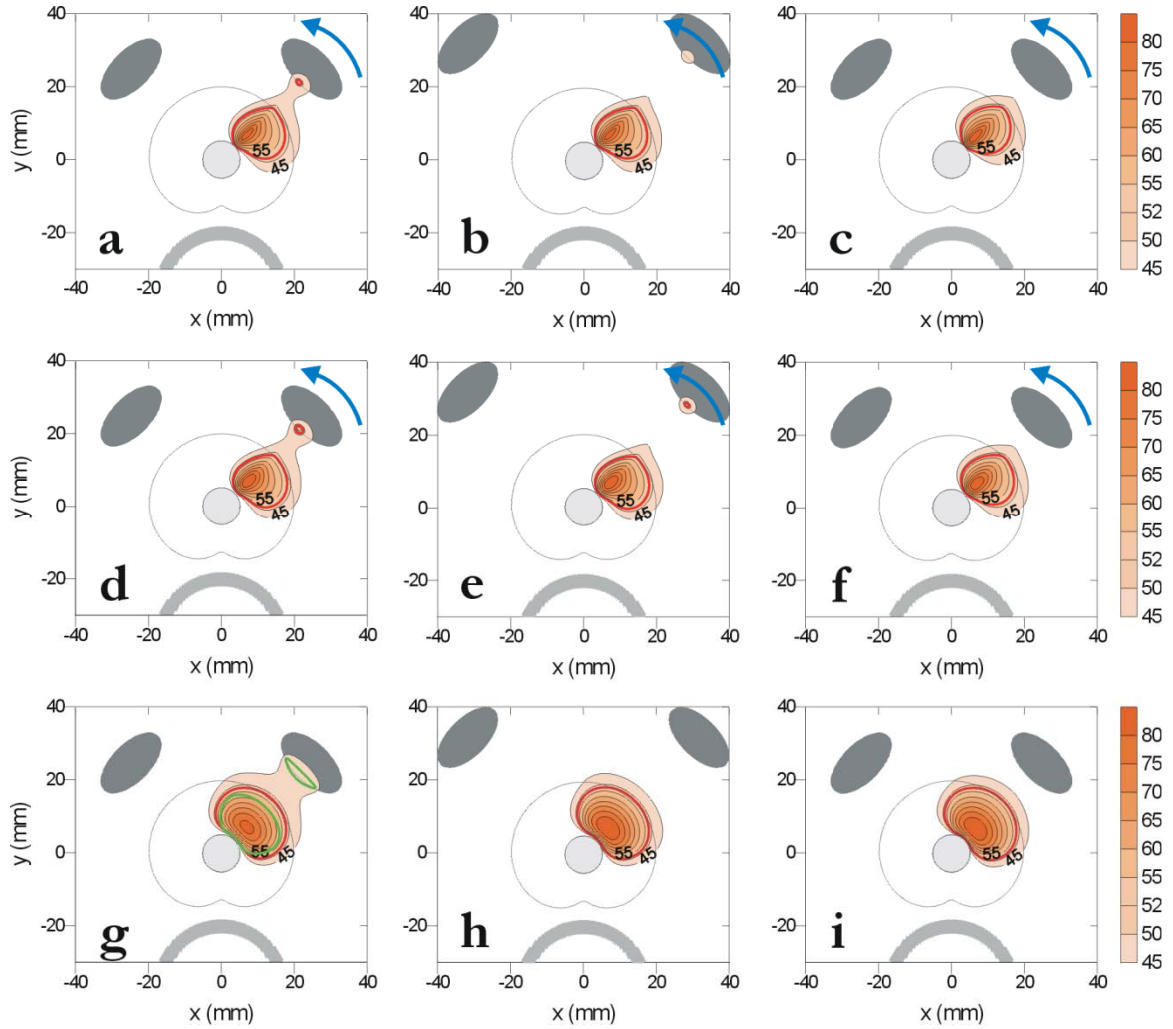


FIG. 2.4: Snapshots of temperature contour profiles for the (a,b,c) curvilinear, (d,e,f) planar, and (g,h,i) tubular applicators. The planar and curvilinear devices will sweep and produce temperature elevations along the entire bone surface (arrow indicates direction of sweeping). Bone heating is compared at 10W with (a,d,g) an applicator frequency of 6.5 MHz and bone 1 cm from the prostate or (b,e,h) 2 cm from the prostate to (c,f,i) heating with an applicator frequency of 10 MHz. The 52°C contour is bolded in red. A 48°C bolded contour is shown in green for the sectored tubular applicator at 6.5 MHz (g) at an earlier time point when bone temperature is higher.

TABLE 2.2: Simulation results comparing the effects of power, frequency, and absorption model on bone temperature, dose, and treatment time with bone 1 cm from the prostate.  
 \*\*Bone is 2 cm from prostate †Prostate attenuation does not change with thermal dose

Prostate size (cm)	Transducer shape	Freq (MHz)	Power (W)	Absorption model	Max bone T (°C)	Treatment time (min)	Max bone TD (EM <sub>43°C</sub> )
3	Planar	8.5	4	Full	61.5	10.9	7.9×10 <sup>4</sup>
		10	4	Full	63.0	10.2	2.2×10 <sup>5</sup>
		8.5	8	Full (65%)	68.4 (58.7)	3.0 (3.0)	1.7×10 <sup>6</sup> (2105)
		10	8	Full	72.8	3.1	2.7×10 <sup>7</sup>
	Curvilinear	8.5	4	Full	61.2	8.3	4.5×10 <sup>4</sup>
		10	4	Full	62.8	8.2	1.5×10 <sup>5</sup>
		8.5	8	Full (65%)	69.4 (58.8)	2.5 (2.4)	1.9×10 <sup>6</sup> (2059)
		10	8	Full	73.5	2.5	2.5×10 <sup>7</sup>
3	Tubular	8.5	4	Full	48.7	11.4	319.9
		8.5	8	Full (65%)	49.8	2.3	101.9
4	Planar	6.5	4	Full	56.8	31.1	1.4×10 <sup>4</sup>
		6.5	10	Full (65%)	57.5 (51.5)	9.2 (8.9)	6297 (133.5)
		8.5	10	Full	54.0	15.4	1312
		10	10	Full	44.9	24.4	5.02
	Curvilinear	6.5	4	Full	53.3	35.3	1933
		6.5	10	Full (65%)	54.5 (49.4)	13.5 (13.2)	976 (53.8)
		8.5	10	Full	51.8	26.2	435.3
		10	10	Full	44.1	54.7	6.07
4	Tubular	6.5	4	Full	47.4	48.6	514.5
		6.5	10	Full (65%)	50.3 (46.6)	4.7 (4.8)	370.2 (35.9)
		8.5	10	Full	44.1	6.4	7.56
4**	Planar	6.5	10	Full	54.2	9.3	760.0
		8.5	10	Full	41.0	15.3	0.07
5	Planar	6.5	6	Full	54.2	41.0	3854
		6.5	10	Full (65%)	54.7 (49.6)	35.2 (35.7)	3524 (144.7)
		7.5	10	Full	45.8	62.2	21.7
	Curvilinear	6.5	6	Full	51.7	68.2	1116
		6.5	10	Full (65%)	52.1 (47.8)	67.4 (68.8)	1082 (86.6)
		7	10	Full	47.7	90.5	93.0
5	Tubular	6.5	6	Full	44.3	29.0	21.5
		6.5	10	Full (65%)	45.1 (42.8)	15.4 (15.9)	20.7 (4.17)
5†	Planar	6.5	10	Full	90.0	6.8	1.2×10 <sup>13</sup>

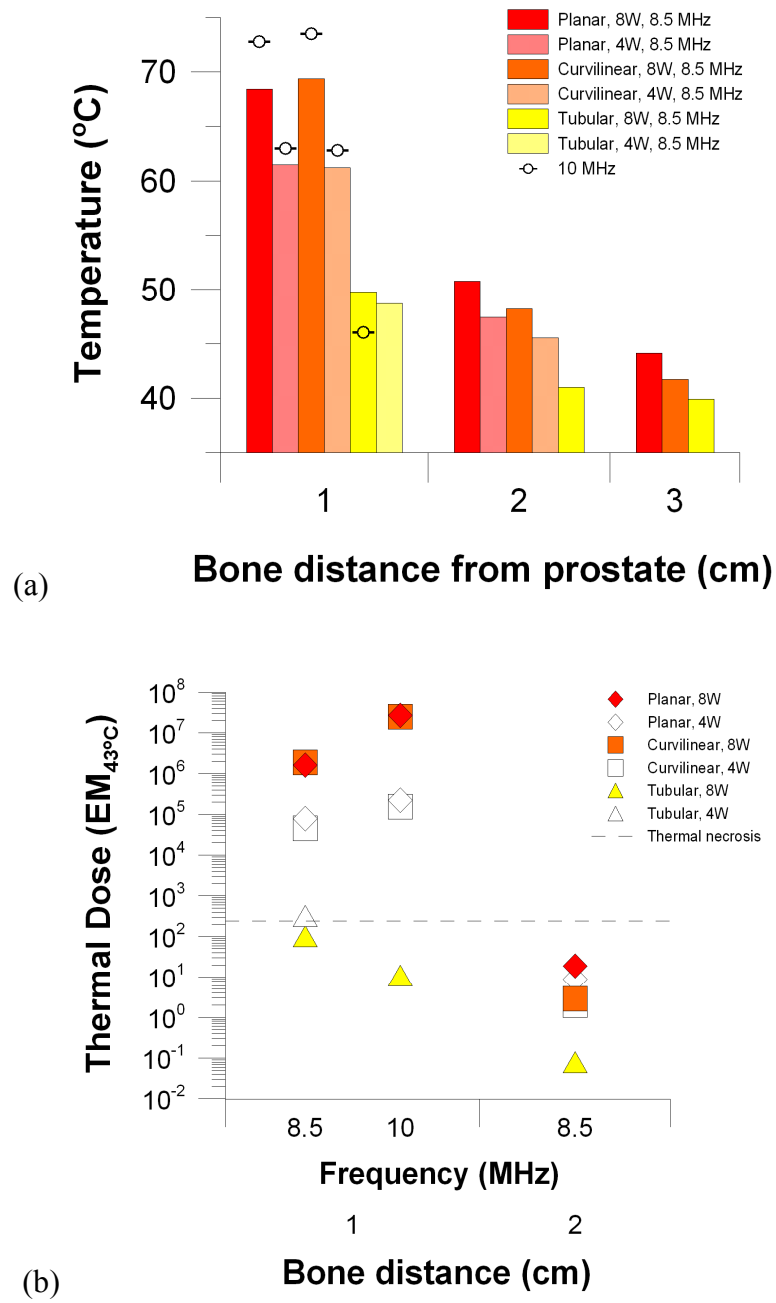


FIG. 2.5: (a) Peak temperatures and (b) maximum cumulative thermal dose at the bone surface for a 3 cm prostate treated with a planar, curvilinear, or tubular applicator at 4 – 8 W and 8.5 – 10 MHz.

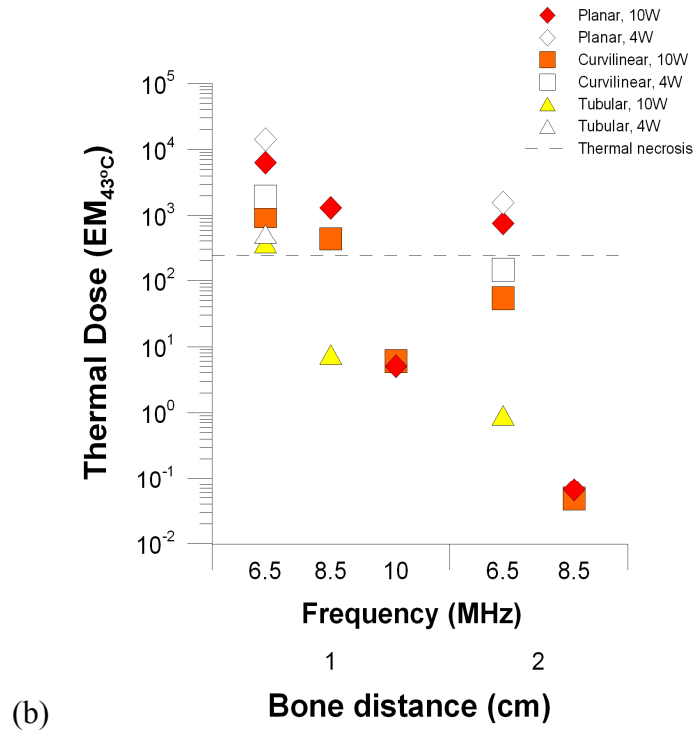
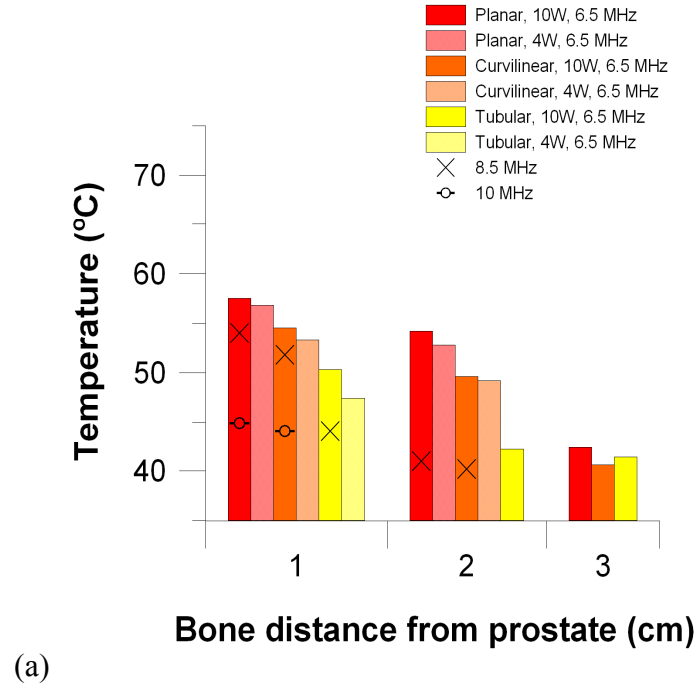


FIG. 2.6: (a) Peak temperatures and (b) maximum cumulative thermal dose at the bone surface for a 4 cm prostate treated with a planar, curvilinear, or tubular applicator at 4 – 10 W and 6.5 – 10 MHz.

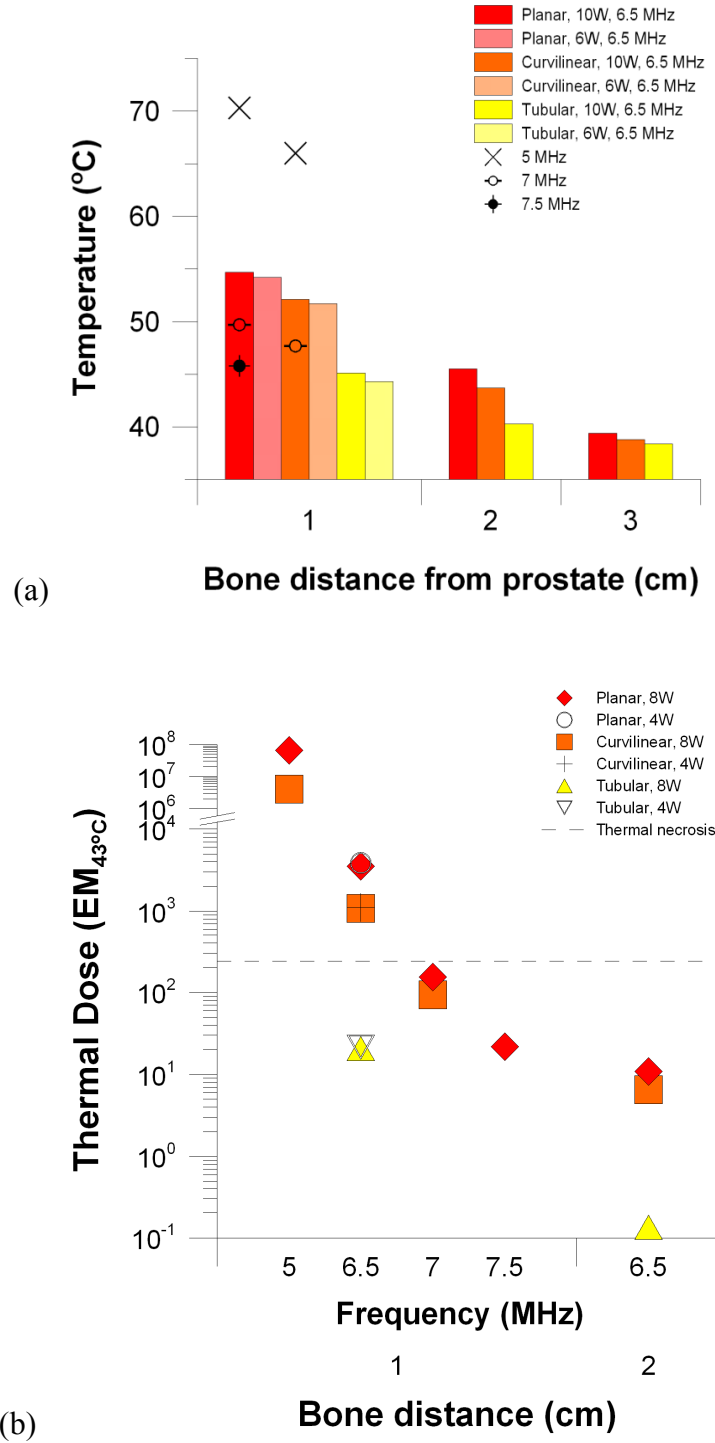


FIG. 2.7: (a) Peak temperatures and (b) maximum cumulative thermal dose at the bone surface for a 5 cm prostate treated with a planar, curvilinear, or tubular applicator at 6 – 10 W and 5 – 7.5 MHz.

reduce bone heating for all applicators. Fig. 2.b illustrates that bone necrosis can be avoided if the tubular applicator frequency is increased to 8.5 MHz (44°C, 7 EM<sub>43°C</sub>) and the planar and curvilinear applicator frequencies are increased to 10 MHz (planar – 45°C, 5 EM<sub>43°C</sub>; curvilinear – 44°C, 6 EM<sub>43°C</sub>). Increasing the frequency increases treatment time slightly for the tubular applicator from 4.7 min to 6.4 min (6.5 MHz vs. 8.5 MHz) and dramatically for the planar and curvilinear applicators from 9 min to 24 min and from 14 min to 55 min, respectively (6.5 MHz vs. 10 MHz). Reducing the power from 10 to 4 W at 6.5 MHz slightly lowers bone temperature but increases thermal dose to the bone due to increased treatment time (planar – 9 min to 31 min, curvilinear – 14 min to 35 min, tubular – 5 min to 49 min). Bone necrosis is still predicted with 2 cm bone separation for the planar applicator at 6.5 MHz, but can be avoided by increasing the operating frequency to 8.5 MHz.

Calculations for the 5 cm prostate model are depicted in Fig. 2., indicating the lower frequency range employed to obtain adequate penetration to the prostate boundary and reduce treatment duration. With 1 cm bone separation, at a 5 MHz drive frequency, treatment is complete for the planar and curvilinear applicators within 22 and 29 minutes, respectively, but bone temperatures exceed 65°C and thermal doses to the bone exceed 10<sup>6</sup> EM<sub>43°C</sub>. At 6.5 MHz bone heating is lower but still potentially problematic for these applicators (planar - 55°C, 3524 EM<sub>43°C</sub>; curvilinear - 52°C, 1082 EM<sub>43°C</sub>) and treatment times have increased to 35 minutes for the planar device and 67 minutes for the curvilinear device. With a small frequency increase to 7 MHz, bone temperatures below 50°C and doses below the necrosis threshold of 240 EM<sub>43°C</sub> are obtained, but the treatment times increase further to 42 minutes for the planar device and to 90 minutes for



the curvilinear device. Simulations for the curvilinear device at higher frequency were not performed due to clinically impractical treatment durations. The planar device can be operated at 7.5 MHz to reduce thermal dose at the bone to 22 EM<sub>43°C</sub> in a 62.2 minute treatment and operated at 8 MHz to further reduce the thermal dose at the bone to 14 EM<sub>43°C</sub> but the treatment time is 104 minutes. The tubular applicator at 6.5 MHz produces non-lethal temperature elevations at the 1 cm bone interface (45°C, 20 EM<sub>43°C</sub>) with a treatment time of 15 min. The bone heating and thermal dose exposures were minimal for the 2 cm bone case and negligible for the 3 cm bone case for all applicator configurations.

### 2.4.3 Other Parameters

Increasing the rotation step size greater than 10° can cause marked increases in bone temperature but decreasing it can only slightly reduce bone heating. When rotation step size is increased above 10°/turn (planar applicator, 10W, 5 MHz, 5 cm prostate, bone 1 cm from prostate boundary), bone temperature is maximal when the applicator stops at one step to aim directly at bone (10°/turn – 70.3 °C, 15°/turn – 75.4 °C, 20°/turn – 80.9 °C) and lesser but still notably increased with respect to the 10°/turn step (that does stop to aim directly at bone) when the applicator never aims directly at bone (15°/turn – 74.1 °C, 20°/turn – 73.7 °C). If the applicator is not aimed directly at bone for a 10°/turn step the bone temperature is only reduced from 70.3 to 70.1 °C. Bone temperature decreases with decreasing sweep step below 10°/turn by only ~1°C at most (5°/turn – 69.8 °C, 2°/turn - 69.3 °C). Treatment times were not greatly increased or reduced by changing

step size (2°/turn – 23.4 min, 5°/turn – 22.6 min, 10°/turn – 21.5 min, 15°/turn – 20.8 min, 20°/turn – 18.0 min).

Increasing the radius of curvature or applicator width for the curvilinear applicator had small effects on bone heating. When the radius of curvature was increased from the default of 15 mm to 22 mm (6.5 MHz, 10 W, 5 cm wide prostate, bone 1 cm from prostate boundary), peak bone temperature increased from 52.1°C to 53.7°C while treatment time decreased from 67 min to 55 min. When the transducer width was increased from the default of 3.5 mm to 5 mm, peak bone temperature decreased from 52.1°C to 50.4°C while treatment duration decreased to 60 min.

#### **2.4.4 Full Absorption and Partial Transmission Models**

Table 2.2 summarizes a comparison between maximum temperature and thermal dose calculated for example cases using both absorption models for bone located within 10 mm of the prostate capsule. Maximum temperatures and thermal dose exposures using the partial absorption model, which only accounts for partial transmission of the incident ultrasound, are lower than values predicted with the full absorption model for each case as anticipated, but still predictive of trends in producing potentially lethal bone heating (>49°C) and thermal damage (>50 EM<sub>43°C</sub>) for all applicator types and prostate dimensions for bone 1 cm away. An exception is the 6.5 MHz tubular applicator in the 4 cm wide prostate, which produced potentially non-deleterious bone heating (47°C, <36 EM<sub>43°C</sub>). The change in treatment times calculated between the two models is less than 1%.

Also shown in Table 2.2 is the marked effect that changing the attenuation within the prostate as described earlier can have on simulation results. When the attenuation does not increase with increasing thermal dose, treatment duration is dramatically reduced and bone temperatures are dramatically increased. For the planar applicator at 6.5 MHz in the 5 cm gland, treatment duration is reduced from 35 min to 7 min and the bone temperature increases from 55°C to 90°C.

## 2.5 Discussion

Recent experimental and theoretical studies have demonstrated the potential advantages of applying transurethral ultrasound for prostate thermal therapy compared to other clinical modalities, most notably speed of treatment, a high degree of spatial selectivity or targeting, and compatibility with MR guidance [12, 109-113, 121, 163]. The three general types of transducer configurations being considered (planar, curvilinear, tubular) each have positive performance data supporting continued development and eventual clinical implementation. Explicit study regarding the potential for bone heating and recommendations for avoiding heating with these approaches is important prior to finalizing designs and implementation in the clinic. Although these devices can be integrated with MR temperature monitoring for therapy control, limitations of these monitoring techniques at bone-tissue interfaces reduce the ability to effectively monitor in areas adjacent to and within bone as a means to avoid or control bone heating. The results herein clearly demonstrate that bone heating can be significant and should be considered in applying any of the three techniques. If bone is not properly accounted for, unwanted temperature elevations could potentially generate bone necrosis,

treatment limiting pain, and extension or generation of unpredictable soft tissue damage zones. The presence of pelvic bone is most problematic for these transurethral techniques when the bone interface is 2 cm or less from the outer boundary of the prostate or target region. Proper selection of frequency and applied power with a concomitant increase in treatment duration can be applied *a priori* to reduce unwanted heating in most cases.

The amount of bone heating generated with these transurethral devices is related to the transducer shape as well as to the bone distance, prostate size, and applicator frequency (Fig. 2.4 – 2.7, Table 2.2). The curvilinear applicator has the narrowest treatment zone, the planar applicator has a slightly wider treatment zone, and the sectored tubular device can heat over an entire 90° section of the prostate (Fig. 2.). The curvilinear and planar devices, while under temperature feedback control, will rotate in sequence over the scan time and produce temperature rises along the bone surface in discrete steps, typically aligned with the centerline direction of the transducer at each step. Varying the rotation step size to 10° or smaller (2°, ~continuous) was found to produce insignificant differences in the extent of predicted bone heating. However, if the rotation step size was greater than 10°, the amount of bone heating was dramatically increased. In comparison, the small step sizes ( $\leq 10^\circ$ ) produce less bone heating since lower applied power and/or duration is required at each position for achieving 52°C at the prostate boundary; this is due to more significant pre-heating of the current target zone from thermal spreading or overlap from the adjacent previously targeted zone, which is in closer proximity when small step sizes are implemented. The sectored tubular applicator is stationary and remains aimed directly at the bone during the complete treatment sequence. Decreasing power can reduce temperatures in bone, but the resultant increase

in treatment duration (and timing between rotation movement for curvilinear and planar) can increase thermal dose accumulation. This effect is most dominant in 3 – 4 cm glands, and less so for the larger 5 cm gland (Fig. 2.5 – 2.7).

Some of the treatment times calculated in this work appear greater than those predicted for planar applicators in the work of Chopra et al. [109]. These differences can partly be attributed to slight variations in applicator and tissue parameters and control mechanisms between the studies, but the dominant factor is likely the incorporation of attenuation changes in the prostate with accumulated thermal dose in these simulation studies. Coagulation and thermal fixation of prostate tissue at high temperature will cause an increase in ultrasound absorption, effectively mimicking a higher frequency transurethral applicator during a portion of the therapy delivery and therefore limiting energy penetration. It will then become increasingly difficult to extend the coagulation zone to the outer prostate boundary and will require longer treatment duration if the tissue temperature is to be maintained below a maximum threshold. As shown in Table 2.2, these differences can be considerable, and not taking attenuation changes in the prostate into account may underestimate treatment duration and are also predictive of much greater bone temperatures.

The sectorized tubular transducer device proved advantageous with respect to the planar and curvilinear device in its ability to treat a predefined or prescribed zone of prostate tissue underlying the pubic bone at lower frequencies with notably less bone heating and shorter treatment times. This was particularly evident when bone was closest; in the 3 cm gland with bone 1 cm from the prostate boundary, necrotic thermal doses in the bone could only be avoided by treatment with the tubular applicator.

Reduced temperature elevation at the bone with the tubular applicator is related to the radial decay and divergence of ultrasound energy from the transducer. This ensures that there is lower ultrasound intensity outside of the prostate so that unwanted thermal doses are less likely to develop in structures such as the bladder, rectum, and pubic bones. However, since the tubular applicator is stationary and remains aimed directly at the bone during the complete treatment sequence, bone temperature may be lower but the thermal dose exposure can be considerable and on level with the curvilinear or planar devices. The tubular applicator does have less spatial selectivity compared to curvilinear and planar configurations, so in practice this advantage could be diminished in situations where boundary control outweighs overall treatment duration and bone heating.

Frequency is the predominant applicator parameter for a given transducer shape that affects the amount of bone heating. Increasing frequency for the tubular applicator reduced bone temperatures in all cases. High frequency operation of the planar and curvilinear applicators enabled a dramatic reduction in bone heating, but only in the 4 and 5 cm glands. In the 3 cm gland, selecting a higher operating frequency for the same applied power level increases bone heating due to a combination of close proximity of the bone to the applicator and higher absorption of the propagated energy within the bone. In larger glands, bone heating is reduced at higher frequency (i.e. 7 – 10 MHz vs. 5 – 6.5 MHz) because the bone is sufficiently far from the applicator and the ultrasound intensity is sufficiently attenuated by increased absorption within the prostate to compensate for increased absorption by the bone. Higher frequency can be used to limit energy penetration outside the target region, but comes at a cost – increased treatment duration due to limited energy penetration out to the prostate boundary. A novel design

configuration of planar transurethral applicators has been developed that utilizes transducers which are capable of emitting multiple distinct frequencies (4.7 MHz and 10 MHz) that can be modulated or blended during treatment delivery [123, 164] as a means of controlling the depth of power penetration. Based upon the results of our study, such a device could prove advantageous to a single frequency device in treating a 4 cm prostate. In the simulations performed in this study, a planar applicator at 10 W and 10 MHz produced bone temperatures of 44.9°C but took 24.4 min to treat a 90° portion of the prostate. Operating at 6.5 MHz, the target zone could be treated in 9.4 min but a much higher peak bone temperature of 57.5°C was produced. A dual frequency device could be operated at 10 MHz adjacent to bone and at 4.7 MHz away from bone to minimize treatment duration and bone temperature. In the 3 cm gland, high frequency operation does not limit bone heating, and in the 5 cm gland, treatment duration may be prohibitively long at higher frequency, and so the utility of this type of device in small or large glands is not as clear.

A thermal dose of 240 EM<sub>43°C</sub> and a bone temperature of 50°C were used in this study as thresholds for deleterious effects on the bone and surrounding tissue. These values are well established for predicting extensive necrosis in soft tissue, including prostate [10, 165]. Thermal necrosis in bone has been observed at 50°C with exposure times from 30 seconds to 6 minutes, which corresponds to thermal doses of 64 to 768 EM<sub>43°C</sub> [166-169]. While a thermal dose of 240 EM<sub>43°C</sub> is used as a threshold for complete necrosis, the thresholds for less complete tissue damage may be much lower [7]. Energy accumulated within the cortical bone can contribute to damaging adjacent soft tissue due to thermal redistribution (thermal conduction and blood flow

mechanisms). Unwanted temperature elevations near pelvic bone are of particular concern for adjacent nerves, which have a high thermal sensitivity with low thermal dose thresholds for permanent or transient damage [7, 170-172].

Results from the full absorption model are indicative of worst case bone heating. The full absorption model accounts for longitudinal wave transmission and shear wave generation over a large range of incident angles, while the partial absorption model neglects shear waves and can underestimate the resultant bone temperature elevations and thermal dose accrual. The angle of incidence of ultrasound waves on bone affects their reflection, absorption, and generation of shear waves, leading to different amounts of bone heating. These effects, rather than being specifically addressed in the simulations, were approximated by bracketing potential temperature rises with a 65% and a full absorption model of a simplified “pubic bone”. A more precise mathematical consideration of wave propagation effects with full anatomically correct models could make the estimates of bone heating and validation of treatment strategies more accurate. Since bone position varies greatly between patients, a pretreatment determination of individual patient anatomy and treatment planning systems [173] could be used to avoid bone heating, and could be used to choose appropriate treatment parameters specific for each patient [173-175].

## **2.6 Conclusions**

In summary, the potential exists for producing unwanted temperature rises at the pubic bone interface during transurethral ultrasound thermal therapy of the prostate using tubular, curvilinear, or planar transducer configurations when the bone is less than 3 cm



of the outer target boundary. These temperature elevations and cumulative thermal dose exposures can compromise the integrity of the bone tissue, cause treatment limiting patient pain, and potentially damage sensitive or non-targeted tissue adjacent to the bone. Temperature rises may be mitigated by the selection of appropriate ultrasound parameters such as transducer shape, power, frequency, and treatment duration. Treatment planning that uses individual patient anatomy as a guide to selecting these parameters is indicated for the successful administration of transurethral thermal ablation in the prostate for cases where the bone is within 3 cm from the outer target boundary.

## Chapter 3

# Endocavity Hyperthermia in the Cervix

### 3.1 Abstract

An endocavity device using multi-sectored tubular transducers is proposed for localized, conformal hyperthermia delivery adjunct to high-dose-rate (HDR) brachytherapy in the uterine cervix. The feasibility of this device to heat clinically relevant target volumes is explored by comparing heating patterns in thermal simulation to patient data. Treatment planning images from 35 patients who underwent HDR brachytherapy for locally advanced cervical cancer were inspected to assess the dimensions of radiation clinical target volumes (CTV) and gross tumor volumes (GTV) surrounding the cervix along with the proximity of organs at risk. Transducer and catheter parameters including frequency, sectoring, catheter thickness, catheter attenuation, and cooling water temperature and flow rate were varied to determine their effects on temperature distributions in homogeneous uterine tissue. Blood perfusion was varied from  $1 - 3 \text{ kg m}^{-3} \text{ s}^{-1}$ . Temperature distributions were compared to patient data to

determine target coverage and devise strategies for adequately heating the cervix with minimal heating of organs at risk. Simulations indicate that for 60-minute treatments the applicator can heat  $>41^{\circ}\text{C}$  and deliver  $>5 \text{ EM}_{43^{\circ}\text{C}}$  over 4 – 5 cm diameter with  $T_{\text{max}} < 45^{\circ}\text{C}$  and  $1 \text{ kg m}^{-3} \text{ s}^{-1}$  blood perfusion. The  $41^{\circ}\text{C}$  contour diameter is reduced to 3 – 4 cm at  $3 \text{ kg m}^{-3} \text{ s}^{-1}$  perfusion. Differential power control to transducer elements and sectors demonstrated tailoring of heating profiles. Dead zones in heating between sectors can be aligned to limit temperature elevation in the rectum and bladder. Feasibility of heating clinically relevant target volumes was demonstrated with power control along the device length and in angle to treat the cervix with minimal thermal dose delivery to the rectum and bladder.

The work in this chapter represents part of a published paper (J. H. Wootton, I.-C. J. Hsu, C. Diederich. An endocervical ultrasound applicator for integrated hyperthermia and HDR brachytherapy in the treatment of locally advanced cervical carcinoma. *Med Phys*, 37(12), 2010 (in press)).

## 3.2 Introduction

Hyperthermia improves tumor control and patient survival when delivered adjunct to radiotherapy for cervical cancer [43, 46, 93, 94]. The most prominent technology for delivering hyperthermia to the cervix is deep regional heating equipment consisting of electromagnetic dipole antennas whose phase interactions can be used to steer energy deposition. This steering is limited, however, so low thermal dose is delivered throughout the pelvis [97], and hot spots may be created outside the cervix which can lead to thermal toxicity [98, 99]. Ultrasound is a much more highly controllable energy

source; by varying frequency, transducer size, and transducer shape, highly conformable heating patterns can be produced in three dimensions. Hyperthermia efficacy can be maximized and toxicity minimized by precisely targeting the cervix and limiting thermal delivery to sensitive organs.

An intrauterine ultrasound device, shown in Fig. 3., has been proposed to create 3-D conformable heating zones in close proximity to cervical lesions. Applicators contain several multi-sectored tubular transducers to allow power control radially and along the length. The device is integrated within a tandem and ring HDR brachytherapy catheter to facilitate sequential or potentially simultaneous thermoradiotherapy. The development of this device will depend on careful selection of ultrasound and applicator parameters relevant to the anatomy and treatment site. The objective of this work is to perform parametric biothermal simulation to characterize heating patterns and identify ultrasound transducer and applicator properties appropriate to delivering therapeutic endocavity hyperthermia in the cervix.

### **3.3 Methods**

#### **3.3.1 Anatomical Inspection**

Treatment planning data based on CT and MRI scans were evaluated for 35 patients implanted for HDR brachytherapy delivery to the cervix. The HDR source ( $\text{Ir}^{192}$ ) is introduced through an applicator (Nucletron, Inc.) consisting of an endocavity catheter, or tandem, along with 1) a ring surrounding the cervical os, 2) two ovoid-shaped structures placed in the vaginal fornices, or 3) a vaginal cylinder. The dimensions of gross tumor volumes (GTV) and target clinical treatment volumes (CTV) identified by

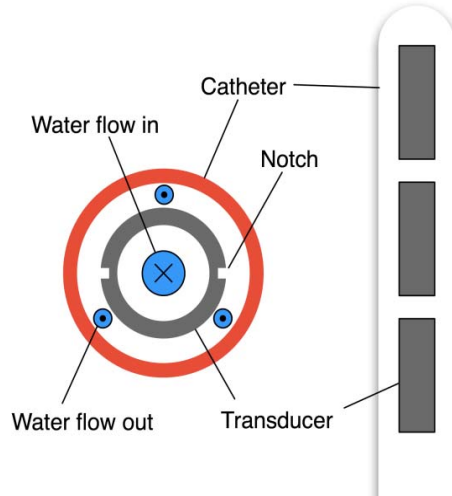


FIG. 3.1: Schematic of catheter-cooled endocavity applicator with a linear array of multi-sectored transducers.

the physician for radiation dose delivery were measured to assess the dimensions of potential clinical targets for hyperthermia. The distances of the rectum and bladder from the tandem, CTV, and GTV were measured. The relative positions of GTV, CTV, tandem and organs at risk are shown in Fig. 3.2.

### 3.3.2 Biothermal Model

The influence of applicator design parameters on heating profiles was investigated using an acoustic and biothermal model of ultrasound hyperthermia in homogeneous uterine tissue. Temperature distributions in cross-section and along the applicator length where  $\rho$  is density ( $\text{kg m}^{-3}$ ),  $c$  is heat capacity ( $\text{J kg}^{-1} \text{ } ^\circ\text{C}^{-1}$ ),  $T_b$  the blood temperature ( $^\circ\text{C}$ ),  $k$  the thermal conductivity ( $\text{W m}^{-1} \text{ } ^\circ\text{C}^{-1}$ ),  $\dot{w}$  the mass flow rate of blood ( $\text{kg m}^{-3} \text{ s}^{-1}$ ), and  $\dot{q}$

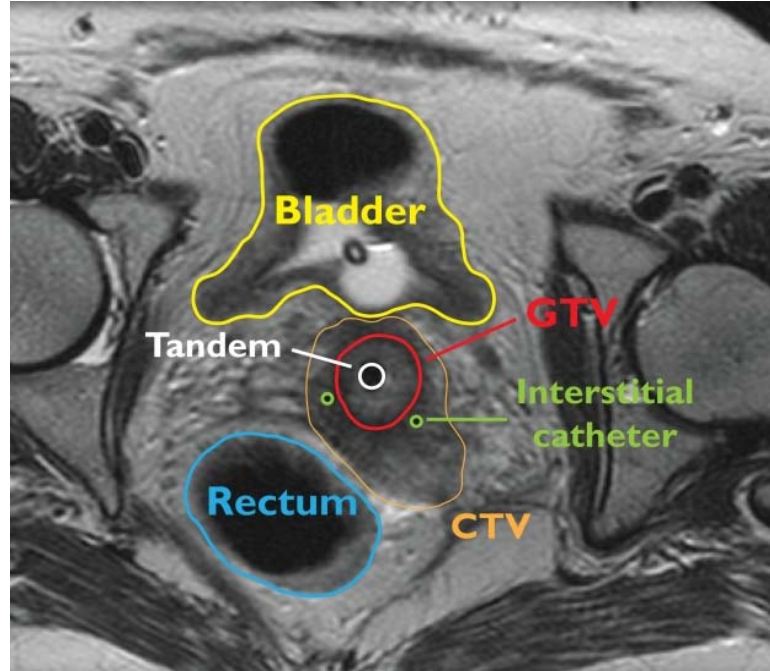


FIG. 3.2: Axial MR section with clinical target volume (CTV), gross tumor volume (GTV), rectum, bladder, endocervical tandem and interstitial catheters. The rectum and bladder closely approach the CTV and GTV on the posterior and anterior aspect, respectively, requiring angular control of heating distributions to treat the tumor without inducing thermal damage in these organs. Interstitial catheters can be used for thermal monitoring and feedback control of power levels.

the ultrasound power deposition ( $\text{W m}^{-3}$ ). The finite difference solution for tissue temperature  $T$  was computed using the Crank-Nicholson method with mixed implicit and explicit integration to improve numerical stability with fine grid spacing [140]. The correlation of the finite difference acoustic and biothermal model to *ex vivo* and *in vivo* temperature and thermal lesion data has been demonstrated in past work [111, 133, 140]. Thermal dose was computed by the Sapareto and Dewey formulation for equivalent minutes at  $43^\circ\text{C}$  ( $\text{EM}_{43^\circ\text{C}}$ ) [8]. The ultrasound power deposition is related to the acoustic intensity by [176]:

$$\dot{q} = 2\alpha \frac{1}{r} I_0 e^{-2\mu(r-r_0)} \quad (3.2)$$

where  $\alpha$  is acoustic absorption ( $\text{Np m}^{-1} \text{ MHz}^{-1}$ ),  $I_0$  the surface intensity of the transducer,  $\mu$  the acoustic attenuation ( $\text{Np m}^{-1} \text{ MHz}^{-1}$ ),  $r$  the radial distance from the center of the applicator (m), and  $r_0$  the outer radius of the transducer (m). Ultrasound intensity was modeled as uniform across sectors, along the applicator length at a given radius, and set to zero between transducer sectors over a defined dead zone angle. The electrical power applied to the transducers was converted to acoustic power by assuming a 50% acoustic efficiency. The model was solved in cylindrical coordinates in cross-section ( $r$ - $\theta$ ) or along the device length ( $r$ - $z$ ). The applicator was a 3.5 mm diameter tubular transducer operated at 6.5 – 8 MHz and housed within a 6 mm outer diameter (OD) catheter with 0.25 – 0.50 mm wall, embedded in homogenous uterine tissue. In order to accurately resolve temperature elevation in the catheter wall with overall reduced computation time, variable radial node spacing was employed following a sigmoidal function that increased from 0.005 mm near the transducer surface to 0.5 mm at 4 cm radial depth in tissue. Acoustic and thermal tissue properties used in the biothermal model are given in Table 3.1 [124, 177-179]. Blood temperature  $T_b$  was 37°C and blood specific heat capacity  $c_b$  was 3825  $\text{W m}^{-2} \text{ }^\circ\text{C}^{-1}$  [124]. Attenuation and absorption were set equal under the assumption that scattered energy is locally absorbed and contributes to heating. A range in blood perfusion from 0.5 – 3  $\text{kg m}^{-3} \text{ s}^{-1}$  was considered to bracket physiological variation in cervical cancers [180]. A convective boundary was applied at the inner catheter wall to model heat removal as  $h(T_{cool} - T_t)$  by cooling water flow with  $h$  the convective cooling coefficient ( $\text{W m}^{-2} \text{ }^\circ\text{C}^{-1}$ ) and  $T_{cool}$  the cooling flow temperature ( $^\circ\text{C}$ ).

TABLE 3.1: Thermal and acoustic properties of cervix and catheter materials employed in the finite-difference model.

Property	Uterus	Catheter
$\rho$ (kg m <sup>-3</sup> )	1060 <sup>a,b</sup>	1100 <sup>f</sup>
$c$ (J kg <sup>-1</sup> °C <sup>-1</sup> )	3600 <sup>a,b</sup>	1600 <sup>f</sup>
$k$ (W m <sup>-1</sup> °C <sup>-1</sup> )	0.56 <sup>a,b,c</sup>	0.23 <sup>f</sup>
$\omega$ (kg m <sup>-3</sup> s <sup>-1</sup> )	0.5 - 3 <sup>d</sup>	0
$\mu$ (Np m <sup>-1</sup> MHz <sup>-1</sup> )	6.9 <sup>e</sup>	
$\alpha$ (Np m <sup>-1</sup> MHz <sup>-1</sup> )		20 - 80 <sup>g</sup>
$T_{cool}$ (°C)		20 - 25
$h$ (W m <sup>-2</sup> °C <sup>-1</sup> )		500 - 1000

<sup>a</sup>Duck 1990

<sup>b</sup>Baldwin 2001

<sup>c</sup>Olsrud 1998

<sup>d</sup>Lyng 2001

<sup>e</sup>Siddiqi 1999

<sup>f</sup>Nominal values for plastic, Kaye 1995

<sup>g</sup>Bloomfield 2000, Guess 1995, Hung 1983, Kaye 1995

An adaptive power control scheme using PID control was implemented following Lin et al [181].

$$P = \begin{cases} P_{\max}, & T < T_{\max} - 2 \\ K \left[ (T_{\max} - T_n) + \frac{\tau}{80} \sum_n (T_{\max} - T_n) - \frac{3}{\tau} (T_{\max} - T_n) \right], & T_{\max} - 2 < T < T_{\max} + 1 \\ 0, & T > T_{\max} + 1 \end{cases} \quad (3.3)$$

with the maximum power  $P_{\max}$ , gain  $K$  and time constant  $\tau$  as adjustable parameters with the goal of ramping temperature from baseline to a set  $T_{\max}$  in 5 minutes with minimal overshoot and oscillation. The power value was updated every 5 seconds.

### 3.3.3 Catheter Material



The effects of ultrasound absorption by the catheter on temperature profiles were examined by parametrically varying catheter material properties along with cooling water flow rate in the catheter. Catheter absorption was set to 20, 40, 60, or 80 Np m<sup>-1</sup> MHz<sup>-1</sup> to reflect the range of values in the materials considered for use in the catheter design: Nylon 6/6, Pebax (Arkema Inc.), TPX (Matsui Plastics, Inc.), polyethylene terephthalate (PET) (Advanced Polymers, Inc.), and Celcon (Ticona Polymers Inc.) [182-185]. These materials differ in stiffness and may require different wall thickness to avoid kinking and to be compatible with 2 – 3 day HDR brachytherapy implantation. Catheter thickness was therefore varied from 0.125 to 0.500 mm in 0.125 mm intervals. Ranges in thermal conductivity from 0.15 – 0.30 W m<sup>-2</sup> °C<sup>-1</sup> and  $\rho c$  product from  $1.5 \times 10^6$  –  $2.1 \times 10^6$  J m<sup>-3</sup> °C<sup>-1</sup> for the catheter were tested but effects on penetration of the 41°C contour were negligible and so these variations were not considered in further analysis. Nominal values used for the plastic catheter were 0.23 W m<sup>-2</sup> °C<sup>-1</sup> for thermal conductivity, 1100 kg m<sup>-3</sup> for density, and 1600 J kg<sup>-1</sup> °C<sup>-1</sup> for heat capacity [185]. Cooling water temperature  $T_{cool}$  was set to 20 or 25 °C and convective cooling coefficient  $h$  to 500 or 1000 W m<sup>-2</sup> °C<sup>-1</sup> based on other catheter-cooled endocavity devices [117, 186, 187]. Catheter material and cooling flow effects were assessed at 1 and 3 kg m<sup>-3</sup> s<sup>-1</sup> tissue blood perfusion. Catheter material comparison tests were conducted using bi-sectored transducers (2×180°) operating at 7 MHz with 30° acoustic dead zones.  $T_{max}$  was set to 43°C, 45°C, or 47°C in the power controller. Temperature profiles were evaluated at 15 minutes, after steady-state had been reached.

### 3.3.4 Transducer Sectoring

The impact of acoustic dead zones on temperature distributions in angle was assessed in a series of simulations. Temperature elevation induced by tri-sectored ( $3 \times 120^\circ$ ) and bi-sectored ( $2 \times 120^\circ$ ) transducers with inactive dead zones (zero acoustic output) of  $20^\circ$ ,  $30^\circ$ ,  $40^\circ$ , or  $50^\circ$  between transducer sectors were compared to an unsectored ( $360^\circ$ ) transducer at blood perfusion levels of 0.5, 1, 2 or  $3 \text{ kg m}^{-3} \text{ s}^{-1}$ .  $T_{cool}$  was set to  $25^\circ\text{C}$  and  $h$  to  $500 \text{ W m}^{-2} \text{ }^\circ\text{C}^{-1}$  for cooling flow. Maximum acoustic power levels in the adaptive controller were set from 0.75 – 3.75 W ( $1.8 - 4.1 \text{ W cm}^{-2}$  surface acoustic intensity) to achieve a  $T_{max}$  of  $43^\circ\text{C}$ ,  $45^\circ\text{C}$ , or  $47^\circ\text{C}$  and 15 minutes was again used as a time point for comparison of steady-state temperature profiles. The catheter was given a nominal absorption of  $40 \text{ Np m}^{-1} \text{ MHz}^{-1}$  and wall thickness of 0.250 mm.

### 3.3.5 Patient Treatment Simulations

A series of simulations were performed in which transducer length, number, frequency, and sectoring were varied to shape the heating profile in axial and sagittal planes to illustrate how the endocervical ultrasound device might be used to treat tumor targets from clinical data while avoiding overheating of rectum and bladder. Applicators with 1 – 3 transducers that were 10 – 15 mm in length and operated at 6.5 – 8 MHz were modeled. Transducers were unsectored or multi-sectored with  $2 \times 180^\circ$  or  $3 \times 120^\circ$  sectoring. Acoustic dead zones between sectors were set to  $30^\circ$ . Cooling flow parameters were set at  $h = 500 \text{ W m}^{-2} \text{ }^\circ\text{C}^{-1}$  and  $T_{cool} = 25^\circ\text{C}$ . 60 minute hyperthermia treatment simulations were conducted, with  $T_{max}$  of  $43^\circ\text{C}$ ,  $45^\circ\text{C}$  or  $47^\circ\text{C}$ . As hyperthermia would likely be administered in multiple fractions, single fraction thresholds of  $41^\circ\text{C}$  and  $5 \text{ EM}_{43^\circ\text{C}}$  were used as indicators of therapeutic heating profiles,

in accordance with suggested guidelines for cumulative thermal dose delivery of 6 – 10  $EM_{43^{\circ}C}$  obtained over multiple treatment sessions [51, 52, 188, 189]. Power control was implemented based on  $T_{max}$  or pilot points in tissue representing the location of interstitial catheters or intraluminal temperature sensors within organs at risk. The rectum temperature was limited to  $41.5^{\circ}C$  while bladder temperature was limited to  $42.5^{\circ}C$ , as the bladder has a higher thermal damage threshold of  $>80 EM_{43^{\circ}C}$  ( $43.5^{\circ}C$  for 1 hr) compared to rectal damage thresholds of 20 – 40  $EM_{43^{\circ}C}$  ( $42.2 - 42.8^{\circ}C$  for 1 hr) [7, 10, 61].

## 3.4 Results

### 3.4.1 Anatomical Inspection

A summary of the anatomical data describing target volume dimensions and location of organs at risk is given in Table 3.2. The CTV averages  $20.5 \pm 5.0$  (standard deviation) per patient in maximum distance in any direction from the tandem. The CTV is often eccentric with respect to the uterine cavity, with the posterior aspect typically extending farther than the anterior aspect ( $20.0 \pm 5.1$  vs.  $17.7 \pm 4.7$ ,  $p = 2 \times 10^{-5}$ , Student's paired t-test). The GTV, representative of the hypoxic tumor core that is the true thermal therapy target, is contained within the CTV and contoured in only the 5 patients who had MRI in addition to CT. The GTV averages  $19.4 \pm 7.3$  mm per patient in maximum radial distance from the tandem with a range of 5 – 28 mm. The GTV is 12 – 20 mm in length. The minimum distance of the rectum and bladder to the tandem is 12.1 and 10.4 mm with

TABLE 3.2: Summary of clinical target volume (CTV) and gross tumor volume (GTV) dimensions and distances of organs at risk from CTV and applicator based on 35 HDR brachytherapy treatment plans (GTV is available for 5 patients).

Parameter	Average $\pm$ SD (mm)	Range (mm)
Max CTV radius (anterior)	$17.7 \pm 4.7$	0 – 42
Max CTV radius (posterior)	$20.0 \pm 5.1$	5 – 44
Max CTV radius (overall)	$20.5 \pm 5.0$	10 – 44
Max GTV radius (overall)	$19.4 \pm 7.3$	6 – 32
GTV length	$15.6 \pm 3.6$	12 – 20
Rectum distance from applicator	$23.5 \pm 4.5$	12 – 44
Rectum distance from CTV	$7.4 \pm 3.6$	1 – 33
Bladder distance from applicator	$17.7 \pm 5.5$	10 – 66
Bladder distance from CTV	$4.7 \pm 3.6$	0 – 47

an average distance of  $23.5 \pm 4.5$  and  $17.7 \pm 5.5$  per patient, respectively. Both rectum and bladder are  $<1$  mm from the CTV boundary in some patients and average  $<8$  mm from the CTV boundary (rectum:  $7.4 \pm 3.6$  mm, bladder:  $4.7 \pm 3.6$  mm).

### 3.4.2 Catheter Material

The maximum radial extent of the steady-state  $41^\circ\text{C}$  contour ranges from 13.7 to 23.8 mm (with  $T_{max} = 45^\circ\text{C}$ ) depending on catheter, cooling flow, and tissue parameters. The effects of the catheter on thermal penetration are minimal for a 0.125 – 0.250 mm wall but become more apparent with a 0.375 – 0.500 mm wall and absorption of  $80 \text{ Np m}^{-1} \text{ MHz}^{-1}$  (Fig. 3.a). Increased catheter thickness and attenuation cause increased heating within the catheter wall, which decreases the effectiveness of cooling flow, bringing the  $T_{max}$  closer to the catheter and reducing the thermal penetration for a given  $T_{max}$  (Table 3.3). The effects of changes in cooling flow parameters for a given catheter

configuration are slight, with a 1.1 – 2.3 mm range in the radial extent of the 41°C contour across all cooling levels. Tissue perfusion has a marked and consistent effect on thermal penetration; high tissue perfusion of  $3 \text{ kg m}^{-3} \text{ s}^{-1}$  reduces the radial extent of the 41°C contour by  $3.7 \pm 0.2 \text{ mm}$  with respect to a lower perfusion case of  $1 \text{ kg m}^{-3} \text{ s}^{-1}$ . The perfusion effect will likely be less consistent *in vivo* as perfusion may increase or decrease during the course of heat delivery [190-193]. The 45°C  $T_{max}$  point is located 2.8 – 9.0 mm from the transducer and  $10.8 \pm 1.1 \text{ mm}$  closer to the transducer than the 41 °C contour. Thermal penetration can be increased if  $T_{max}$  is allowed to increase; for an intermediate case of catheter properties ( $\alpha = 40 \text{ Np m}^{-1} \text{ MHz}^{-1}$ , 0.25 mm wall), cooling flow ( $h = 500 \text{ W m}^{-2} \text{ }^{\circ}\text{C}^{-1}$ ,  $T_{cool} = 20^{\circ}\text{C}$ ), and tissue perfusion ( $1 \text{ kg m}^{-3} \text{ s}^{-1}$ ), the radial extent of the 41°C contour increases from 21.7 mm to 23.8 mm if  $T_{max}$  is increased from 45°C to 47°C.

Temperature within the catheter wall ranges from 27.8 – 44.0°C over the parameters tested and is predominately dependent on catheter thickness. The peak temperature in the catheter wall always occurs at the outer edge of the catheter. The catheter wall is effectively cooled with  $T < 37^{\circ}\text{C}$  for wall thickness  $< 0.375 \text{ mm}$ . At 0.375 mm wall thickness, cooling becomes less effective, resulting in peak catheter wall temperatures from 32.6 – 42.4°C. Catheter wall temperature is  $> 41^{\circ}\text{C}$  at high attenuation values ( $60 - 80 \text{ Np m}^{-1} \text{ MHz}^{-1}$ ) with  $h = 500 \text{ W m}^{-2} \text{ }^{\circ}\text{C}^{-1}$ ,  $T_{cool} = 25^{\circ}\text{C}$ , and  $3 \text{ kg m}^{-3} \text{ s}^{-1}$  perfusion. At 0.500 mm catheter wall thickness, peak catheter wall temperatures of 34.5 – 44.0°C occur, equivalent to 0 – 120  $\text{EM}_{43^{\circ}\text{C}}$  over 60 minutes.

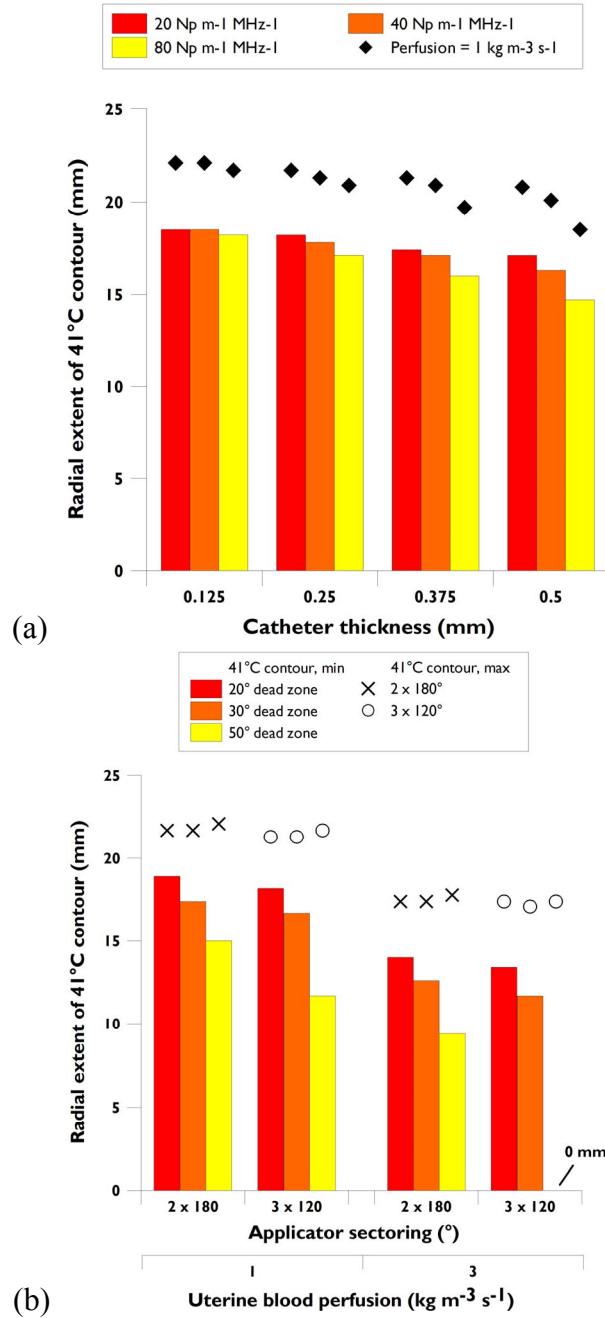


FIG. 3.3: Therapeutic thermal penetration assessed at 15 minutes with parametric changes in ultrasound transducer, catheter, and tissue properties. (a) Radial extent of 41°C contour for a higher ( $3 \text{ kg m}^{-3} \text{ s}^{-1}$ , indicated by bars) or lower ( $1 \text{ kg m}^{-3} \text{ s}^{-1}$ , indicated by symbols) perfusion for 0.125 – 0.500 mm catheter wall thickness and 20 – 80  $\text{Np m}^{-1} \text{ MHz}^{-1}$  catheter attenuation. Empty symbols correspond to  $T_{\max} = 47^\circ\text{C}$  in the lower perfusion case ( $T_{\max} = 45^\circ\text{C}$  for all other data points). (b) Minimal and maximum radial extent of 41°C contour for  $2 \times 180^\circ$ , and  $3 \times 120^\circ$  transducers with an acoustic dead zone of  $20^\circ$  –  $50^\circ$  between sectors at blood perfusion levels of 1 or  $3 \text{ kg m}^{-3} \text{ s}^{-1}$  and  $T_{\max} = 45^\circ\text{C}$ .

TABLE 3.3: The effects of catheter parameters on thermal penetration and thermal dead zone with  $2 \times 180^\circ$  applicator. A range of values for catheter attenuation, thickness, convective cooling coefficient ( $h$ ), and cooling flow temperature  $T_{cool}$  with  $3 \text{ kg m}^{-3} \text{ s}^{-1}$  or low  $1 \text{ kg m}^{-3} \text{ s}^{-1}$  uterine blood perfusion are considered in their influence on steady-state electrical power level  $P_{electric}$  (50% acoustic efficiency), location of  $T_{max}$  ( $45^\circ\text{C}$ ), minimum radial extent of the  $41^\circ\text{C}$  contour in the dead zone and maximum radial extent of the  $41^\circ\text{C}$  contour within the transducer sector.

Attenuation Np $\text{MHz}^{-1}$	Wall $\text{m}^{-1}$ mm	Perfusion $\text{kg m}^{-3} \text{ s}^{-1}$	$h, T_{cool}$ $\text{W m}^{-2} \text{ }^\circ\text{C}^{-1},$ $^\circ\text{C}$	$P_{electric}$ W	$T_{max}$ radius mm	41°C radius	
						Min mm	Max mm
20	0.25	1	500, 25	1.4	9	15.3	20.9
20	0.25	1	1000, 20	1.7	10.3	16	22.5
20	0.5	1	1000, 20	1.6	9.4	15.7	21.3
20	0.25	3	1000, 20	2.3	8.9	11.5	18.9
80	0.25	1	500, 25	1.5	8.3	15	20.1
80	0.25	1	1000, 20	1.9	9.8	15.7	21.7
80	0.5	1	1000, 20	1.9	8	14.7	19.7
80	0.25	3	1000, 20	2.6	8.2	11.5	18.2

### 3.4.3 Transducer Sectoring

Thermal coverage in angle depends on sectoring and acoustic dead zone size (Fig. 3.b). Tri-sector (3×120°) transducers maintain better thermal penetration within dead zones than bi-sector (2×180°) transducers; the minimum extent of the 41°C contour with 40° dead zones between sectors is 16.0 mm vs. 14.0 mm for a 3×120° vs. 2×180° device at  $1 \text{ kg m}^{-3} \text{ s}^{-1}$  perfusion and 11.2 mm vs. 8.5 mm at  $3 \text{ kg m}^{-3} \text{ s}^{-1}$  perfusion ( $\alpha_{cath} = 40 \text{ Np m}^{-1} \text{ MHz}^{-1}$ , 0.25 mm wall,  $h = 500 \text{ W m}^{-2} \text{ }^\circ\text{C}^{-1}$ ,  $T_{cool} = 20^\circ\text{C}$ ). Within sectors, the maximum radial extent of the 41°C contour between these devices differs by <0.5 mm from each other and from the 360° device. Sufficient power to sectors is necessary to provide therapeutic heating throughout dead zones; if  $T_{max}$  is  $43^\circ\text{C}$  or  $T_{max} = 45^\circ\text{C}$  with

50° dead zones, tissue temperature does not reach 41°C within the dead zones at a perfusion of  $3 \text{ kg m}^{-3} \text{ s}^{-1}$ .

### 3.4.4 Patient Treatment Simulations

The 41°C and 5 EM<sub>43°C</sub> contours extend >2 cm radially with  $T_{max} = 45^\circ\text{C}$  at 7 MHz operating frequency and moderate perfusion ( $1 \text{ kg m}^{-3} \text{ s}^{-1}$ ) in simulated 60-minute hyperthermia treatments (Fig. 3.). Multi-sectored applicators have similar penetration within sectors as 360° applicators with a radial reduction <5 mm in the 41°C and 5 EM<sub>43°C</sub> contours within the 30° dead zone at the sector cut (Fig. 3.a-c). The 5 EM<sub>43°C</sub> contour within dead zones can be pushed out 3 – 5 mm radially by applicator rotation 30 – 45 minutes into a 60 min treatment. The PID-based power controller can be used to control angular temperature distributions based on a pilot point set to 41.5°C in the rectum and  $T_{max} = 45^\circ\text{C}$  within sectors (Fig. 3.c). Power can be controlled to individual transducers along the device length to tailor penetration, such as in Fig. 3.d, where the thermal profile follows the typical radiation dose profile with more extensive coverage in the cervix that tapers towards the fundus of the uterus. Temperature and thermal dose overlays from patient-specific simulations demonstrate coverage of target volumes with an unsectored applicator with organs at risk far from the target (Fig. 3.e) or with the use of transducer sectoring and power control guided by thermal feedback based on a pilot point in the rectum limited to 41.5°C and interstitial pilot points within the target limited to  $T_{max} = 47^\circ\text{C}$  (Fig. 3.f).



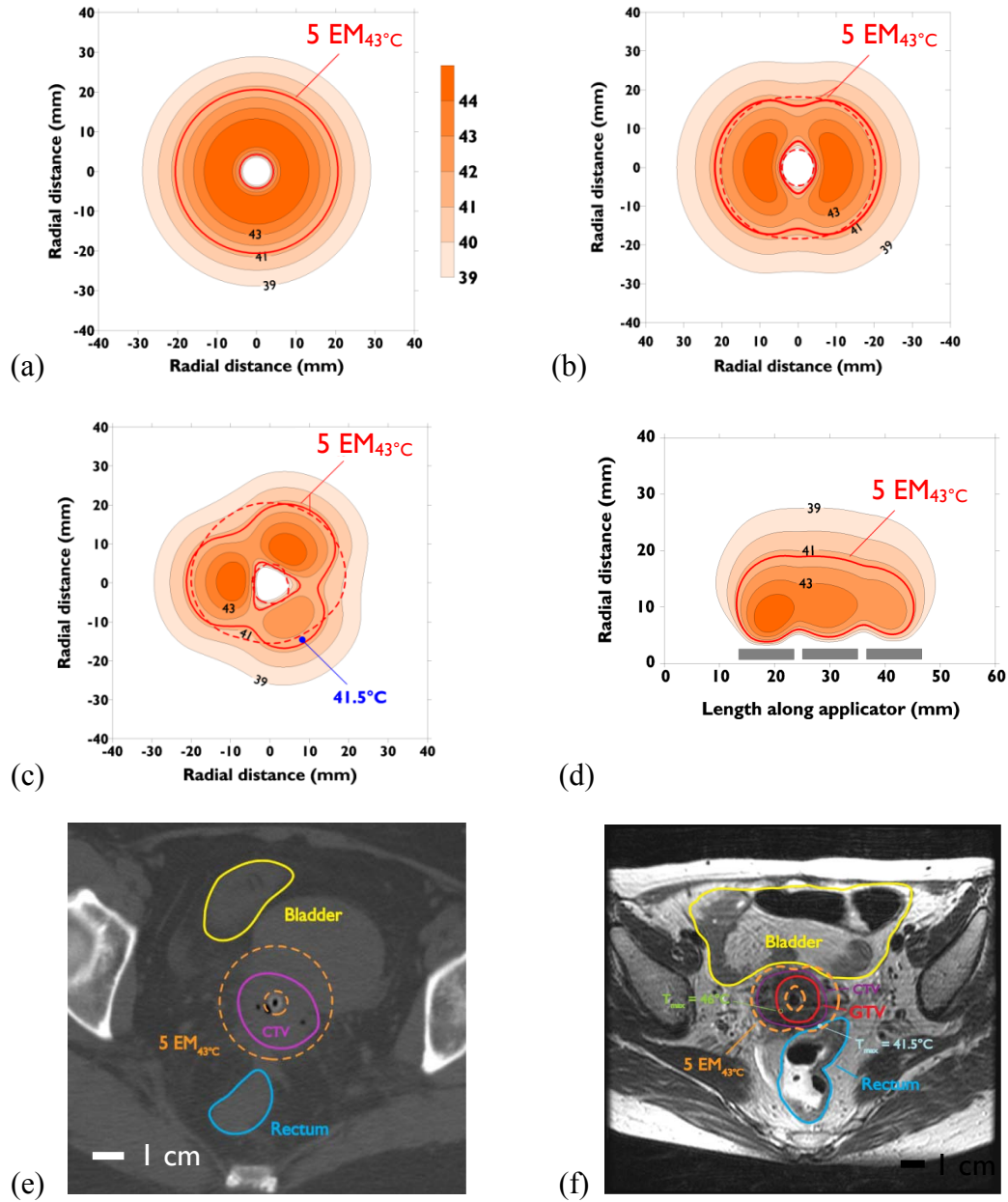


FIG. 3.4: Temperature and thermal dose distributions after 60 min hyperthermia in uterine tissue (thick lines indicate thermal dose of 5 EM<sub>43°C</sub>) with  $1 \text{ kg m}^{-3} \text{ s}^{-1}$  perfusion in the biothermal model. (a) The 41°C contour extends >4 cm in diameter for an unsectored transducer with  $T_{max} = 45^\circ\text{C}$ . (b) A 2×180° with both sectors under PID control to  $T_{max} = 45^\circ\text{C}$  demonstrates a temperate reduction at sector cuts which can be mitigated by rotating the applicator 90° at 45 minutes (5 EM<sub>43°C</sub> contour for treatment with rotation indicated by dashed line). (c) A 3×120° applicator demonstrating power control to sectors based on the use of a pilot control point with  $T_{max} = 41.5^\circ\text{C}$  (dashed 5 EM<sub>43°C</sub> contour for rotation at 30 minutes). (d) Power control along the device length shapes the longitudinal heating profile. (e) Thermal dose overlay for a 360° device encompassing the CTV. (f) Demonstration of laterally directed energy output with a 2×180° device using reduced heating at sector cuts to limit temperature rise in rectum and bladder.

### 3.5 Discussion

The likely feasibility for clinical use of the endocavity ultrasound device can be determined by comparing the extent of therapeutic temperature achieved in thermal simulation, influenced by transducer, catheter wall, and tissue parameters, to tumor volumes and radiation target volumes from a set of patients who underwent radiotherapy for locally advanced cervical cancer. Theoretical analysis indicates that the endocervical ultrasound applicator can apply therapeutic levels of hyperthermia to 4 – 5 cm diameter regions localized around the cervix. HDR brachytherapy treatment planning data present CTV that average 4 cm in diameter, and the GTV, which is the site of hypoxic regions that can lead to radioresistance and recurrence [39, 85, 86], is a smaller region still within this target (Table 3.2). Hyperthermia simulations indicate that a GTV <4 cm in diameter can be covered by therapeutic heating ( $>41^{\circ}\text{C}$ ) with the endocervical ultrasound applicator at moderate perfusion levels ( $0.5 - 2 \text{ kg m}^{-3} \text{ s}^{-1}$ ) and with low maximum temperature ( $T_{max} = 45^{\circ}\text{C}$ ). Catheter material properties have a moderate impact on temperature distributions, with catheter thickness  $<0.5 \text{ mm}$  and attenuation  $<60 \text{ Np m}^{-1} \text{ MHz}^{-1}$  preferable to maximize thermal penetration and reduce temperature elevation in the catheter wall (Fig. 3.).

At higher perfusion levels, higher power with increased maximum temperature ( $T_{max} = 47^{\circ}\text{C}$ ) may be required to extend therapeutic thermal coverage in the target volume. Maximum temperatures reported for clinical hyperthermia in the pelvis range from  $41 - 42^{\circ}\text{C}$  for deep heating systems to  $43 - >45^{\circ}\text{C}$  for endocavity or interstitial, respectively [97, 103, 193, 194]. Past clinical studies using RF heating technology with little control over spatial heating distributions note increased toxicity and complication

rates (rectal or bladder fistula) associated with temperatures  $>43^{\circ}\text{C}$  [195-197]. In contrast to RF sources, tandem ultrasound technology can direct heating energy and maximum temperatures to tumor target sites while maintaining temperatures much less than  $43^{\circ}\text{C}$  in the bladder and rectum so that higher maximum temperatures may be achieved with possibly reduced complications. Furthermore, the volumes of tissue at  $45 - 47^{\circ}\text{C}$  would be small, confined within the tumor and in close proximity to the ultrasound source.

For tumors or target volumes  $>4 - 5$  cm in diameter, the endocervical ultrasound applicator could be used in conjunction with interstitial ultrasound applicators, which are smaller than the endocervical device (2.4 mm vs. 6 mm diameter) and placed within brachytherapy catheters implanted directly in the tumor [107] in order to extend heating to the outer margin of the implant. Larger tumors may alternatively be treated by a combined hyperthermia approach involving deep regional heating and endocervical conformal heating as a thermal dose boost to the hypoxic tumor core, as regional heating devices may only achieve tumor temperatures of  $39 - 39.5^{\circ}\text{C}$  [95, 100].

Concomitant with a consideration of adequate thermal coverage of the tumor volume to the successful administration of hyperthermia is minimization of thermal exposure to the rectum and bladder. The selection of unsectored or sectored devices in clinical hyperthermia delivery will depend on the location of organs at risk with respect to the target volume. These organs can lie  $<10 - 12$  mm from the delivery catheter and  $<1$  mm from the CTV boundary (Table 3.2); thermal delivery must be well controlled in these situations to treat the target while minimizing thermal dose deposition in organs at risk. As shown in Fig. 3., in cases where the rectum and bladder are  $>2 - 3$  cm from the

applicator, unsectored transducers can be safely employed. If the bladder and rectum are  $<2 - 3$  cm from the applicator, sectored applicators can be positioned so that the sector sites are aimed towards the bladder and rectum in order to limit heating of these organs and direct thermal penetration laterally into the parametrium.

The implications of dead zones in the acoustic field between transducer sectors are complex. It is possible to use regions of reduced heating advantageously by aligning them with non-targeted tissues that will cause undesirable side effects if over-treated. When zones of low acoustic intensity are present within the target volume, however, care must be taken to maintain adequate thermal dose delivery, particularly in the presence of high perfusion. With a given sectoring configuration, the effects of reduced heating at the sector site can be mitigated by applicator rotation during treatment, as illustrated in Fig. 3.b-c. This allows the overall heating pattern to be retained but higher thermal dose to be achieved closer to the applicator and farther in depth at the original orientation of the sector cuts. This comes at the expense of a reduced maximum radial extent of therapeutic thermal dose within the sectors.

Treatment control aided by thermal monitoring will ensure adequate thermal dose delivery to the treatment target and thermal protection of non-targeted organs. Interstitial catheters routinely implanted within the cervix lateral to the treatment catheter for HDR brachytherapy can be adapted for thermometry within the treatment zone and intraluminal catheters with temperature sensors may be placed in the bladder and rectum similar to deep hyperthermia for additional feedback. Catheter-based ultrasound technology is also amenable to non-invasive MR temperature imaging for feedback power control of multiple transducer elements and sectors [12, 114, 119].

Treatment planning can aid the clinical delivery of hyperthermia by the endocervical ultrasound device. Geometric information obtained from brachytherapy planning can be used to determine applicator positioning. Temperature-based hyperthermia treatment planning [198] could be used to determine *a priori* power levels that are likely to provide adequate thermal coverage of the target with minimal temperature elevation in the rectum and bladder.

### 3.6 Conclusions

Conformal heating from simulated hyperthermia treatments was compared to clinical target volumes for HDR brachytherapy. Radiation target volumes averaged 4 cm diameter, with tumor volumes smaller than the radiation target. Biothermal simulation demonstrated that treatment zones <4 – 5 cm diameter could be adequately covered with therapeutic temperature ( $>41^{\circ}\text{C}$ ) by a single endocervical ultrasound device within a catheter and at moderate perfusion ( $1 \text{ kg m}^{-3} \text{ s}^{-1}$ ). At high perfusion ( $3 \text{ kg m}^{-3} \text{ s}^{-1}$ ), the heating zone is reduced to 3 – 4 cm diameter. Thermal exposure to the rectum and bladder, which can be located 10 – 12 mm from the applicator and within 1 mm of the target volume, is reduced when using a multi-sectored applicator configuration by aiming acoustic dead zones between sectors towards these structures. Interstitial catheters routinely placed within the target can be implanted with therapeutic devices to extend the heating volume or with thermometry probes to provide temperature feedback in order to guide power control.

## **Chapter 4**

# **Implant Strategies for Catheter-Based Ultrasound Hyperthermia Adjunct to HDR Brachytherapy in the Uterine Cervix**

### **4.1 Abstract**

Catheter-based ultrasound devices deliver locally targeted, 3-D conformable heating easily integrated with HDR brachytherapy delivery. Characterization of heating patterns is performed and strategies identified to determine how these devices can be used to heat cervical tumors. A COMSOL/MATLAB thermal treatment planning platform that uses constrained temperature-based optimization is the basis for analyzing heating patterns. The volume of tissue  $>41^{\circ}\text{C}$  is maximized with the following

constraints:  $T_{\max} = 47^{\circ}\text{C}$ ,  $T_{\text{rectum}} = 41.5^{\circ}\text{C}$ , and  $T_{\text{bladder}} = 42.5^{\circ}\text{C}$ . Heating volumes are assessed with sectorized and unsectorized interstitial (2.4 mm OD) and an endocavity (6 mm OD) device, spaced at 3-4 cm in cervix at 1 or 3  $\text{kg m}^{-3} \text{s}^{-1}$ , or with perfusion varying with location and temperature. Hyperthermia treatment is modeled in 14 patients implanted for HDR brachytherapy. Catheter positions from the brachytherapy implant are used for introduction of endocavity ( $360^{\circ}$  or  $2 \times 180^{\circ}$  output) or interstitial ( $180^{\circ}$ ,  $270^{\circ}$ , or  $360^{\circ}$  output) applicators. Device positioning, sectoring, length, and aiming are varied in order to treat clinical target volumes (CTV) for radiation delivery with the given temperature constraints.  $T_{90}$  in the CTV is used as an indicator of treatment efficacy. Tight control of heating is achieved between sectorized applicators. Control is highly important to treating patient CTV; sectorized applicators were used in nearly all patients to improve  $T_{90}$  while satisfying temperature constraints. Conformable heating of appreciable volumes is possible using multiple sectorized, catheter-based ultrasound devices. Thermal monitoring in clinical treatments will be important for adapting to unknown perfusion levels.

## 4.2 Introduction

Hyperthermia improves tumor control and overall survival when delivered adjunct to radiotherapy and has shown a particularly significant benefit in the treatment of cervical cancer [43, 46, 93, 103]. Favorable efficacy and toxicity profiles are obtained by sufficiently heating the tumor while minimizing temperature elevation in organs at risk such as the rectum and bladder.

Catheter-based ultrasound devices have been developed for minimally invasive, locally targeted, 3-D conformal heat delivery to sites in the cervix and prostate [107, 112,

118]. These devices consist of linear arrays of sectored tubular transducers with power control along the device length and in angle. The ability of catheter-based ultrasound to deliver conformal heating has been demonstrated *in vivo*, *ex vivo*, and in phantom using benchtop thermometry and MR temperature imaging [12, 119, 199]. The implantation of ultrasound devices into catheters used for HDR brachytherapy delivery affords spatial and temporal alignment of hyperthermia with radiotherapy. A device has been developed for endocervical implantation that can heat 2 – 4 cm targets within the cervix [118], and the heating zone can be potentially extended to treat larger tumors by the additional implantation of interstitial devices.

The use of implant configurations with multiple applicators will require extensive treatment planning to determine power levels that will result in adequate thermal coverage of the tumor with minimal thermal toxicity to organs at risk. A treatment planning platform has been developed for modeling and optimizing thermal delivery by multiple catheter-based ultrasound devices [198]. This software uses CT images from HDR brachytherapy planning to create a 3-D model of the tumor target, organs at risk, and catheter locations, which are used as a basis for temperature-based optimization using pre-defined thermal goals.

The hyperthermia treatment planning platform will be a basis for further exploring heating capabilities and limitations of multiple catheter-based ultrasound device implants as well as implant configurations that satisfy thermal goals related to treatment efficacy and toxicity. The aims of this work are to describe 1) heating volumes attainable with interstitial and endocavity ultrasound technology, 2) characterize thermal coverage achievable in heating radiation clinical target volumes using brachytherapy



catheter locations and in doing so, 3) determine implant geometry and device selection that maximizes thermal coverage with minimal concomitant thermal damage to the rectum and bladder. The effects of blood perfusion in tissue on temperature profiles are considered in depth.

### 4.3 Methods

The thermal modeling and optimization software has been described previously [198]. Briefly, CT images on which the target for HDR brachytherapy and organs at risk (rectum and bladder) have been contoured are imported and these structures are rendered in COMSOL with a finite element mesh. The locations of catheters are noted from patient images and catheter positions are selected for ultrasound device placement. Two types of devices are modeled: a 6 mm device that is implanted in the uterine cavity and a 2.4 mm interstitial device for direct implantation in the tumor. The endocavity device has transducers that are unsectored ( $360^\circ$  output) or have two  $180^\circ$  sectors with separate power control ( $2 \times 180^\circ$ ). A  $30^\circ$  dead zone in acoustic output is applied between the sectors. The interstitial device has transducers that are unsectored ( $360^\circ$ ) or have a single sector of  $180^\circ$  or  $270^\circ$ . The temperature-based optimization method varies power levels of all sectors and transducers in order to maximize the proportion of the target volume  $>41^\circ\text{C}$  with constraints placed on the maximum tissue temperature ( $T_{\text{max}}$ ) and the temperature in the rectum ( $T_{\text{rectum}}$ ) and bladder ( $T_{\text{bladder}}$ ).

The heating performance of the catheter-based ultrasound devices depends on their frequency, sectoring, dimensions, catheter material properties, cooling flow, and tissue properties. All devices consist of 1 – 3 transducers that operate at 7 MHz, are 1 cm

TABLE 4.1: Thermal and acoustic properties of cervix and catheter.

Property	Uterus	Catheter
$\rho$ (kg m <sup>-3</sup> )	1060 <sup>a,b</sup>	1100 <sup>f</sup>
$c$ (J kg <sup>-1</sup> °C <sup>-1</sup> )	3600 <sup>a,b</sup>	1600 <sup>f</sup>
$k$ (W m <sup>-1</sup> °C <sup>-1</sup> )	0.56 <sup>a,b,c</sup>	0.23 <sup>f</sup>
$\omega$ (kg m <sup>-3</sup> s <sup>-1</sup> )	1 - 3 <sup>d</sup>	0
$\mu$ (Np m <sup>-1</sup> MHz <sup>-1</sup> )	6.9 <sup>e</sup>	
$\alpha$ (Np m <sup>-1</sup> MHz <sup>-1</sup> )		40 <sup>f</sup>
$T_{cool}$ (°C)		30
$h$ (W m <sup>-2</sup> °C <sup>-1</sup> )		1000
$f$ (MHz)	7.0	

<sup>a</sup>Duck 1990<sup>b</sup>Baldwin 2001<sup>c</sup>Olsrud 1998<sup>d</sup>Lyng 2001<sup>e</sup>Siddiqi 1999<sup>f</sup>Nominal values for plastic, Kaye 1995

in length, and have a 2 mm gap between elements. The endocavity device consists of 3.5 mm diameter elements within a 6 mm OD catheter with 0.25 mm wall, while the interstitial device consists of 1.5 mm diameter elements within a 2.4 mm OD catheter with 0.25 mm wall. Power deposition by the endocavity and interstitial ultrasound devices is calculated by a simplified model for cylindrical radiators [176] and temperature distributions in tissue are determined by the classic Pennes bioheat equation [141]. Electrical power is converted to acoustic power by assuming a 50% efficiency. The effect of ultrasound absorption by the catheter material is considered, with sub-millimeter mesh elements at the applicator surface to resolve temperature elevation. Mesh elements increase in size to a maximum of 1.5 mm in order to increase computational

efficiency without compromising temperature accuracy. Acoustic and thermal properties of the catheter and tissue are shown in Table 4.1 [124, 177-180, 185]. Tissue blood perfusion has a dominant effect on thermal distributions in tissue and a range in perfusion of  $1 - 3 \text{ kg m}^{-3} \text{ s}^{-1}$  based on measurements in cervical tumors [180] is used with the effects of spatial and temporal variations in perfusion considered in their effects on temperature patterns. Annular cooling flow runs within the catheter-housed ultrasound devices and provides acoustic coupling between the transducer and catheter wall, protection of device overheating, and increases thermal penetration by pushing the maximum temperature further into the tissue. Cooling flow is modeled by a convective boundary condition at the inner catheter wall with energy removal dictated by  $h(T_{cool} - T_{ci})$  where  $h$  is the convective cooling coefficient ( $\text{W m}^{-2} \text{ }^{\circ}\text{C}^{-1}$ ),  $T_{cool}$  is the cooling flow temperature ( $^{\circ}\text{C}$ ) and  $T_{ci}$  is the temperature at the inner catheter wall ( $^{\circ}\text{C}$ ). In this study  $h$  is set to  $1000 \text{ W m}^{-2} \text{ }^{\circ}\text{C}^{-1}$  and  $T_{cool}$  to  $30^{\circ}\text{C}$ .

### 4.3.1 Regular Implant Spacing

The heating capabilities of endocavity and interstitial devices were investigated for various regularly spaced implant configurations that might be feasible using a template for introduction of HDR brachytherapy catheters. The implant configurations tested are shown in Fig. 4.1. Interstitial devices were separated by 3 cm from each other and 4 cm from the endocavity device, based on the ability of endocavity devices to heat further in depth. For each implant geometry, two cases were tested, one in which all applicators have  $360^{\circ}$  acoustic output, and one in which all devices are sectorized. Sectorized interstitial devices have  $180^{\circ}$  output while the endocavity applicator has  $2 \times 180^{\circ}$

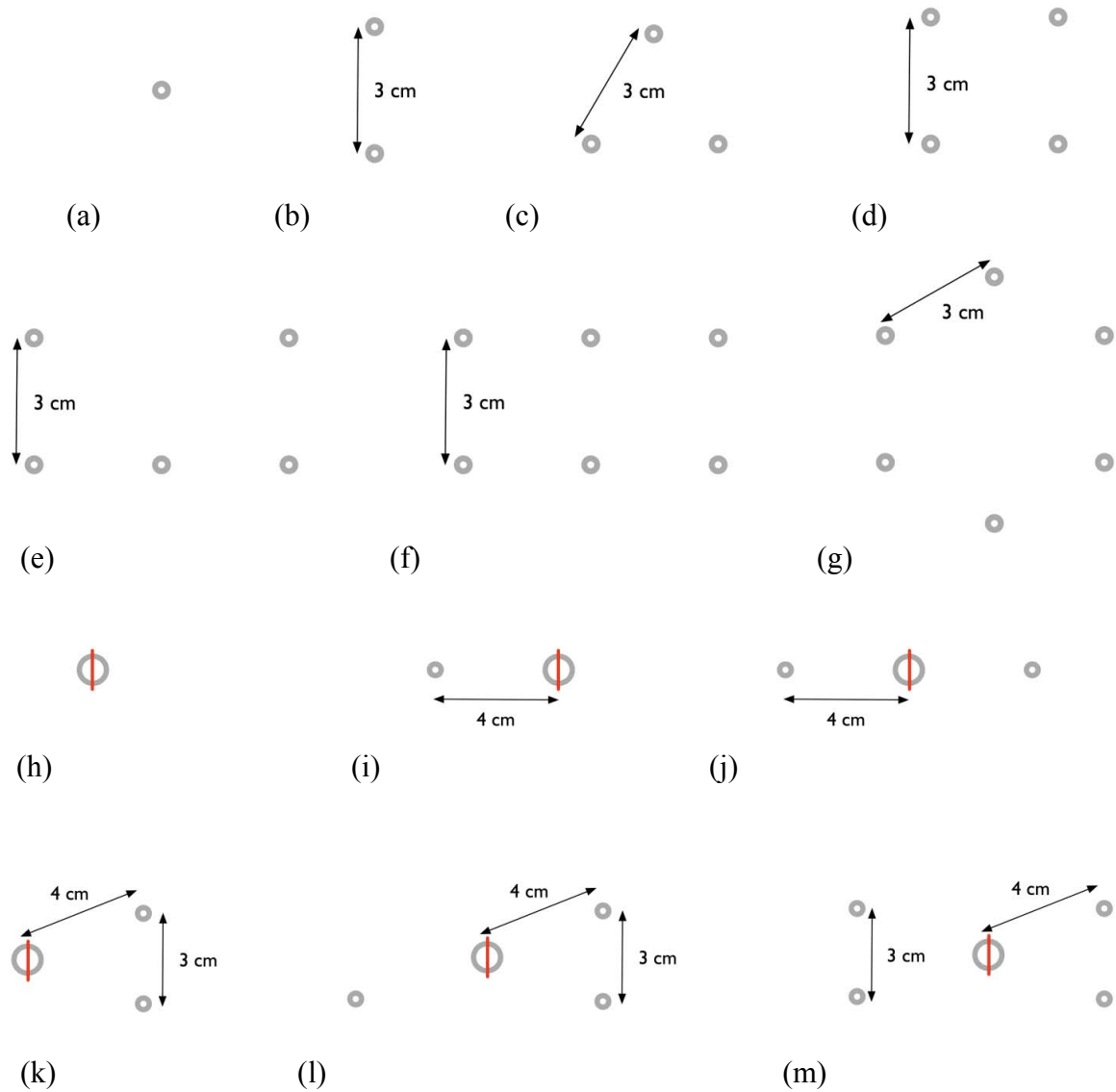


FIG. 4.1: Implant geometries tested for heating volume characterization in homogeneous uterine tissue.

output. All applicators consist of 3 elements in length. Directional interstitial devices were aimed towards the center of the implant while the bi-directional endocavity device was oriented to aim left and right towards the interstitial applicators. A simplified optimization method was employed in which the volume of tissue  $>41^{\circ}\text{C}$  is maximized

with the only constraint that  $T_{\max} < 47^{\circ}\text{C}$ . In order to ensure that heating volumes were relatively symmetrical, power values were constrained to be within a range of 0.25 W electrical across all interstitial devices and across all transducers and sectors within the endocavity device.

Spatial and temperature-based variations in blood perfusion were considered by employing three perfusion models: 1) blood perfusion is homogeneous and constant, 2) a 6-cm diameter tumor is present in the center of the implant with a perfusion higher or lower than the surrounding tissue, and 3) perfusion is temperature-dependent and follows the relationship described in Tompkins et al. [200] for tumor periphery. In the homogeneous model, optimizations were performed to determine power values  $P_{\text{per1}}$  and  $P_{\text{per3}}$  that resulted in the largest therapeutic heating volume with a uniform perfusion of  $1 \text{ kg m}^{-3} \text{ s}^{-1}$  and  $3 \text{ kg m}^{-3} \text{ s}^{-1}$ , respectively. The power values  $P_{\text{per1}}$  and  $P_{\text{per3}}$  were then applied with a perfusion of  $3 \text{ kg m}^{-3} \text{ s}^{-1}$  and  $1 \text{ kg m}^{-3} \text{ s}^{-1}$ , respectively, to determine the extent of under- or overheating if perfusion differs from the planned value. As data have shown that perfusion in tumors may be higher or lower than normal tissue [201-203], power values were optimized to determine the largest attainable heating volume for two situations: (a) tumor perfusion =  $1 \text{ kg m}^{-3} \text{ s}^{-1}$  and surrounding tissue perfusion =  $3 \text{ kg m}^{-3} \text{ s}^{-1}$ , and (b) tumor perfusion =  $3 \text{ kg m}^{-3} \text{ s}^{-1}$  and surrounding tissue perfusion =  $1 \text{ kg m}^{-3} \text{ s}^{-1}$ . Power levels for these situations are designated  $P_{\text{tumper1}}$  and  $P_{\text{tumper3}}$ . Plans were run for case (a) with power levels  $P_{\text{per3}}$  and for case (b) with powers  $P_{\text{per1}}$  to determine how the heating volume changes when the tumor has higher or lower perfusion than planned in surrounding tissue. The effects of perfusion changes with temperature were considered

by running plans with power values  $P_{\text{per1}}$  and  $P_{\text{per3}}$  using a base perfusion of  $1 \text{ kg m}^{-3} \text{ s}^{-1}$  or  $3 \text{ kg m}^{-3} \text{ s}^{-1}$  in the Tompkins model [200].

### 4.3.2 Patient-Specific Optimization

The ability of endocavity and interstitial devices to treat clinical targets in the cervix was explored by modeling hyperthermia in 14 patients implanted for HDR brachytherapy at UCSF. Patients were implanted with tandem and ring or tandem and cylinder brachytherapy applicators with an additional 2 – 6 interstitial catheters implanted for extended radiation coverage of the target volume. None of the patients with vaginal cylinder implants selected for analysis had vaginal wall involvement. Catheter positions along with the contoured clinical target volume (CTV) for radiation, rectum, and bladder were imported into the COMSOL model as described previously. Patients 13 and 14 underwent hyperthermia treatment as part of a Phase I clinical trial. In these patients, a hyperthermia target volume (HTV) was defined based on the tumor location and used as the target in hyperthermia simulations. In the other 12 patients, the CTV, which is larger than the tumor volume, was used as the target in the thermal model. In order to standardize the patient models for comparison of angular temperature distributions, the first 2 cm of the CTV was used. This is typically where the hypoxic tumor core is located that is the site of radio-resistance and recurrence [39, 85, 86]. For each patient, the following iterative approach to generating thermal treatment plans was taken: 1) a combination of the endocavity and interstitial devices were modeled in the positions of brachytherapy catheters with length, insertion depth, sectoring, and orientation selected *a priori*, 2) A temperature-based constrained optimization was performed to maximize coverage of the target volume with prescribed limits on  $T_{\text{max}}$ ,  $T_{\text{rectum}}$ , and  $T_{\text{bladder}}$ , 3) The

$T_{90}$ , or temperature exceeded by 90% of the target volume, was computed, 4) ultrasound device positions, length, and sectoring were modified to improve coverage, 5) optimization was re-run,  $T_{90}$  re-computed, device parameters changed, and so on until  $T_{90}$  could no longer be improved. This procedure was first performed using a perfusion of  $1 \text{ kg m}^{-3} \text{ s}^{-1}$  to determine power levels  $P_{\text{per1\_pt}}$  that resulted in the best thermal coverage of the target volume. A power optimization was then performed using this implant configuration to determine the thermal coverage achieved at  $3 \text{ kg m}^{-3} \text{ s}^{-1}$  without changing the implant. Changes in device placement, length, and sectoring were made and power values optimized in order to attempt to improve the thermal coverage at  $3 \text{ kg m}^{-3} \text{ s}^{-1}$  perfusion. For select patients, a transient simulation was run to determine thermal dose delivery to the target volume. Power was decreased from 30% above the optimized level down to  $P_{\text{per1\_pt}}$  to achieve a ramp-up to steady-state with minimal overshoot at 10-15 minutes followed by 60 – 65 minutes of steady-state hyperthermia for a 75-minute total simulation time. Temperature constraints used in patient-specific simulations are:  $T_{\text{max}} < 47^\circ\text{C}$ ,  $T_{\text{rectum}} < 41.5^\circ\text{C}$ , and  $T_{\text{bladder}} < 42.5^\circ\text{C}$ . The temperature limits for organs at risk are based on thermal damage thresholds from *ex vivo* and *in vivo* data [7, 10, 61].

## 4.4 Results

### 4.4.1 Regular Implant Spacing

The volume of tissue that could be feasibly heated by a combination of 3-element, unsectored interstitial devices alone in the implant configurations shown in Fig. 4.1a-g to  $>41^\circ\text{C}$  in uterine tissue with  $1 \text{ kg m}^{-3} \text{ s}^{-1}$  perfusion is  $31 - 220 \text{ cm}^3$ . A single interstitial device heated  $>41^\circ\text{C}$  over a 3.6 cm diameter while 6 devices as configured as in Fig. 4.1f

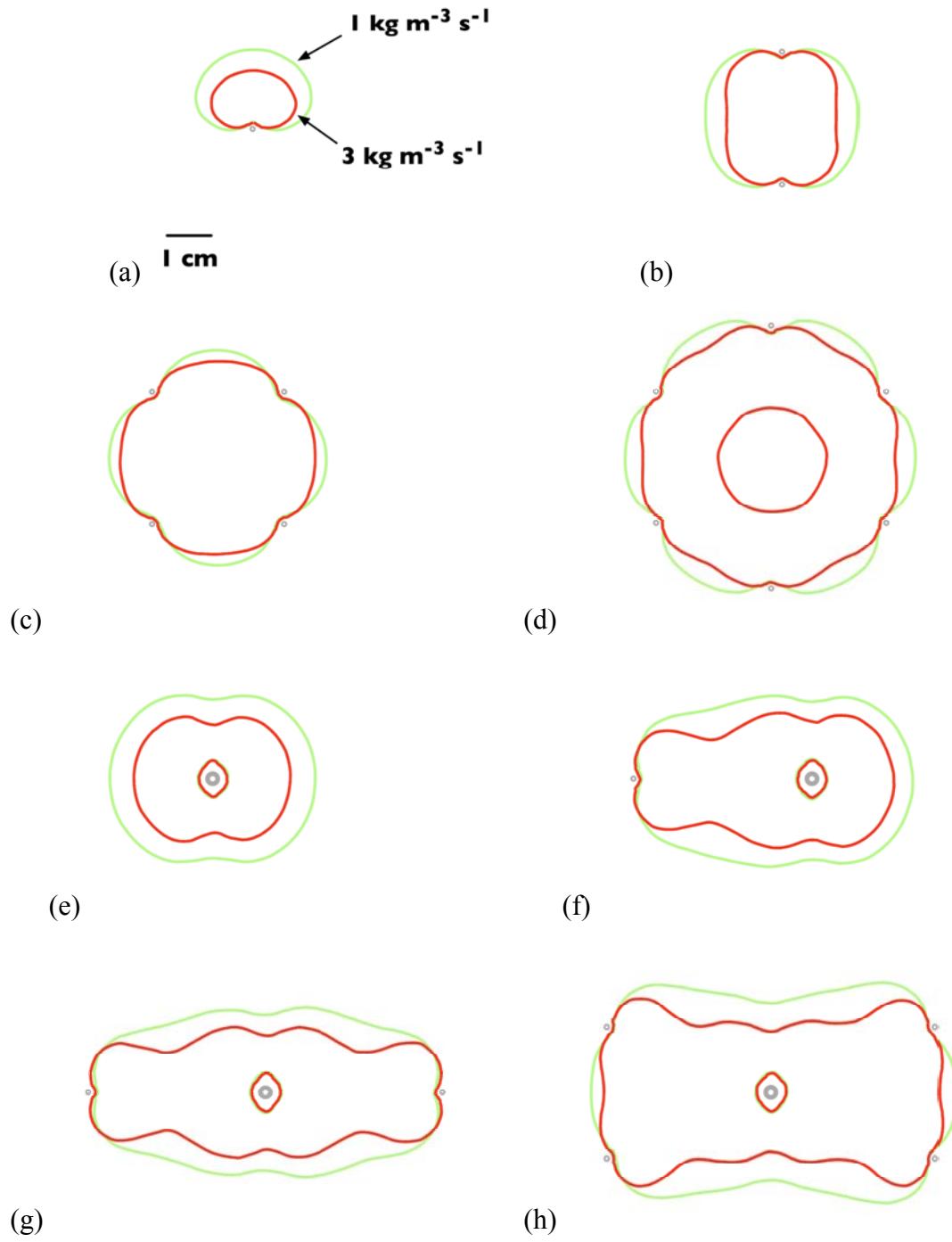


FIG. 4.2: Extent of  $41^{\circ}\text{C}$  contour shown for select implant geometries with directional interstitial and endocavity devices at  $3 \text{ kg m}^{-3} \text{ s}^{-1}$  or  $1 \text{ kg m}^{-3} \text{ s}^{-1}$  blood perfusion.



heated  $>41^{\circ}\text{C}$  over 9.4 cm in width. When  $180^{\circ}$  sector devices were employed, the tissue volume  $>41^{\circ}\text{C}$  for 1 – 6 interstitial devices was reduced to  $13 - 116 \text{ cm}^3$ . The heating pattern for directional devices was tightly controlled to the device spacing; 2 directional devices spaced at 3 cm (Fig. 4.1b) heated  $>41^{\circ}\text{C}$  over a height of 3.2 cm and 6 directional devices spaced at 3 cm (Fig. 4.1f) heated  $>41^{\circ}\text{C}$  over a width of 7.0 cm. At  $3 \text{ kg m}^{-3} \text{ s}^{-1}$  blood perfusion, tissue volumes  $>41^{\circ}\text{C}$  for unsector devices shrank to  $16 - 131 \text{ cm}^3$ , a single applicator heated  $>41^{\circ}\text{C}$  over a 2.6 cm diameter, and 6 devices heated  $>41^{\circ}\text{C}$  over a 8.6 cm width. For 1 – 6 sector devices at  $3 \text{ kg m}^{-3} \text{ s}^{-1}$  blood perfusion, the therapeutic heating volumes were  $7 - 76 \text{ cm}^3$ . As shown in Fig. 4.2, the temperature elevation between directional interstitial devices spaced at 3 cm were highly robust to perfusion changes (given increased power to reach the same  $T_{\text{max}}$ ); 2 directional devices heated  $>41^{\circ}\text{C}$  over 3.2 cm height at 1 and  $3 \text{ kg m}^{-3} \text{ s}^{-1}$  blood perfusion, while 6 directional devices in a rectangular configuration (Fig. 4.1f) heated  $>41^{\circ}\text{C}$  over a 6.8 cm width at  $3 \text{ kg m}^{-3} \text{ s}^{-1}$  perfusion and 7.0 cm at  $1 \text{ kg m}^{-3} \text{ s}^{-1}$  perfusion. An exception is the hexagonal implant configuration (Fig. 4.1g), in which a portion of tissue at the center of the implant fails to reach  $41^{\circ}\text{C}$  with sector or unsector devices at  $3 \text{ kg m}^{-3} \text{ s}^{-1}$ , given the imposed limit of  $T_{\text{max}} < 47^{\circ}\text{C}$ .

The endocavity tandem was able to heat larger volumes with a given  $T_{\text{max}}$  than the interstitial device, and interstitial devices could be strategically employed to augment the lateral thermal coverage. At  $1 \text{ kg m}^{-3} \text{ s}^{-1}$  blood perfusion, a 3-element, unsector tandem heated  $>41^{\circ}\text{C}$  over a 4.6 cm diameter and  $51 \text{ cm}^3$  volume compared to a 3-element interstitial, which heated  $>41^{\circ}\text{C}$  over a 3.6 cm diameter and  $31 \text{ cm}^3$  volume. At  $3 \text{ kg m}^{-3} \text{ s}^{-1}$  perfusion, the relative difference was greater, with the tandem heating  $>41^{\circ}\text{C}$  over a

3.8 cm diameter and 31 cm<sup>3</sup> volume and the interstitial heating >41°C over a 2.6 cm diameter and 16 cm<sup>3</sup> volume. The bi-sectored (2×180°) tandem applicator also heated >41°C to a maximum 4.6 cm diameter, but the 41°C contour was reduced to 3.8 cm in diameter due to the presence of the 30° acoustic dead zone between sectors. This reduced the tissue volume >41°C for a 3 element tandem device from 51 to 46 cm<sup>3</sup>. The tandem device allowed for large heating zones to be created with few applicators; using only 2 interstitial devices spaced at 4 cm laterally to an unsectored tandem (Fig. 4.1j), the 41°C contour is 11 cm in diameter and 141 cm<sup>3</sup> in volume. Using 4 interstitial applicators as in Fig. 4.1m, the tissue volume >41°C was increased only to 150 cm<sup>3</sup>. The heating zone can again be tightly controlled by using directional applicators; with a tandem and 2 interstitial devices (Fig. 4.1j), the width of the 41°C contour was 7.8 cm to an overall applicator spacing of 8 cm. Although large, tightly controlled heating volumes could be covered by using directional interstitial devices spaced at 4 cm from a tandem, some scalloping of heating volumes occurred at a higher perfusion of 3 kg m<sup>-3</sup> s<sup>-1</sup> (Fig. 4.2) and is particularly pronounced with unsectored devices in Fig. 4.1i-j. This can be mitigated by closer spacing or employing more devices for heating.

Power levels for maximal thermal coverage with  $T_{\max} = 47^{\circ}\text{C}$  varied with applicator type and implant configuration. As shown in Fig. 4.3, the power level for the 2×180° tandem to achieve maximal thermal coverage was nearly constant, ranging from 1.55 – 1.80 W cm<sup>-2</sup> at 1 kg m<sup>-3</sup> s<sup>-1</sup> perfusion and 2.22 – 2.37 W cm<sup>-2</sup> at 3 kg m<sup>-3</sup> s<sup>-1</sup> perfusion whether or not it was used with directional interstitial devices. This indicates that there was little coupling of the interstitial devices with the tandem in contributing to

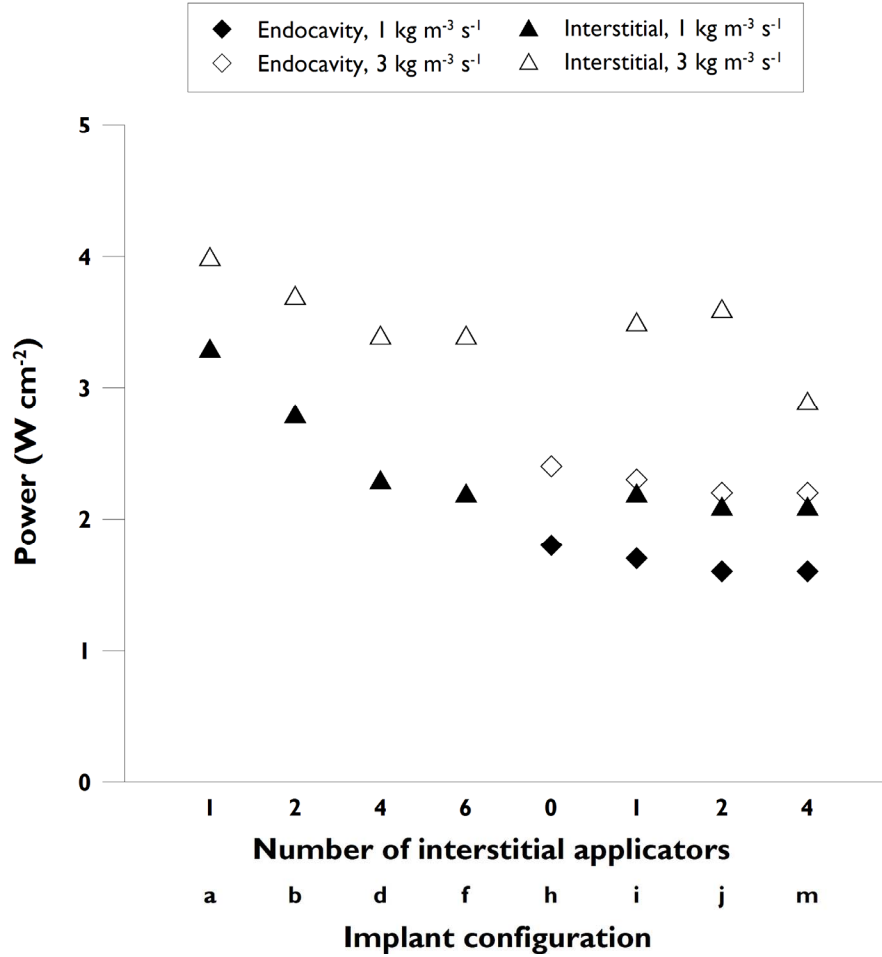


FIG. 4.3: Power values  $P_{\text{per1}}$  and  $P_{\text{per3}}$  used to produce maximal tissue volume  $> 41^\circ\text{C}$  for the regular implant geometries in Table 4.1.

the maximum temperature elevation. It also represented a nearly constant increase in power of 34 – 43% from 1 to 3 kg m<sup>-3</sup> s<sup>-1</sup> perfusion. The 180° interstitial devices, when used with the 2×180° tandem, had similar power levels (1.38 – 1.66 W cm<sup>-2</sup>) for maximum thermal coverage regardless of the number of devices used at 1 kg m<sup>-3</sup> s<sup>-1</sup>, but at 3 kg m<sup>-3</sup> s<sup>-1</sup> perfusion there was more variation in the power values, with power  $> 3.5$  W cm<sup>-2</sup> with 1 or 2 interstitial devices and  $< 3$  W cm<sup>-2</sup> with 4 interstitial devices. The

increase in power levels of 38 – 70% from 1 to 3 kg m<sup>-3</sup> s<sup>-1</sup> for the interstitial devices was more pronounced and variable than for the tandem. The interstitial devices, when used alone, required less power to achieve thermal coverage of larger volumes as the number of implanted devices increases, but there was a limit to the reduction in power that was observed. For directional devices at 1 kg m<sup>-3</sup> s<sup>-1</sup>, the average power levels for optimal thermal coverage decreased from 3.31 to 2.30 W cm<sup>-2</sup> from 1 to 4 applicators but only to 2.20 W cm<sup>-2</sup> for 6 applicators. At 3 kg m<sup>-3</sup> s<sup>-1</sup>, the power levels decreased from 3.95 to 3.41 W cm<sup>-2</sup> from 1 to 4 applicators but only to 3.35 W cm<sup>-2</sup> for 6 applicators. The relative difference between power levels at 3 and 1 kg m<sup>-3</sup> s<sup>-1</sup> increased with an increasing number of applicators, as well, with 19% higher power with 1 applicator, 30% higher power with 4 applicators, and 52% higher power with 6 applicators.

Perfusion that differs from the planned value had a prominent effect on temperature distributions in tissue (Table 4.2). If the planned power levels  $P_{\text{per}3}$  are used with 1 kg m<sup>-3</sup> s<sup>-1</sup> perfusion, the heating volumes increased from a range of 31 – 220 cm<sup>3</sup> to a range of 45 – 305 cm<sup>3</sup> (45 – 102% rise) compared to heating volumes using  $P_{\text{per}1}$ .  $T_{\text{max}}$  increased to 50.5 – 52.9°C, which would likely lead to thermal destruction of tissue [146-148]. The extent of over-heating increased with a greater number of interstitial devices;  $T_{\text{max}}$  was 50.5°C with 1 interstitial device alone, 51.6°C with 2 devices, and 52.8°C with 6 devices. This was due to the higher relative difference between optimal power levels  $P_{\text{per}3}$  and  $P_{\text{per}1}$  with an increasing number of devices.  $T_{\text{max}}$  was 51.7° for the tandem alone, 52.1°C for the tandem with 1 interstitial, and 52.6°C for the tandem with 4 interstitial. If power levels  $P_{\text{per}1}$  were used with 3 kg m<sup>-3</sup> s<sup>-1</sup> perfusion, the heating

TABLE 4.2: Tissue volumes  $>41^{\circ}\text{C}$  ( $\text{cm}^3$ ) with  $[T_{\text{max}} (^{\circ}\text{C})]$  for cases with regular implant spacing.  $T_{\text{max}} = 47^{\circ}\text{C}$  if unspecified.

Implant	Power values					
	$P_{\text{per1}}$	$P_{\text{per3}}$	$P_{\text{per3}}$	$P_{\text{per1}}$	$P_{\text{per1}}$	$P_{\text{per3}}$
	Perfusion ( $\text{kg m}^{-3} \text{ s}^{-1}$ )					
	1	1	3	3	1, Tompkins	3, Tompkins
a	31	45 [50.5]	16	10 [44.6]	29 [47.8]	14 [48.1]
b	65	101 [51.6]	38	19 [44.1]	65 [48.7]	33 [48.4]
d	138	208 [52.9]	90	40 [43.3]	162 [50.8]	88 [47.3]
f	200	305 [52.8]	138	45 [43.0]	224 [51.0]	128 [48.6]
h	51	82 [51.7]	31	18 [43.7]	50 [48.3]	32 [49.6]
i	81	138 [52.1]	50	19 [43.5]	73 [48.4]	46 [49.6]
j	141	208 [52.4]	77	37 [43.9]	143 [49.1]	70 [49.7]
m	150	303 [52.6]	124	16 [42.8]	147 [48.3]	124 [46.8]

volumes decreased from  $16 - 138 \text{ cm}^3$  to  $10 - 109 \text{ cm}^3$  ( $38 - 87\%$  decrease) compared to heating volumes using  $P_{\text{per3}}$ , there were gaps in temperature  $>41^{\circ}\text{C}$  between devices for all multi-applicator implant configurations, and  $T_{\text{max}}$  decreased to  $42.8 - 44.6^{\circ}\text{C}$ . Again, the extent of under-treatment scaled with the number of applicators due to an increasing relative difference in the power levels  $P_{\text{per1}}$  and  $P_{\text{per3}}$ , with a  $T_{\text{max}}$  of  $44.6^{\circ}\text{C}$  for 1 interstitial device,  $44.1^{\circ}\text{C}$  for 2 devices, and  $43.0^{\circ}\text{C}$  for 6 devices. When combined with the tandem, this relationship did not hold, with a  $T_{\text{max}}$  of  $43.7^{\circ}\text{C}$  for the tandem alone increasing to  $43.9^{\circ}\text{C}$  with 2 interstitial devices and decreasing to  $42.8^{\circ}\text{C}$  with 4 interstitial devices.

Spatial and temperature-based variations in perfusion had a wide ranging effect on thermal profiles. When the optimized power values  $P_{\text{per1}}$  were employed to heat a central 6 cm diameter tumor at a perfusion of  $3 \text{ kg m}^{-3} \text{ s}^{-1}$  with the surrounding tissue at  $1 \text{ kg m}^{-3} \text{ s}^{-1}$ , there were gaps in thermal coverage  $>41^{\circ}\text{C}$  between devices in multi-implant

configurations similar to homogeneous perfusion of  $3 \text{ kg m}^{-3} \text{ s}^{-1}$ , although heating volumes were  $10 - 109 \text{ cm}^3$  vs.  $10 - 45 \text{ cm}^3$  due to the extension of heating into the lower perfused tissue surrounding the tumor. Using power values  $P_{\text{per}3}$  to treat a central tumor at  $1 \text{ kg m}^{-3} \text{ s}^{-1}$  with the surrounding tissue at  $3 \text{ kg m}^{-3} \text{ s}^{-1}$  perfusion, the extent of overheating was similar to a homogeneous perfusion of  $1 \text{ kg m}^{-3} \text{ s}^{-1}$ , with  $T_{\text{max}} = 50.3^\circ\text{C} - 52.3^\circ\text{C}$  vs.  $50.5^\circ\text{C} - 52.9^\circ\text{C}$  for the homogeneous case, but with smaller heating volumes of  $42 - 194 \text{ cm}^3$  vs.  $45 - 305 \text{ cm}^3$  due to the reduction of thermal penetration into the surrounding tissue at higher perfusion. When perfusion was varied with temperature as per Tompkins [200],  $T_{\text{max}}$  exceeded  $47^\circ\text{C}$  with a base perfusion of both  $1$  and  $3 \text{ kg m}^{-3} \text{ s}^{-1}$  using optimized powers  $P_{\text{per}1}$  and  $P_{\text{per}3}$ , the extent to which varied greatly, with  $T_{\text{max}}$  ranging from  $47.3^\circ\text{C} - 51.0^\circ\text{C}$ . Despite the variation in  $T_{\text{max}}$ , the total heating volumes  $>41^\circ\text{C}$  were similar for the uniform perfusion and temperature-dependent perfusion cases; all heating volumes were within 17% of each other and most were within 3%.

#### 4.4.2 Patient-Specific Optimization

Control of energy delivery was tantamount to the ability to provide therapeutic thermal coverage of the CTV without excessive heating of the rectum and bladder. The use of sectorized interstitial and bi-sectorized endocervical devices allowed for increased temperature elevation in the CTV within the given temperature constraints for overall  $T_{\text{max}}$ ,  $T_{\text{rectum}}$ , and  $T_{\text{bladder}}$  in nearly all patients. The use of sectorized applicators to provide therapeutic coverage of clinical targets is demonstrated in Fig. 4.4. The bi-directional tandem can be used to extend heating laterally with the inter-sector acoustic dead zone oriented to limit temperature rise in the rectum and bladder posterior and anterior to the

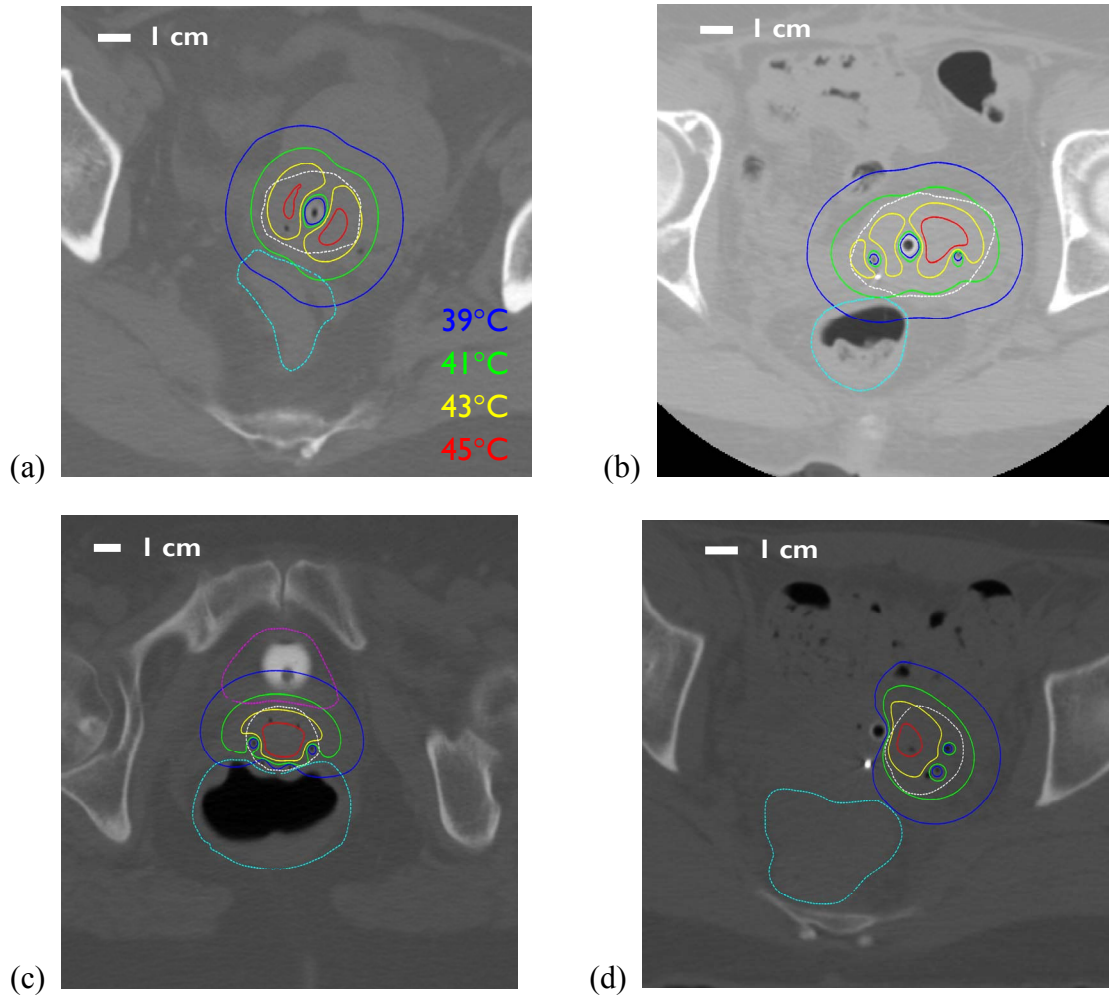


FIG. 4.4: Patient-specific optimization results demonstrating thermal coverage of clinical target volumes by (a) a single  $2 \times 180^\circ$  endocavity applicator using a dead zone to minimize rectal heating, (b) a  $2 \times 180^\circ$  endocavity applicator with two directional interstitial applicators to extend heating laterally, (c) four directional interstitial applicators treating a target in close proximity to the rectum and bladder, and (d) a  $180^\circ$  directional endocavity device with two unsectored interstitial applicators (Perfusion =  $1 \text{ kg m}^{-3} \text{ s}^{-1}$ ).

target (Fig. 4.4a,b) or to treat an eccentric target (Fig. 4.4d). Secteded interstitial devices can be used to extend lateral heating by the bi-directional tandem without increasing  $T_{\text{max}}$  (Fig. 4.4b) or, when in close proximity to organs at risk can direct energy into the target to protect these structures (Fig. 4.4c).

Thermal coverage as defined by  $T_{90}$  for all patients is shown in Fig. 4.5. At a perfusion of  $1 \text{ kg m}^{-3} \text{ s}^{-1}$ , the  $T_{90}$  ranged from  $40.3 - 42.7^\circ\text{C}$  and 10 out of 14 patients had  $T_{90} \geq 41^\circ\text{C}$ . An endocervical applicator was used in 10 out of 14 patients and in all cases a bi-directional ( $2 \times 180^\circ$ ) applicator resulted in improved  $T_{90}$  compared to a  $360^\circ$  applicator. 0 – 4 interstitial applicators with 1 – 3 elements and  $180^\circ$ ,  $270^\circ$ , or  $360^\circ$  directivity were employed with 11 out of 14 patients using at least 2 interstitial applicators. When a perfusion of  $3 \text{ kg m}^{-3} \text{ s}^{-1}$  was applied, the implant configuration unchanged, and power values re-optimized,  $T_{90}$  ranged from  $39.1 - 41.7^\circ\text{C}$  with 5 out of 14 patients above  $41^\circ\text{C}$  and 6 out of 14 patients at or below  $40^\circ\text{C}$ . In 8 patients, the implant configuration used at a perfusion of  $1 \text{ kg m}^{-3} \text{ s}^{-1}$  also resulted in the highest  $T_{90}$  at a perfusion of  $3 \text{ kg m}^{-3} \text{ s}^{-1}$  compared to other configurations tested. For these patients, the  $T_{90}$  at  $3 \text{ kg m}^{-3} \text{ s}^{-1}$  ranged from  $39.1 - 41.7^\circ\text{C}$  with 5 out of these 8 patients  $> 41^\circ\text{C}$ . For the other 6 patients, by changing the implant configuration from the configuration used at a perfusion of  $1 \text{ kg m}^{-3} \text{ s}^{-1}$ , the  $T_{90}$  was improved by  $0.4 - 1.0^\circ\text{C}$  from  $39.2 - 40.7^\circ\text{C}$  to  $39.6 - 40.9^\circ\text{C}$  at  $3 \text{ kg m}^{-3} \text{ s}^{-1}$  perfusion.

Even when the implant configuration did not change, the nature of the heating pattern did change, and the limiting factor in heating differed from 1 to  $3 \text{ kg m}^{-3} \text{ s}^{-1}$  perfusion (Table 4.3). Violation of the  $T_{\text{max}}$  constraint limited the ability to heat for 3 patients at  $1 \text{ kg m}^{-3} \text{ s}^{-1}$  and 5 patients at  $3 \text{ kg m}^{-3} \text{ s}^{-1}$ . The  $T_{\text{rectum}}$  constraint limited the ability to heat the CTV in 3 patients at  $1 \text{ kg m}^{-3} \text{ s}^{-1}$  perfusion and in 0 patients at  $3 \text{ kg m}^{-3} \text{ s}^{-1}$ . The  $T_{\text{bladder}}$  constraint limited the ability to heat in 2 patients at both 1 and  $3 \text{ kg m}^{-3} \text{ s}^{-1}$ . The  $T_{\text{max}}$  increased or remained nearly unchanged in all of these patients from 1 to  $3 \text{ kg m}^{-3} \text{ s}^{-1}$ .



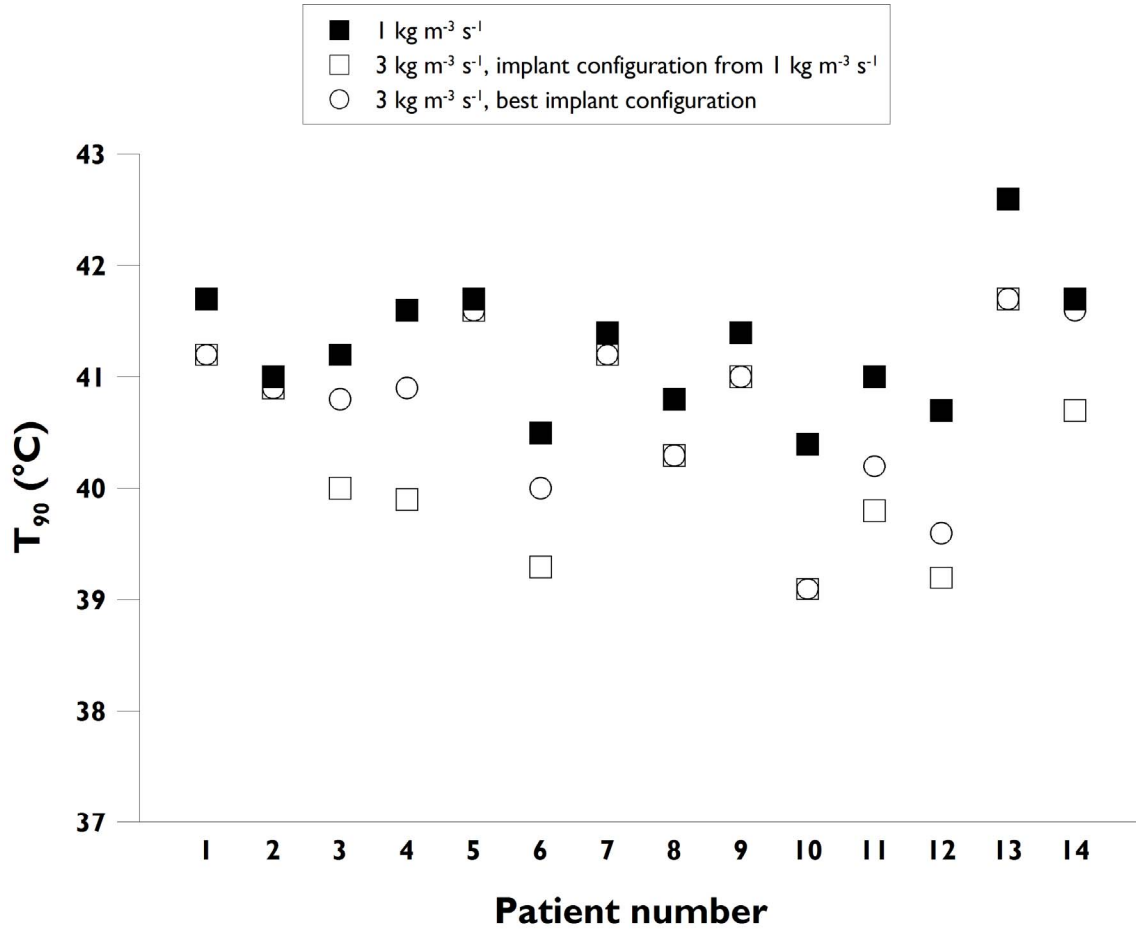


FIG. 4.5:  $T_{90}$  values for all patient cases considered for temperature-based optimization. The optimal result at  $1 \text{ kg m}^{-3} \text{ s}^{-1}$  is compared to the same configuration optimized at  $3 \text{ kg m}^{-3} \text{ s}^{-1}$  along with the configuration that resulted in the highest  $T_{90}$ .

For the patients in which no change in implant configuration was necessary to optimally deliver heating at a higher perfusion level, only the power of the devices needs to be increased; a comparison of power values used to produce plans for these patients is made in Fig. 4.6. At  $1 \text{ kg m}^{-3} \text{ s}^{-1}$  perfusion, power levels for the endocavity applicator ranged from  $1.09 - 1.55 \text{ W cm}^{-2}$  and at  $3 \text{ kg m}^{-3} \text{ s}^{-1}$  from  $1.47 - 2.26 \text{ W cm}^{-2}$ . For 4 out of

TABLE 4.3: Thermal descriptors for the 8 patients with the same implant configuration at 1 and 3 kg m<sup>-3</sup> s<sup>-1</sup> perfusion. Thermal dose values from transient simulations for patients 5, 7, and 8 are shown as (EM43°C).

Pt #	Interstitial directivity (°)	CTV (cm <sup>3</sup> )	T <sub>90</sub> (°C)		T <sub>max</sub> (°C)		T <sub>rectum</sub> (°C)		T <sub>bladder</sub> (°C)	
			Perfusion (kg m <sup>-3</sup> s <sup>-1</sup> )		1	3	1	3	1	3
			1	3						
1		13.0	41.7	41.2	45.9	47.1	41.6	40.6	41.9	40.7
2	180, 180	23.4	41.0	40.9	45.3	46.5	41.2	40.4	42.5	42.5
5	360, 360, 360	16.3	41.7 (10.0)	41.6	45.4	47.1	41.6	41.3	41.3	37
7	270, 270, 360	23.7	41.4 (7.8)	41.2	44.5	46.2	41.1	40.2	42.5	42.6
8	180, 180	16.3	40.8 (2.6)	40.3	45.4	47.0	41.5	40.9	42.2	42.0
9	270, 180, 180, 270	10.1	41.3	41.0	47.1	47.0	40.9	41.2	42.0	40.3
10	360, 270, 270, 360	58.0	40.4	39.1	47.0	47.1	41.2	40.3	39.2	37.9
13	360, 360, 270	6.3	42.6	41.7	47.1	47.1	37.8	37.3	42.2	40.8

5 of these patients the power scaled very closely from 1 to 3 kg m<sup>-3</sup> s<sup>-1</sup> perfusion, with a 43 – 47% increase. Patient 9 had only a 17% increase in power from 1 to 3 kg m<sup>-3</sup> s<sup>-1</sup>. There was more variation in the power scaling of the interstitial devices, with applied powers of 1.16 – 2.00 W cm<sup>-2</sup> at 1 kg m<sup>-3</sup> s<sup>-1</sup> perfusion and 1.56 – 2.59 W cm<sup>-2</sup> at 3 kg m<sup>-3</sup> s<sup>-1</sup> perfusion, for a 22 – 71% power increase from 1 to 3 kg m<sup>-3</sup> s<sup>-1</sup> perfusion. Within patients, the power levels of interstitial devices differed by up to 0.7 W cm<sup>-2</sup>.

Transient thermal simulation with 10-15 minute power ramp and 75 minute total simulation time produced thermal dose accumulation in the target similar to dose that would be accrued after an hour at steady state temperature values. As shown in Table 4.3

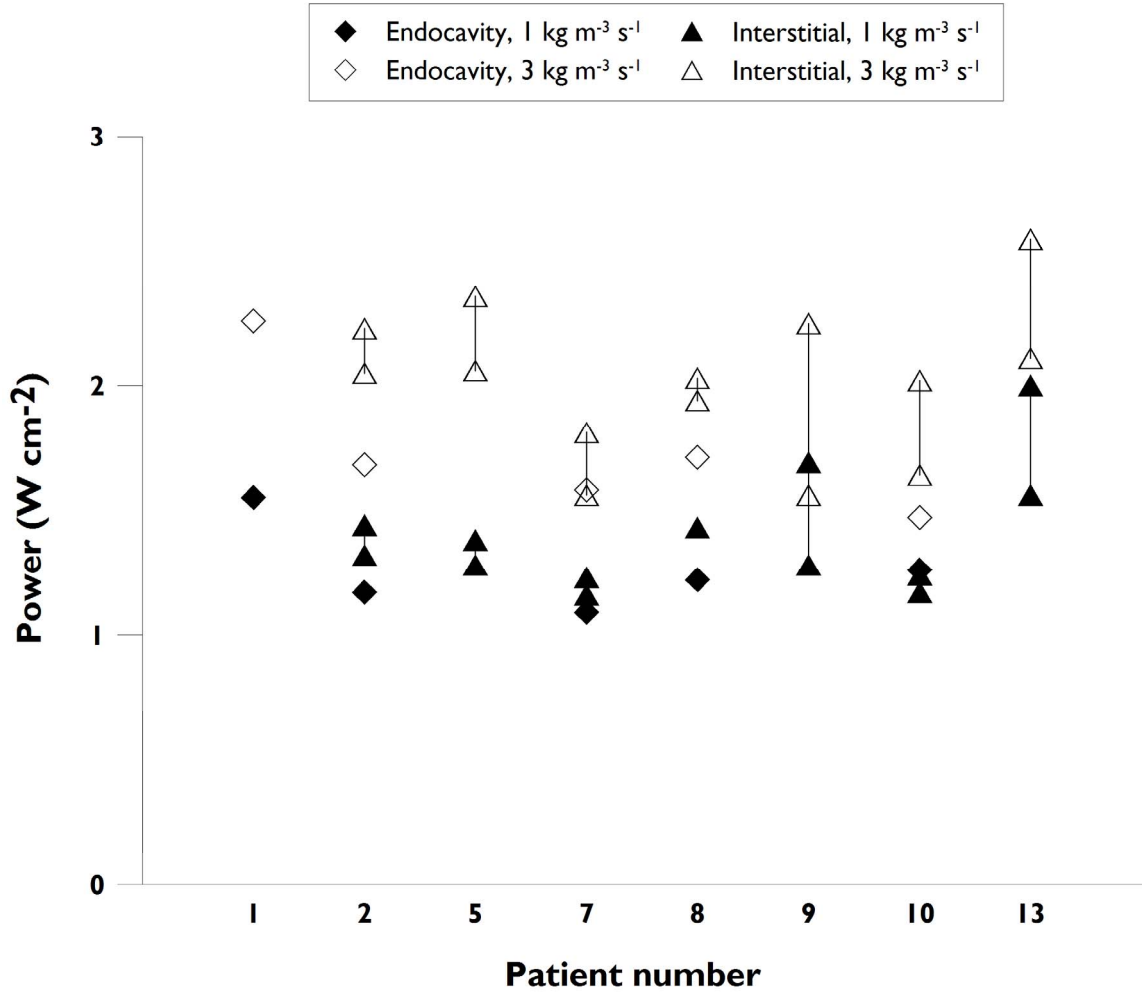


FIG. 4.6: Power values used to create optimal treatment plans in those patients in which the optimal implant configuration at  $3 \text{ kg m}^{-3} \text{ s}^{-1}$  was the same as the optimal configuration at  $1 \text{ kg m}^{-3} \text{ s}^{-1}$ . The range in power values for interstitial devices is indicated by the symbols  $\Delta$  and  $\blacktriangle$  connected with lines.

for 3 patients, the thermal dose exceeded by 90% of points within the CTV was 10.0  $\text{EM}_{43^\circ\text{C}}$  for patient 5, 7.8  $\text{EM}_{43^\circ\text{C}}$  for patient 7, and 2.6  $\text{EM}_{43^\circ\text{C}}$  for patient 8. The thermal dose values for 1 hour at the  $T_{90}$  values for these patients were 9.9  $\text{EM}_{43^\circ\text{C}}$  for patient 5, 6.5  $\text{EM}_{43^\circ\text{C}}$  for patient 7, and 2.8  $\text{EM}_{43^\circ\text{C}}$  for patient 8.

## 4.5 Discussion

Catheter-based ultrasound devices have the ability to create highly conformal heating patterns by controlling thermal delivery in angle and along their length. In combination, they have potential to extend the volume of therapeutic heating over an individual device and compensate for gaps in heating due to sectoring used to create directional energy delivery. The influence of devices on each other and overall heating patterns depends on device spacing, orientation, and the tissue environment in which they are placed. Heating patterns are relatively straightforward for a regularly spaced, parallel implant, but are influenced by tissue properties, particularly blood perfusion, which can vary within the tumor and with temperature. In clinical hyperthermia treatments, it is desirable to employ pre-existing catheter locations used in HDR brachytherapy for thermal delivery in order to avoid increased morbidity from the introduction of additional catheters. The ability of multiple ultrasound devices to heat a patient target volume may be compromised by catheter placement that is irregularly spaced and non-parallel. Therapeutic heating of clinical targets is further limited by a desire to limit maximum temperature elevation and temperature in the rectum and bladder in order to avoid thermal toxicity. The main objective of this work was to investigate the performance of catheter-based ultrasound devices placed in HDR brachytherapy catheters in providing therapeutic heating of cervical tumors. Temperature-based optimization was used to determine power levels that achieve the highest possible thermal coverage of clinical targets from patients while satisfying temperature constraints based on limiting toxicity. Regularly spaced implants were analyzed to characterize heating volumes that may be

achieved using a template for catheter introduction and identify the extent of the perfusion effect.

Blood perfusion in tissue is difficult to predict and hard to measure. Variations in both the spatial and temporal distributions in blood perfusion were tested to assess effects on temperature profiles created. Deviation in perfusion from the level used for power optimization caused overheating of the target volume with  $T_{\max} = 50 - 52^{\circ}\text{C}$  or underheating with  $T_{\max} = 43 - 44^{\circ}\text{C}$ . Temperature distributions that are more robust to perfusion changes were created by using directional applicators in tight configurations with  $<4$  cm spacing between devices (Fig. 4.2). The hexagonal implant configuration in Fig. 4.1g produced large therapeutic heating volumes at low perfusion but is not robust to perfusion changes. Implant configurations with a greater number of devices had a greater chance for over- or underheating with perfusion levels that differ from what is planned, as evident in Table 4.1, and care must be taken in these cases to carefully select power values. Clinical hyperthermia delivery will require thermal monitoring to truly assess how perfusion is affecting temperature distributions and guide power control. Safety would dictate that power levels are planned for a low perfusion level and increased if insufficient temperature elevation is achieved in the target. With more devices, power levels may start lower but need to be increased by a greater relative amount, as evidenced in Fig. 4.3. The endocavity device will likely deliver  $2 - 3 \text{ W cm}^{-2}$  while the interstitial devices may require a much larger range of power values depending on spacing and sectoring (Fig. 4.3, Fig. 4.6).

Control over heating distributions is tantamount to the successful delivery of hyperthermia in the cervix, based on the 14 patients analyzed. In many cases the rectum

and bladder were in close proximity to the target volume ( $<5$  mm) and  $<10$  mm from catheters, requiring precise control (another word) of temperature gradients to target the CTV without overheating the rectum and bladder. This was afforded by the use of  $180^\circ$  or  $270^\circ$  interstitial devices aimed away from organs at risk (Fig. 4.4b,c) as well as a bi-sectored endocervical device with dead zones oriented to be aligned with rectum and bladder (Fig. 4.4a). Sector devices can also be used to extend the therapeutic heating volume over cases in which  $360^\circ$  devices would couple heating to create a high  $T_{\max}$ . This is demonstrated in Fig. 4.4b, in which a sector device is aimed left to extend therapeutic heating without coupling with the endocervical bi-sectored device aimed in the same direction to elevate the  $T_{\max}$ .

Large volumes of tissue can be heated by catheter-based ultrasound devices in regular implant configurations in homogeneous uterine tissue. The  $41^\circ\text{C}$  cloud was extended up to  $220\text{ cm}^3$  with 6 interstitial devices at  $1\text{ kg m}^{-3}\text{ s}^{-1}$  perfusion and  $138\text{ cm}^3$  at  $3\text{ kg m}^{-3}\text{ s}^{-1}$  perfusion. Despite the ability to easily treat targets  $>100\text{ cm}^3$ , some CTV in patients of  $20 - 60\text{ cm}^3$  were difficult to cover with therapeutic heating. This is due to both the inability to fully heat targets without overheating organs at risk, and to applicator spacing that is far from ideal for catheter-based hyperthermia delivery. Patient 8 (Table 4.2), in which a  $T_{90}$  of  $40.8^\circ\text{C}$  was obtained (at  $1\text{ kg m}^{-3}\text{ s}^{-1}$  perfusion), an endocervical applicator was employed for heating along with 2 interstitial directional applicators. In this case, the CTV was in close proximity to bladder and rectum and the interstitial applicators were  $<1$  cm from the endocervical device (Fig. 4.7). Heating of the entire CTV was limited by either overheating of the rectum ( $1\text{ kg m}^{-3}\text{ s}^{-1}$ ) or high temperature from device coupling ( $3\text{ kg m}^{-3}\text{ s}^{-1}$ ). Applicator spacing  $<1$  cm makes it difficult to

increase the volume of therapeutic heating due to coupling of both cooling and device heating at relatively low powers. For patient 10 (Table 4.2), in which a  $T_{90}$  of 40.4°C was obtained at 1 kg m<sup>-3</sup> s<sup>-1</sup> and 39.1°C at 3 kg m<sup>-3</sup> s<sup>-1</sup>, even with  $T_{max}$  at 47.0°C, an endocervical applicator was used in addition to 4 directional interstitial applicators, but all of these were located in the posterior portion of the cervix and limited the ability to provide therapeutic heating in the anterior portion of the cervix (Fig. 4.7). Heating can be coupled between applicators that are non-parallel due to the ability to control energy delivery by each element along the length of the ultrasound device, an advantage of ultrasound over RF heating modalities. When applicators come within 10 mm of each other as in Patient 8, however, it becomes difficult to increase the volume of therapeutic heating due to coupling of cooling and high temperatures obtained between devices at relatively low power. When applicators are not spaced throughout the target volume as in Patient 10, a high  $T_{90}$  is difficult to achieve, especially with high blood perfusion.

Although the majority of patients analyzed could be treated with the same implant configuration at a perfusion of 1 and 3 kg m<sup>-3</sup> s<sup>-1</sup>, 6 patients required some modification of the implant in going from 1 to 3 kg m<sup>-3</sup> s<sup>-1</sup> perfusion. In 3 of the 6 patients, coverage could be improved simply by changing the aiming direction of 1 or 2 applicators. Therefore, 11 of the 14 patients could be treated with the same applicators in place at 1 and 3 kg m<sup>-3</sup> s<sup>-1</sup>. In the remaining 3 patients, coverage could be improved by slightly changing the sectoring of 1 or 2 interstitial applicators. In one patient a 360° applicator was replaced with a 270°, in another a 270° replaced with a 180°, and in a third two 180° devices were replaced with 270° devices. All patients were able to be treated with the

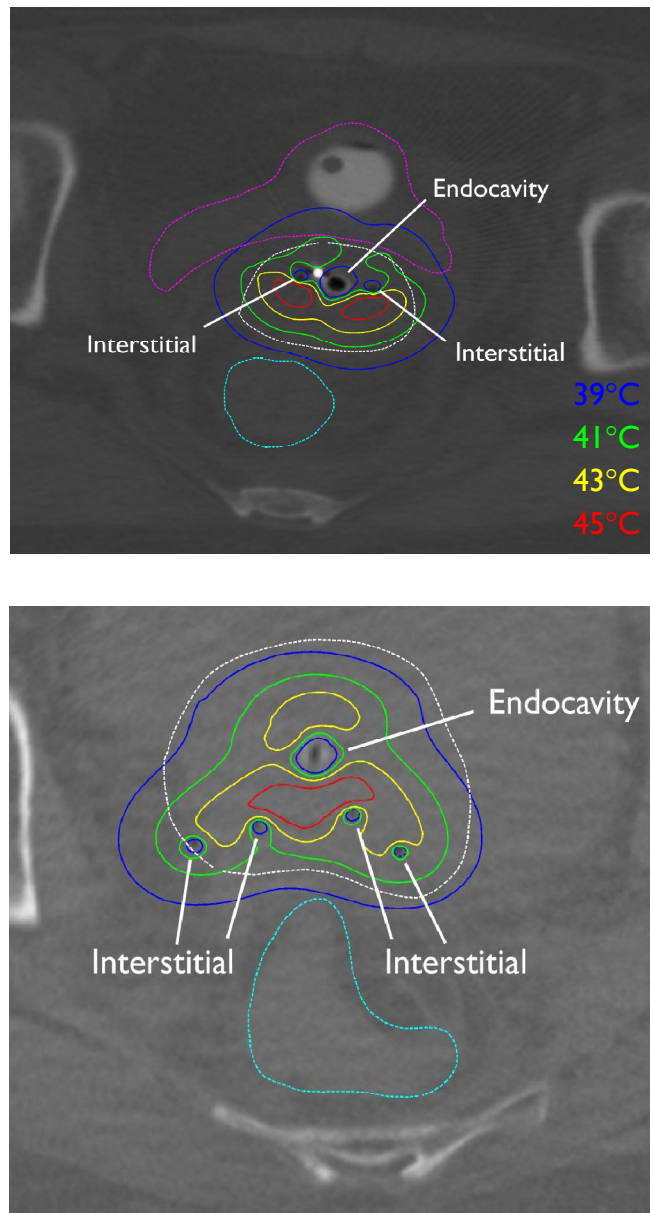


FIG. 4.7: Limitations in the ability to heat throughout clinical target volumes are presented by (a) coupling of cooling and maximum temperature elevation by closely spaced applicators or (b) by catheters that are not placed throughout the target volume.

same types of applicators in the same positions at both perfusion levels tested, with slight changes in aiming or sectoring to improve coverage. This shows promise for being able



to optimize at a low perfusion and use thermal feedback to increase power or aiming as necessary to improve thermal delivery. Sectored applicators can be rotated during treatment if necessary to increase thermal dose deposition to areas that may not be well heated.

## 4.6 Conclusions

The heating capabilities of catheter-based ultrasound devices were investigated in regularly spaced implants and HDR brachytherapy implants in patients treated for locally advanced cervical cancer using a thermal treatment planning model. The influence of different blood perfusion levels along with changes in blood perfusion were considered in their effects on temperature profiles. Two types of applicators were used in thermal simulations: small interstitial devices directly implanted in tissue and a larger endocavity device. Volumes of tissue  $>41^{\circ}\text{C}$  up to  $51\text{ cm}^3$  with the endocavity device and  $31 - 220\text{ cm}^3$  with  $1 - 6$  interstitial devices at  $3\text{ cm}$  separation could be heated. If assumed perfusion levels of  $1$  and  $3\text{ kg m}^{-3}\text{ s}^{-1}$  are switched from the planned value for regularly spaced implants,  $T_{\text{max}}$  up to  $53^{\circ}\text{C}$  and down to  $43^{\circ}\text{C}$  can occur, and  $T_{\text{max}}$  up to  $51^{\circ}\text{C}$  in the temperature-dependent perfusion model; thermal feedback in clinical treatments would be necessary to compensate for unexpected changes in perfusion levels. Patient cases provided a number of difficulties to achieving adequate thermal coverage of clinical target volumes, including highly irregular applicator spacing and close proximity of organs at risk to the target volume, but  $T_{90}$  values of  $40.3 - 42.7^{\circ}\text{C}$  were achieved at  $1\text{ kg m}^{-3}\text{ s}^{-1}$ , and 10 out of 14 patients with  $T_{90} \geq 41^{\circ}\text{C}$ .  $T_{90}$  values decreased to  $39.1 - 41.7^{\circ}\text{C}$  at a higher perfusion of  $3\text{ kg m}^{-3}\text{ s}^{-1}$  due to the inability of irregularly spaced applicators

to achieve thermal penetration throughout the CTV, although thermal coverage will be higher for the hypoxic tumor core within the CTV. Sectored applicators are used in nearly all patients to control heating to the target boundary without overheating of rectum and bladder. Catheter-based ultrasound hyperthermia provides locally delivered, 3-D conformal heating as a feasible option for thermal treatment of locally advanced cervical carcinoma, and thermal delivery can be improved by implanting catheters spaced 15 – 30 mm apart and throughout the target volume.

**Part II**

**Experimental Device Design,  
Performance Characterization and  
Clinical Feasibility**

## **Chapter 5**

# **An endocervical ultrasound applicator for integrated hyperthermia and HDR brachytherapy in the treatment of locally advanced cervical carcinoma**

### **5.1 Abstract**

The clinical success of hyperthermia adjunct to radiotherapy depends on adequate temperature elevation in the tumor with minimal temperature rise in organs at risk. Existing technologies for thermal treatment of the cervix have limited spatial control or rapid energy falloff. An endocervical applicator was developed that uses a linear array of multi-sectored tubular ultrasound transducers to provide 3-D conformal, locally targeted hyperthermia concomitant to radiotherapy in the cervix. The catheter-based device is

integrated within a HDR brachytherapy applicator to facilitate sequential and potentially simultaneous heat and radiation delivery. A family of applicators was fabricated with 1 – 3 tubular transducers operating at 6.6 – 7.4 MHz that are unsectored ( $360^\circ$ ), bi-sectored ( $2 \times 180^\circ$ ), or tri-sectored ( $3 \times 120^\circ$  or  $135^\circ \times 135^\circ \times 90^\circ$ ) for control of energy deposition in angle and along the device length. The device is housed in a 6 mm diameter PET catheter with cooling water flow for endocervical implantation. Acoustic output was characterized by measuring acoustic efficiencies and rotational acoustic intensity distributions. Thermal output was assessed by measuring rotational temperature distributions using benchtop thermometry and MR temperature imaging. Imaging artifacts were moderate with CT and minimal with MRI. The potential for simultaneous heat and radiation delivery was assessed by measuring radiation transmittance through the device, demonstrating a 4 – 6% radiation attenuation. Devices have acoustic output that is well collimated in length, reflects the sectoring strategy, and is strongly correlated with temperature distributions. Power control along the device length and in angle is demonstrated under MR temperature guidance. Dead zones can be oriented for thermal protection of the rectum and bladder. Theoretical simulation (Chapters 3 & 4) and experimental analysis point to the feasibility of the endocervical ultrasound device for clinical implementation in delivering 3-D conformal hyperthermia as an adjunct to HDR brachytherapy in the treatment of locally advanced cervical carcinoma.

The work in this paper represents part of a published paper (J. H. Wootton, I.-C. J. Hsu, C. Diederich. An endocervical ultrasound applicator for integrated hyperthermia and HDR brachytherapy in the treatment of locally advanced cervical carcinoma. *Med Phys*, 37(12), 2010 (in press)) and conference proceedings article (J. H. Wootton, T. Juang, J.

Pouliot, I.-C. J. Hsu, C. Diederich. An intrauterine ultrasound applicator for targeted delivery of thermal therapy in conjunction with HDR brachytherapy to the cervix. *Proc. SPIE*, 7181, 1-9, 2009).

## 5.2 Introduction

The efficacy of thermal therapy depends on the delivery of targeted heating in close spatial and temporal sequence with conformal radiotherapy, while toxicity depends on the extent of heating in non-targeted tissue. Thermal dose delivery has been positively correlated to tumor response, with cumulative thermal dose thresholds of 6 – 10 equivalent minutes at 43°C ( $EM_{43^{\circ}C}$ ) required for hyperthermia to exhibit significant therapeutic enhancement [51, 52, 188, 189]. Inadequate heating techniques resulting in low thermal dose delivery to tumors have been a primary reason for studies failing to demonstrate a clinical benefit of adjunct hyperthermia [48-50].

Treatment monitoring is central to verifying that adequate thermal dose is delivered to the tumor and organs at risk have minimal thermal dose accumulation. Verification of applicator positioning is the first step towards proper thermal delivery, and a catheter-based hyperthermia applicators should be compatible with CT and MRI used for HDR brachytherapy treatment planning. Temperature monitoring during therapy is critical for feedback power control to guide treatment, especially in the face of blood perfusion that may change during the course of therapy [201-203]. Adaption of interstitial catheters for thermometry represents a straightforward method for thermal monitoring. MRI can also be used to assess temperature distributions with  $<1^{\circ}C$

accuracy [18], and compatibility with MRI affords the possibility of non-invasive, 3-D temperature measurement during administration of hyperthermia.

The objective of this work was to develop and characterize an endocervical ultrasound applicator that is catheter-based, compatible with standard imaging techniques, and capable of 3-D conformable hyperthermia delivery adjunct to HDR brachytherapy. This device, shown in concept in Fig. 5., consists of a linear array of tubular transducers to provide power control along the device length, with each transducer divided into acoustically isolated sectors to control energy output in angle. The device is integrated within the endocavity catheter of a HDR brachytherapy delivery applicator for minimally invasive, locally delivered heating targeted to the region surrounding the cervix. The endocervical ultrasound device was developed through a consideration of clinical target volumes, extensive theoretical analysis, and experimental characterization. Theoretical investigations into the design, and analysis of temperature distributions produced by the device is presented in Chapters 3 & 4. Details of device fabrication are presented in this chapter along with expected device performance based on imaging, measurement of acoustic output, and assessment of heating patterns. The potential for simultaneous thermoradiotherapy is explored by measuring radiation attenuation through the ultrasound device.

## **5.3 Methods**

### **5.3.1 Applicator Fabrication**

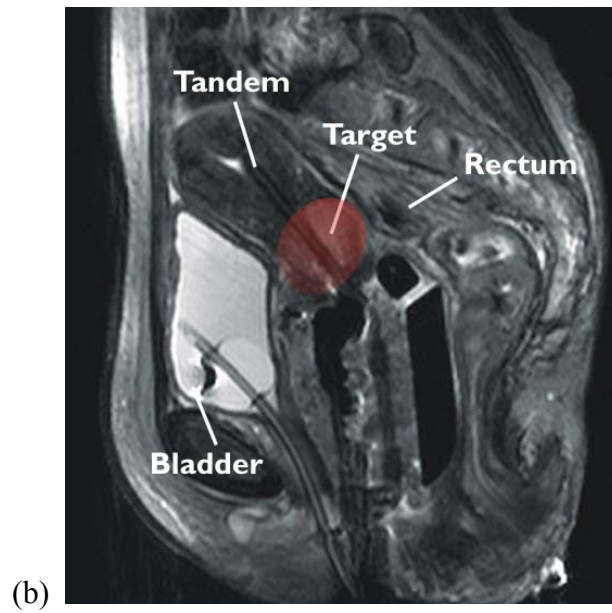
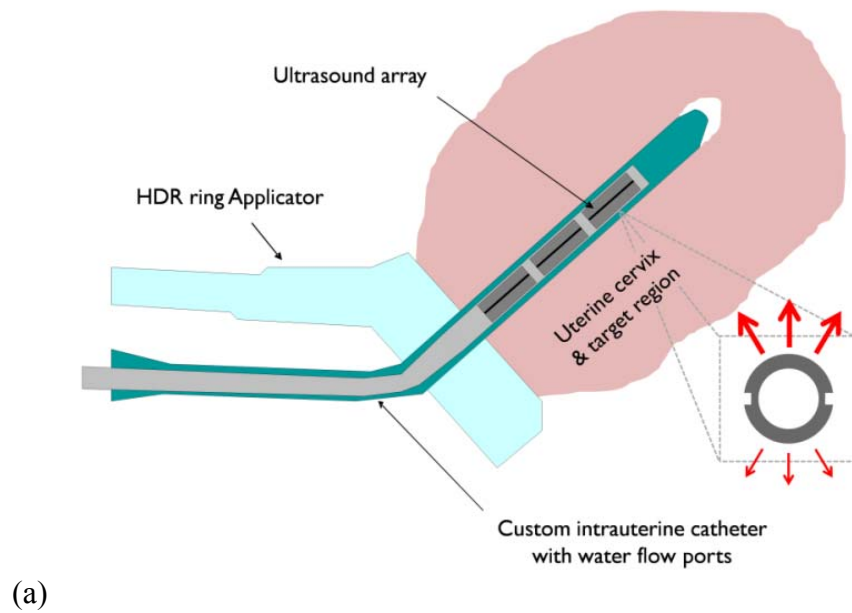


FIG. 5.1: (a) Drawing of endocervical ultrasound applicator integrated within HDR brachytherapy tandem and ring catheter. 3-D conformal hyperthermia is delivered locally to the uterine cervix by a linear array of multi-sectored transducers with differential power control to sectors and transducers. (b) Sagittal MR image of brachytherapy implant showing the position of the endocervical tandem with respect to cervical target, rectum and bladder.



A family of ultrasound applicators was constructed based on input from biothermal simulations. These devices have 2 – 3 tubular transducers (PZT-4, Boston Piezo Optics) that are 3.5 mm in diameter, 10 mm in length, and operate within a 6.5 – 8 MHz range. Uncut tubes are employed along with tubes that have been cut through one-half wall thickness into 2 sectors of  $180^\circ$  ( $2 \times 180^\circ$ ) or 3 sectors of  $120^\circ$  ( $3 \times 120^\circ$ ) using an automatic dicing saw (Disco Corporation). In order to control the size of the dead zone in acoustic output between sectors, tubes are sectorized using either a single cut or two adjacent cuts with 0.1 – 0.2 mm separation. A polyimide tube (1.47 mm OD, Small Parts) at the center of the applicator conducts cooling water flow and acts as a base for mounting the tubular elements. Transducers are mounted on this polyimide tube over smaller polyimide tubes (0.7 mm OD, Cole-Parmer) and secured in place with silicone (NuSil Technology) at the transducer edges to maintain air-backing. Transducer sectors are individually wired with coaxial cable (0.5 mm OD, Temp-Flex Cable) that runs to Redel RF power connectors (Lemo S.A.) at the back end. The transducer assembly is covered with a thin layer of epoxy (310M, Epoxy Technology) and polyester heat shrink (4.8 mm OD, Advanced Polymers). An outer polyimide tubing layer (3.4 mm OD, Professional Plastics) protects the cables and provides structure.

The ultrasound applicators are housed within a custom catheter modeled after an endocervical brachytherapy tandem. The PET catheters (Advanced Polymers) have a 6 mm OD with 0.25 – 0.50 mm wall and are formed with a  $30^\circ$  angle at the distal portion to accommodate the inflection from the vagina to the uterine cavity. Annular water flow couples acoustic energy between the transducers and catheter and cools the catheter surface. The back end of the catheter has a hemostasis valve (Qosina Corporation) for

applicator insertion, positioning in length and angle, and sealing cooling flow. The PET catheter can replace the endocervical tandem portion of the same diameter in the HDR brachytherapy applicator (Nuceltron, Inc.) and can be used for brachytherapy delivery. The fabricated endocervical ultrasound device is shown in Fig. 5..

### **5.3.2 Acoustic Characterization**

Acoustic characterization of endocervical ultrasound applicators consisted of measuring 1) the frequency of peak electrical impedance magnitude for bare tubes, 2) acoustic efficiencies of transducers and transducer sectors on completed applicators, 3) rotational acoustic intensity profiles, and 4) optical displacement

Electrical impedance was determined for unmodified tubes over a 5 – 10 MHz frequency range using a Network Analyzer (HP 3577A, Hewlett-Packard) and the frequency corresponding to peak electrical impedance was measured. Acoustic efficiencies for all tubes and sectors mounted on fabricated applicators were determined using a radiation force balance method adapted for cylindrical transducers [204], in which the device is centered within a brass acoustic reflector with a conical inner surface to direct acoustic waves towards an absorptive rubber target suspended from an electronic balance (Mettler AE200-S, Mettler Instrument Corp.). A function generator (Wavetek 273, Wavetek Corp.) with RF Amplifier (ENI 2100L, Electronic Navigation Industries) was used to apply 3 W electrical power to all transducer sectors. Input electrical power to the device was measured with a power meter (HP 438A, Hewlett-Packard). Acoustic efficiency measurements were first acquired over a 0.6 MHz frequency range with 0.1

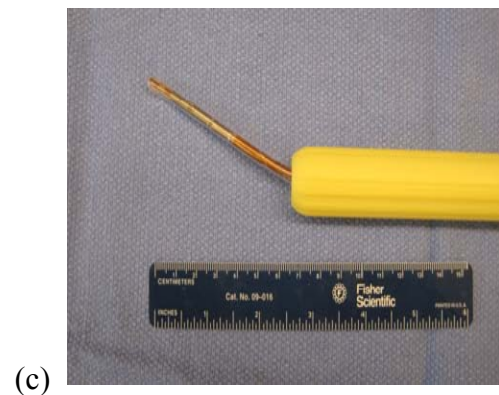
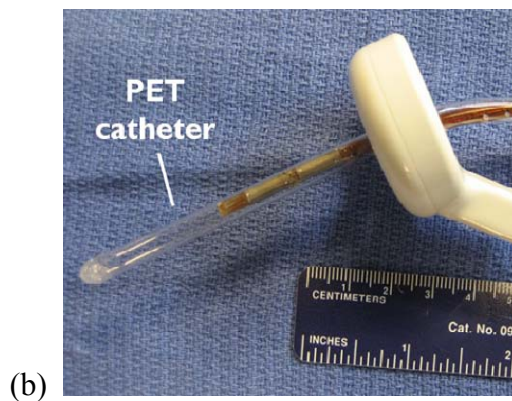
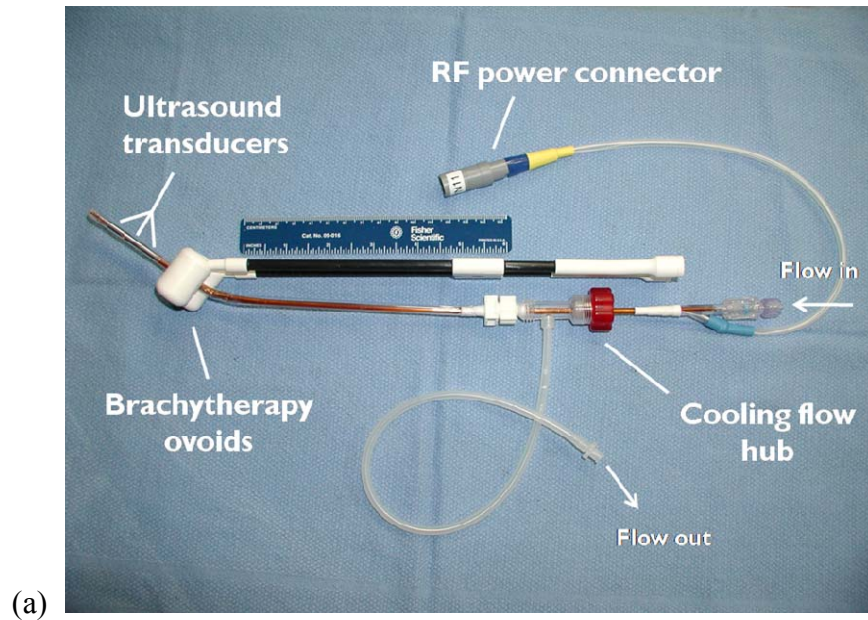


FIG. 5.2: Endocervical ultrasound device integrated within HDR brachytherapy delivery applicators (Nucletron, Inc.). The device is housed in a tipped PET catheter bent at  $30^\circ$  that replaces the endocervical tandem of the brachytherapy applicator. (a) A 3-element tandem and ovoid device with power connector and integrated cooling flow. (b,c) 2-element tandem and ring and 3-element vaginal cylinder devices.

MHz step, centered on the peak frequency determined from the network analyzer, and then over 0.3 MHz within this range in 0.05 MHz intervals. Three measurements were acquired at each frequency, with 0.1 – 0.3% standard error.

Rotational acoustic intensity profiles of endocervical applicators were measured in deionized, degassed water with a hydrophone scanned under motor control [122]. A needle-type hydrophone (Onda HNP-0400, Onda Corp.) was positioned at 8 mm from the device surface with a stepping motor system (XSlide, Velmex Inc.) that moved the hydrophone along the length of the transducers while the applicator was successively rotated by a rotational motor (B5990TS Rotary Table, Velmex Inc.). All motors were under computer control. Plots were obtained over  $360^\circ$  in rotation with  $2^\circ$  angular step size and 0.25 mm step size along the applicator length. The hydrophone signal was read on an oscilloscope (HP 54600A, Hewlett-Packard). A function generator (Wavetek 273, Wavetek Corp.) was used to trigger the amplifiers powering the transducer elements (500-009 RF Generators, Advanced Surgical Systems, Inc.) with a 50% duty cycle at 200 Hz. The oscilloscope window was adjusted to display only the acoustic signal at the end of the 200 cycle pulse. Applicators were scanned with all sectors powered to  $2 \text{ W cm}^{-2}$  surface acoustic intensity at peak acoustic efficiency.

A technique termed optical displacement has been developed as an additional assessment of rotational acoustic output. A brass target ( $3 \times 10 \text{ mm}$ ) is aligned with an ultrasound transducer and positioned at 8 mm from the transducer surface. The transducer is pulsed and the resulting displacement of the brass target is measured with a laser sensor. The size of the target is such that the acoustic output is integrated over its length at each angular position. The transducer is rotated in  $2.5^\circ$  increments over  $360^\circ$  to produce a rotational optical displacement trace for visualization of angular variations in acoustic output.

### **5.3.3 Thermal Characterization**

Short duration heating patterns produced by the devices were investigated in tissue-mimicking phantom. This phantom has thermal and acoustic properties similar to soft tissue ( $k = 0.58 \text{ W m}^{-1} \text{ }^{\circ}\text{C}^{-1}$ ,  $\mu = 0.53 \text{ dB/cm/MHz}$ ) [205]. The applicator was implanted in an 8 cm diameter cylindrical phantom in a water bath held at 22°C. Cooling flow was run at 22°C and 60 mL min<sup>-1</sup> ( $h \approx 1000 \text{ W m}^{-2} \text{ }^{\circ}\text{C}^{-1}$ ). Multi-junction constantan-manganin thermocouple probes (4×2.5 mm spacing, Ella-CZ) encased in polyimide (0.58 mm OD, Small Parts) and housed in 20-gauge stainless steel needles (Becton-Dickerson S.A.) were implanted 10 mm from the transducer surface, vertically centered on the elements, and spaced every 45° around the device. Probe position was verified by CT. Thermometry data were acquired with a 48-channel HP data acquisition system (HP 34970A). Transducer sectors were driven at 1 – 2 W cm<sup>-2</sup> surface acoustic intensity for 5 minutes at peak acoustic efficiency. The phantom was then allowed to equilibrate for 3 hours in order to reach baseline temperature. After equilibration, the applicator was rotated 15° and the sectors were again powered at 1 – 2 W cm<sup>-2</sup> surface acoustic intensity for 5 minutes. This procedure was repeated once more in order to obtain rotational temperature distributions with 15° angular resolution.

### 5.3.4 Imaging Characterization

Prior to any clinical treatment, the position of the endocervical applicator would have to be verified with CT or MR. Artifacts could limit accurate determination of position and registration with treatment planning images. Artifact characterization was performed by implanting the ultrasound device in *ex vivo* bovine tissue and performing 1)

a standard spiral CT scan (transverse plane, 3 mm slice thickness) and 2) a 3T MRI scan ( $T_E/T_R = 10/100$ , FOV = 24 cm, BW = 15.63 kHz, 5 mm slice thickness).

In addition to thermal characterization performed using benchtop thermometry, development of heating patterns in 3-D was assessed using MR temperature imaging. The catheter-based endocavity applicator was implanted in *ex vivo* porcine tissue and placed in a 3T MRI. MR scans ( $T_E/T_R = 14.3/130$ ) were performed based on the widely used proton resonant frequency shift technique [17]. 2 devices were employed for heating: 1) a 1-element,  $135^\circ \times 135^\circ \times 90^\circ$  applicator at 6.6 – 6.7 MHz and 2) a 2-element,  $2 \times 180^\circ$  applicator at 7.9 – 8.0 MHz. Transducer sectors were powered at  $1 - 3 \text{ W cm}^{-2}$  for up to 15 minutes, during which time temperature was assessed every 14 seconds. Tissue was kept at room temperature as well as cooling flow through the device, which was run at  $\sim 100 \text{ mL min}^{-1}$ .

### 5.3.5 Radiation Attenuation

The possibility for simultaneous thermoradiotherapy was explored by measuring the attenuation of radiation transmission from a seed placed within the catheter-based ultrasound device. A bare catheter (6 mm OD, 0.50 mm wall, PET, Advanced Polymers, Inc.) was placed in a well-type ionization chamber used for calibration of HDR brachytherapy seeds. An electrometer records the current produced by the creation of ion pairs by emitted photons. A HDR brachytherapy source  $\text{I}^{192}$  was moved within the catheter at 2.5 mm steps from the tip. The same measurement was performed with the ultrasound device placed within the catheter, and photon transmission was compared to the bare catheter. Measurements were performed for a 2-element and a 3-element device.

## 5.4 Results

### 5.4.1 Acoustic Output

A summary of peak frequencies, acoustic efficiencies, and dead zone sizes measured for 6 of the fabricated applicators is given in Table 5.1. Overall acoustic efficiencies of ultrasound transducers and sectors range from 33.4 – 51.8 % and depend upon peak electrical impedance magnitude, transducer mounting on the applicator, and transducer sectoring. Transducer sectors have significantly increased efficiency over unsectored transducers; 120° and 180° sectors have acoustic efficiencies of  $44.1 \pm 3.6$  % vs.  $39.7 \pm 2.6$  % for unsectored transducers ( $p = 0.005$ , Student's t-test). The frequency corresponding to peak acoustic efficiency ranges from 6.60 to 7.45 MHz. Falloff of efficiency away from peak frequency is moderate and varied, with a  $4.7 \pm 2.3$  % (1.0 – 10.2 %) reduction in efficiency at 0.1 MHz off peak and a  $17.3 \pm 7.1$  % (7.9 – 27.1 %) reduction in efficiency at 0.2 MHz off peak.

Rotational acoustic intensity plots demonstrate collimated energy output from the transducers along the device length and directional acoustic output from device sectors (Fig. 5.). Angular dead zones in acoustic energy between transducer sectors range from 13.8 – 51.0° as defined by the region with relative acoustic intensity <10% of the maximum within each sector. Electrical isolation between transducer sectors is demonstrated in Fig. 5., where no acoustic signal is measured when one sector on each 3×120° transducer in a 2-element device is not powered. Rotational acoustic intensity

TABLE 5.1: Acoustic characterization of fabricated devices. Frequency ranges corresponding to peak acoustic efficiencies (mean  $\pm$  SD) are given for each transducer along with inter-sector dead zone sizes (angle between 10% acoustic intensity contours).

Applicator	Sectoring	Elements	Frequency (MHz)	Efficiency (%)	Dead zone (°)
1	$3 \times 120^\circ$	2	6.95 – 7.10	$43.8 \pm 2.2$	$45.7 \pm 3.3$
2	$3 \times 120^\circ$	2	7.35 – 7.45	$45.1 \pm 4.0$	$17.8 \pm 2.2$
3	$2 \times 180^\circ$	2	6.60 – 6.75	$40.5 \pm 7.3$	$19.4 \pm 1.3$
4	$2 \times 180^\circ$	3	7.05 – 7.15	$43.5 \pm 5.3$	$34.9 \pm 3.0$
5	$360^\circ$	2	7.35	$41.1 \pm 1.3$	none
6	$360^\circ$	3	7.20 – 7.30	$40.3 \pm 3.1$	none

plots are well correlated with optical displacement measurements (Fig. 5.5, Fig. 5.6). Acoustic output within sectors is inhomogeneous with higher intensities generally present near the edges of elements and sectors and dips in acoustic intensity in the center of sectors. Acoustic intensity peaks are relatively sharp, with only 0.25 – 1.8% of measurement points  $>80\%$  maximum intensity and 1.6 – 11% of points  $>60\%$  maximum intensity within transducer sectors.  $360^\circ$  applicators have uniformly higher intensities over the transducer compared to within sectors of  $2 \times 180^\circ$  or  $3 \times 120^\circ$  applicators; 80 – 92% of measurement points are  $>20\%$  maximum acoustic intensity and 20 – 50% of measurement points are  $>40\%$  maximum intensity for unsectored transducers while for multi-sectored applicators, 56 – 76% of points within sectors are  $>20\%$  maximum acoustic intensity and 14 – 38% of points are  $>40\%$  maximum intensity.

#### 5.4.2 Thermal Characterization

Rotational temperature distributions in phantom reflect the patterns observed in



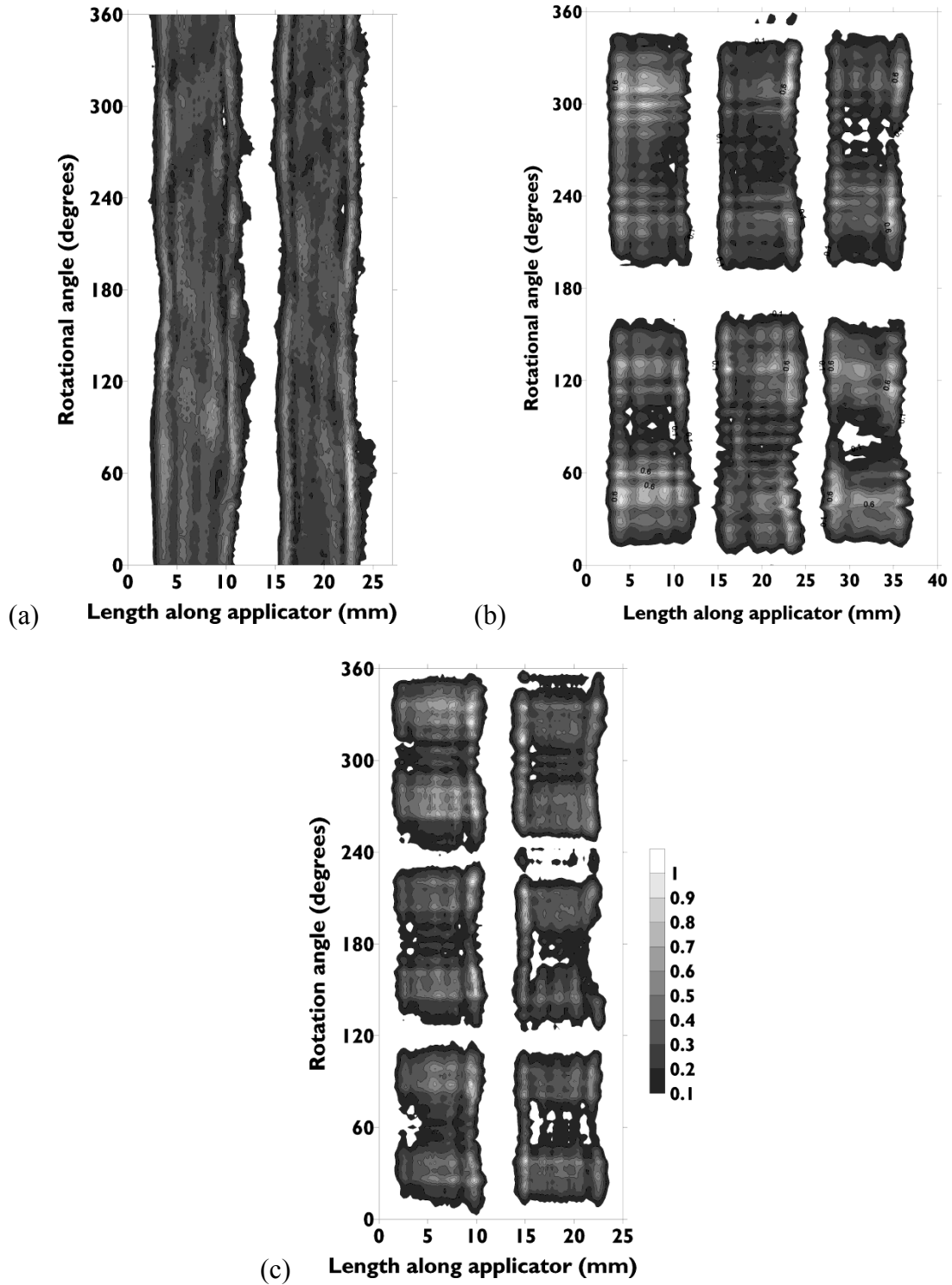


FIG. 5.3: Rotational acoustic pressure-squared distributions in water at 8 mm from the device surface. (a) A 2-element,  $360^\circ$  device with collimated beam output. (b) A 3-element,  $2 \times 180^\circ$  device with discrete zones of higher acoustic intensity separated by large low acoustic intensity zones between sectors. (c) A 2-element,  $3 \times 120^\circ$  device with smaller dead zones between transducer sectors.

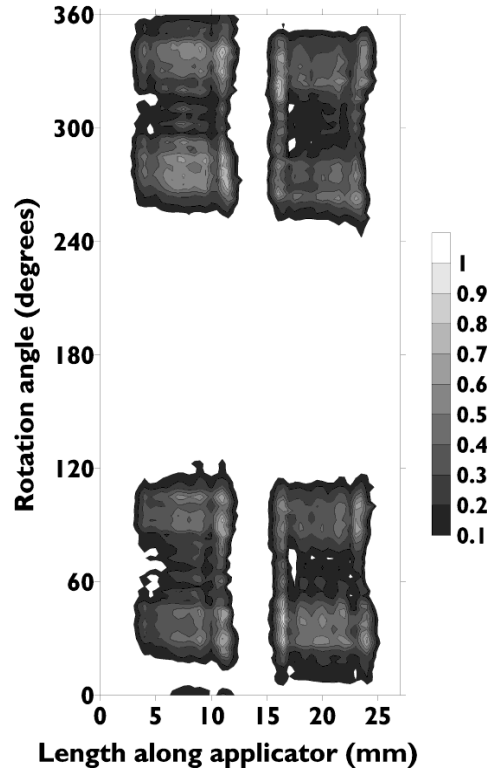


FIG. 5.4: Demonstration of electronic isolation of transducer sectors. A  $3 \times 120^\circ$  device has 2 sectors active, with the sector spanning  $120 - 240^\circ$  receiving 0 power, and produces no acoustic output due to bleed over from the other sectors.

the optical displacement and acoustic intensity plots averaged over transducer length. Zones of reduced temperature elevation correspond to dead zones in acoustic output (Fig. 5.6). Within transducers sectors, greater uniformity is observed in temperature than acoustic intensity profiles, as variations in acoustic intensity are smoothed by thermal conduction. The  $360^\circ$  applicator tested had normalized temperature elevation ranging from  $0.87 - 1.0$  in rotation around the applicator (Fig. 5.6a) corresponding to a normalized acoustic intensity range of  $0.62 - 1.0$ . Control of angular temperature elevation for multi-sectored transducers is achieved by power modulation to individual

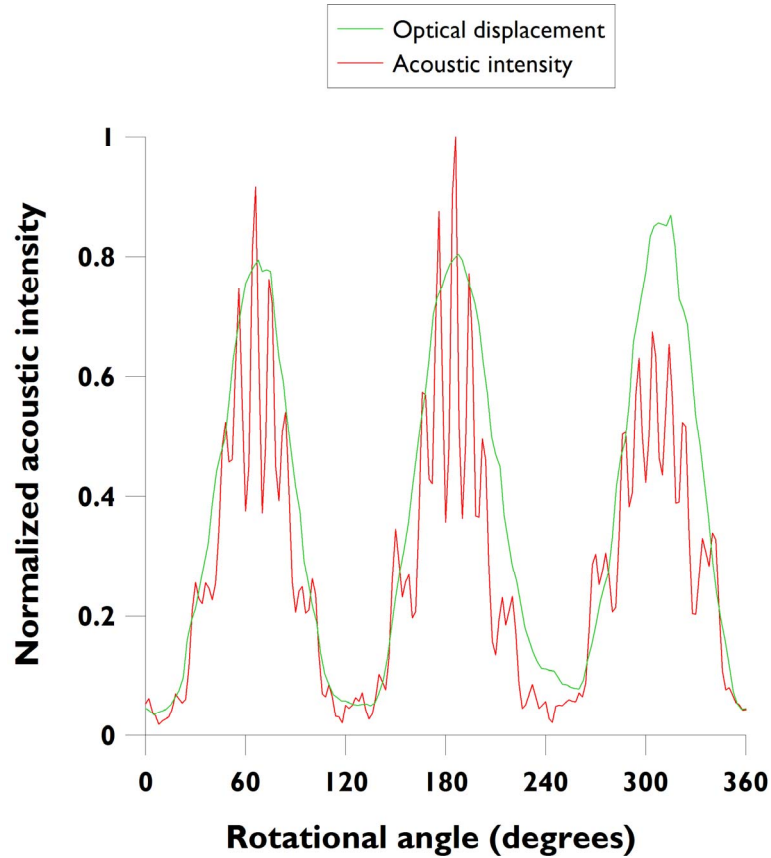


FIG. 5.5: Comparison of acoustic output as assessed by rotational acoustic intensity measurement and the optical displacement technique for a  $3 \times 120^\circ$  transducer. The hydrophone and optical displacement target are both 8 mm from the device.

transducer sectors; Fig. 5.6b demonstrates a normalized temperature elevation of 1.0 with  $2 \text{ W cm}^{-2}$  surface acoustic intensity applied to the sector spanning  $0 - 180^\circ$  and 0.7 with  $1.0 \text{ W cm}^{-2}$  surface intensity applied to the sector spanning  $180 - 360^\circ$ . Fig. 5.6c shows a tri-sector applicator with all sectors powered to  $2.0 \text{ W cm}^{-2}$  surface acoustic intensity or with the sector spanning  $0 - 120^\circ$  receiving zero power, resulting in a  $120^\circ$  zone with normalized temperature elevation  $< 0.5$  of the maximum. Temperature rise was verified to be highly reproducible ( $< 0.2^\circ\text{C}$  variation) at the same time point and applicator

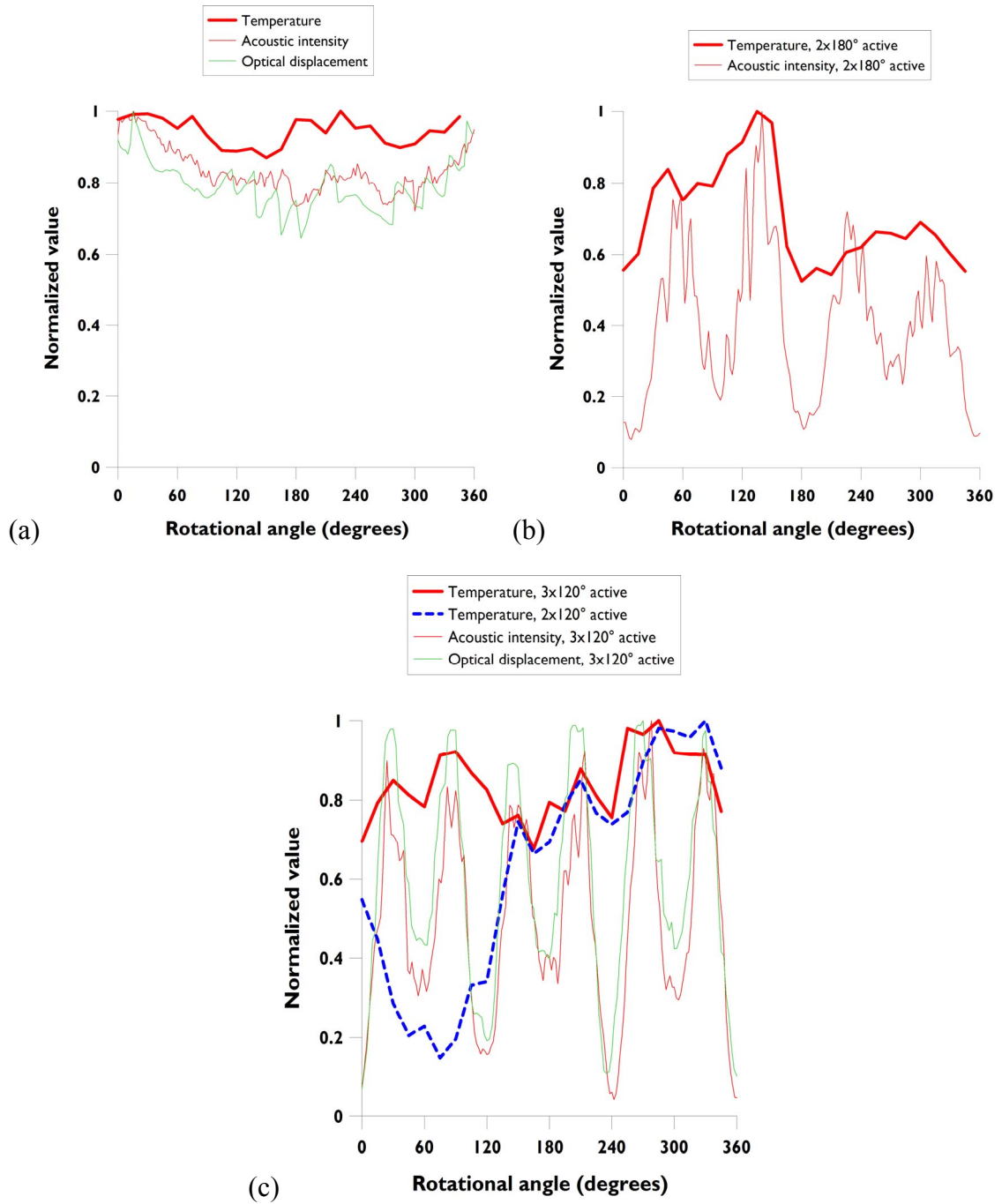


FIG. 5.6: Comparison of normalized temperature elevation in phantom at 10 mm radius after 5 minutes of heating to rotational acoustic intensity in water at 8 mm for the applicators used to produce the acoustic intensity distributions in Fig. 6 (intensity is averaged over the device length every 2° in angle and normalized to the maximum average intensity): (a) a 360° applicator, (b) a 2×180° applicator with one sector at 2 W cm<sup>-2</sup> surface acoustic intensity and the other at 1 W cm<sup>-2</sup> surface acoustic intensity, and (c) a tri-sectored applicator (3×120°) with 2 or 3 sectors active. The normalized output from the optical displacement technique is shown in (a) and (c).

position after 3 hour equilibration for various orientations in the phantom.

### 5.4.3 Imaging Characterization

The CT streaking artifact, as shown in Fig. 5.7, is prominent, due to the dense PZT crystal used to make the ultrasound transducers. Registration with structures several cm from the applicator, however, is likely still possible. The MR artifact is minimal even at 3T, extending 1 – 2 mm from the applicator, allowing MR to be used for precise applicator positioning.

Additional heating experiments conducted with MR temperature imaging give a more comprehensive view of the heating profiles of the ultrasound devices. Real-time monitoring was used to control power to individual sectors and transducers in axial and coronal slices and heat to several cm depth in tissue. Fig. 5.8 shows thermal images obtained during heating of *ex vivo* porcine tissue. Power control along the device length is demonstrated in Fig. 5.8a-b, while power control in angle is illustrated in Fig. 5.8c-d.

### 5.4.4 Radiation Attenuation

The reduction in current read by the electrometer when the seed is within the ultrasound device versus air is shown in Fig. 5.9. Photon emission is lowest when the seed is under the transducers, where the electrometer current is reduced by 4 – 6% due to the high density of the PZT ceramic. The footprint of each applicator can clearly be seen with peaks corresponding to each transducer for the 2- and 3-element devices. Radiation treatment plans that incorporate the attenuation of the ultrasound device could allow simultaneous hyperthermia and radiation to be performed.

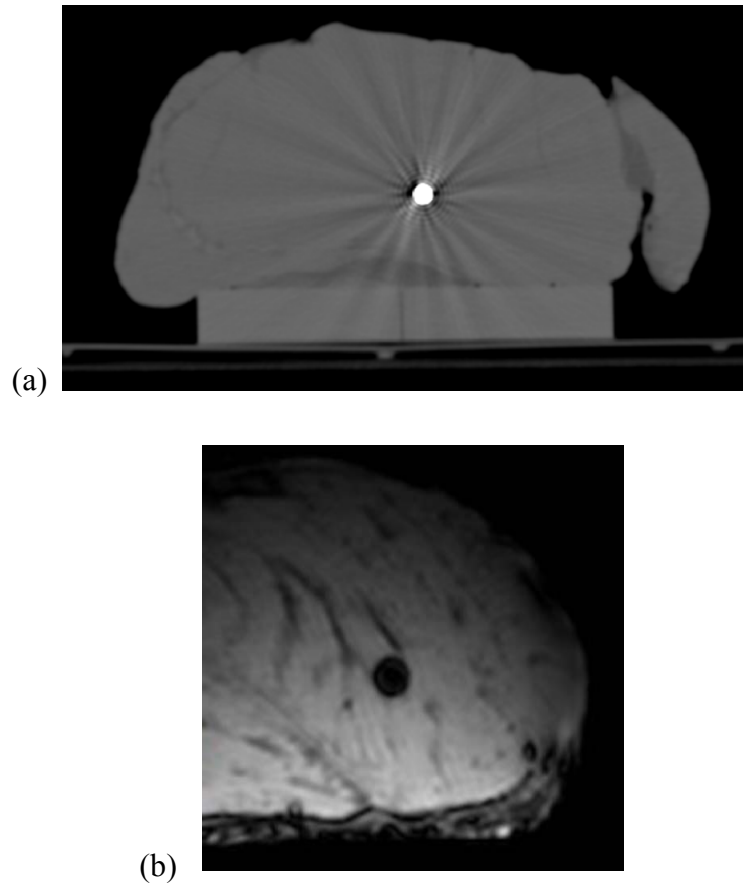


FIG. 5.7: Artifact characterization of the ultrasound applicator implanted in *ex vivo* tissue with (a) standard CT or (b) MRI.

## 5.5 Discussion

The clinical efficacy and adoption of hyperthermia technology relies on its being straightforward to use, adapted to the tumor site, capable of conformal heat delivery, and amenable to combination with radiotherapy. The anatomical location of the cervix allows for access through a natural body cavity for minimally invasive, localized delivery of heat and radiation. Endocavity applicators in existence for locally targeted heating to

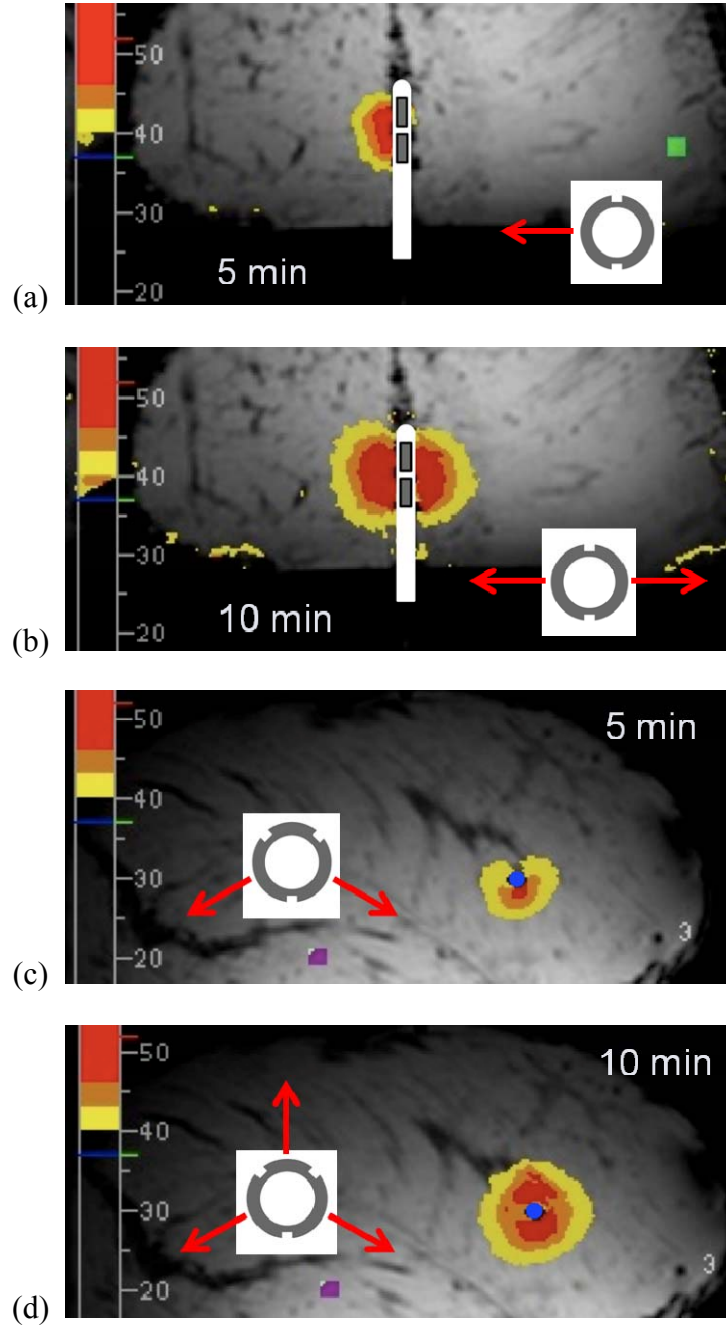


FIG. 5.8: MR temperature imaging in *ex vivo* porcine tissue demonstrating thermal penetration to several cm depth in tissue and the use of power modulation to control temperature distributions along (a,b) the device length and (c,d) in angle over 5 – 10 minutes.

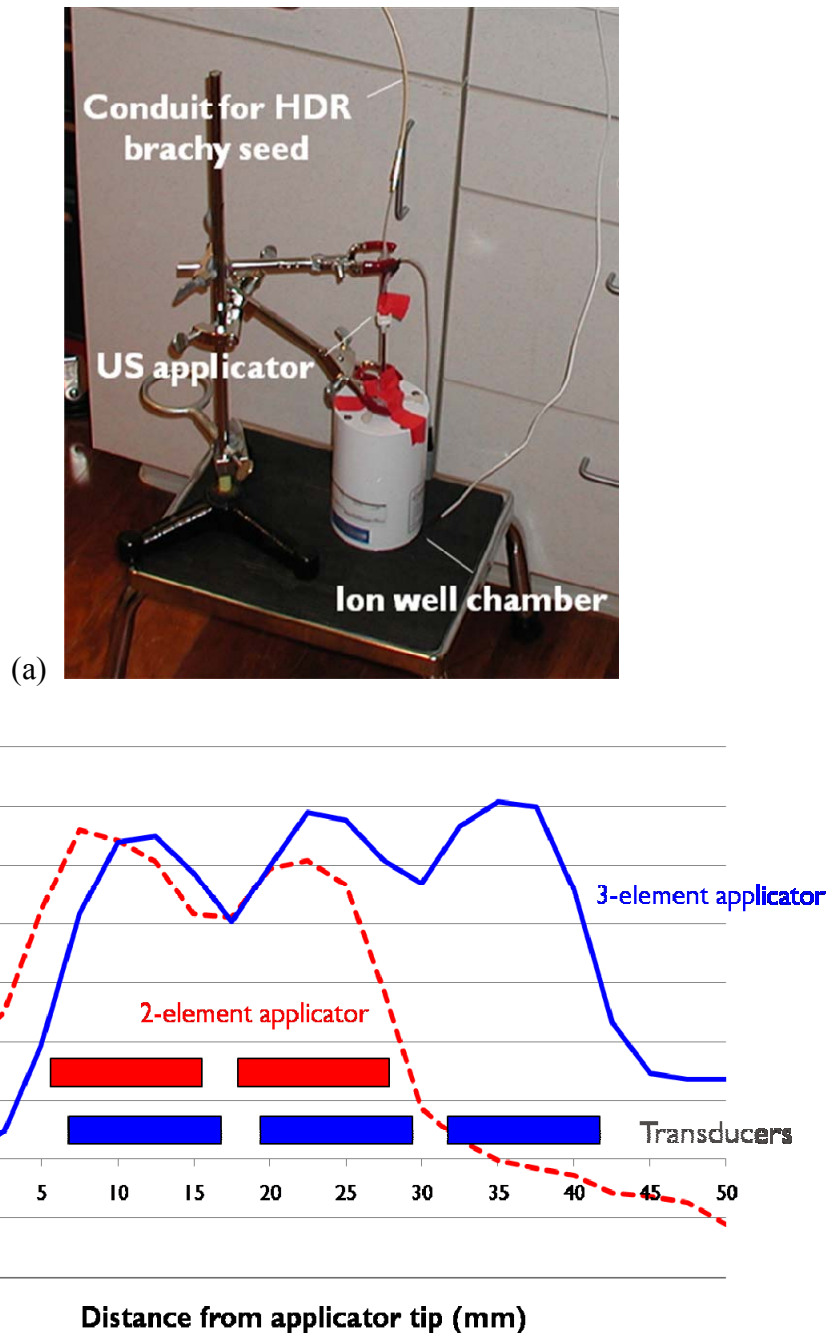


FIG. 5.9: (a) Experimental setup for the radiation attenuation measurements with well-type ionization chamber, ultrasound applicator, and HDR brachytherapy seed. (b) Blockage of radiation emission from a seed within the ultrasound device versus air at various seed positions in the well-type ionization chamber. Photon blockage is indicated by reduction in current from the chamber.



the cervix do not provide sufficient penetration or control of heating to be practical. Deep heating devices, although completely non-invasive, also offer limited control over thermal distributions with creation of hot spots outside the cervix. The objective of this work was to develop a device that uses arrays of multi-sectored tubular transducers to deliver localized heating that is more controllable than existing heating technology so that a more favorable efficacy-toxicity profile can be achieved by creating a higher differential between tumor temperatures and temperatures in organs at risk. Control over thermal delivery, demonstrated in thermal simulation and experiment, is afforded by power selection to transducer elements and sectors along with orientation of inter-sector dead zones. Integration of the endocervical applicator with an HDR brachytherapy catheter facilitates the alignment of conformal hyperthermia with radiation dose profiles.

The intent of this study was to develop an endocervical ultrasound applicator to deliver conformal hyperthermia concurrent with the HDR boost portion of radiotherapy. In this setting the tandem catheter is placed during surgery, CT/MR is performed for position verification and planning purposes to tailor treatment to the target, and thermometry can be placed in ancillary catheters for treatment monitoring and control. This intrauterine technology can be complementary with deep heating techniques in the sense that hyperthermia can be delivered in the HDR brachytherapy session, in addition to deep regional heating concurrent with the external beam radiotherapy phase of treatment [46, 206], thereby allowing greater cumulative thermal dose delivery. Although not investigated in this study, it may be possible to integrate the intrauterine ultrasound tandem with a Smit Sleeve to allow simple, reproducible insertion and

placement within the cervix for local hyperthermia delivery sequential to specific fractions of external beam radiotherapy.

A range in demands on angular heating profile can be accommodated by modifying the size of acoustic dead zones. By adjusting the width of sector cuts, dead zones in acoustic output between sectors ranged from 18 to 46° (Table 5.1). In the face of higher perfusion, an applicator with smaller dead zones could be used to avoid under-treatment. When organs at risk are in close proximity to the applicator, larger dead zones can be used and aligned with these organs to minimize thermal toxicity. Transducers can also be sectored to any angular dimension to create dead zones in acoustic output of any size.

The effects of uniformity of acoustic output within sectors, variations in the inter-sector dead zones, and acoustic power modulation observable in beam plots and optical displacement correlate to differences in the resulting temperature elevation in tissue-mimicking phantom. Temperature profiles are smoothed out with respect to acoustic intensity by thermal conduction mechanisms, the extent to which depends on the homogeneity of transducer sectors (Fig. 5.6). Unsectored transducers have more uniform acoustic output than multi-sectored elements and thus induce more uniform temperature elevation. The impact of relatively large dips (50-75% reduction from maximum) in acoustic intensity within sectors are reflected in temperature profiles as much more moderate dips in temperature (10-25% reduction from normalized maximum). Acoustic dead zones <20°, even with minimum intensity <5% of the maximum, cause minimal perturbations in the temperature profile that are comparable to dips in temperature associated with low intensity zones within sectors. Acoustic dead zones >30° cause more

prominent drops in temperature ( $>40\%$  reduction from normalized maximum) that can be oriented for thermal protection of organs at risk.

Imaging can indicate the location of ultrasound applicators within the tumor volume prior to treatment. Due to the presence of the streaking artifact in CT images, treatment planning images for HDR brachytherapy delivery may be obtained without the ultrasound applicators in place, with implant locations defined by catheter positioning. In cases where MR is used for treatment planning, which represents a small subset of patients, there does not seem to be a need to remove ultrasound applicators prior to imaging. Although catheter positions can be verified in transverse slices, there is no imaging method that can gauge the insertion depth of ultrasound applicators. The applicator must be well marked to gauge insertion depth externally by visual inspection.

The 4 – 6% attenuation of radiation emittance by a HDR brachytherapy source could potentially be accounted for in brachytherapy treatment planning. The exact depth of the ultrasound device would have to be known, since, as evidenced in Fig. 5.9, radiation attenuation falls rapidly when the brachytherapy seed is not under the transducers. Given the inability to ensure device insertion depth with imaging, transducer position as determined by a combination of imaging and manual inspection of device length would have to be relayed to brachytherapy treatment planning. In implementing simultaneous thermoradiotherapy, the benefit of increased cell kill in the tumor must be weighed against possibly increased toxicity in surrounding tissues, and remains an important topic of discussion. In this intracavitary setting, the multi-sectored ultrasound applicator is immediately adjacent to the target tissue and can direct heating to the tumor while limiting heating of normal tissue at risk, and thus may provide for an improved

technique to deliver simultaneous heat and radiation while minimizing increased toxicity to non-targeted tissue.

## 5.6 Conclusions

An endocervical ultrasound applicator has been developed for locally targeted, 3-D conformal hyperthermia delivery to the uterine cervix in conjunction with HDR brachytherapy. The device consists of a linear array of multi-sectored tubular transducers, allowing control of heating in length and angle. Acoustic and thermal characterization confirms conformal energy delivery capabilities, and temperature distributions correlate strongly with acoustic output. The acoustic dead zone between sectors can be used for thermal protection of organs at risk, and dead zone size can be controlled by the sectoring technique. Compatibility of the device with CT and MR imaging for image-guided placement is confirmed, and real-time MR temperature imaging during sonication for thermometry feedback during sonication is possible. MR thermometry confirmed the ability to heat several cm in depth and use power control to tailor thermal profiles. Simultaneous thermoradiotherapy may be feasible by the delivery of HDR brachytherapy from within the endocervical ultrasound device, but treatment planning would have to compensate for the 4 – 6% radiation attenuation by the ultrasound transducers. The endocervical ultrasound device is now under clinical investigation to assess the safety and feasibility of endocervical ultrasound hyperthermia in the cervix adjunct to HDR brachytherapy. Hyperthermia delivery can be guided by the use of treatment planning for *a priori* selection of proper device sectoring, length, aiming, and power levels.

## **Chapter 6**

### **Clinical Feasibility of Endocavity**

### **Ultrasound Hyperthermia**

#### **6.1 Abstract**

Catheter-based ultrasound devices have been developed for interstitial and endocervical heating through theory and experiment. Based on past experiments demonstrating controlled, conformal heating capabilities, a clinical trial was merited to investigate the safety and feasibility of catheter-based ultrasound hyperthermia as an adjunct to HDR brachytherapy in the treatment of cervical cancer. The results of the first 2 treatments in 1 patient involving the use of the endocervical device, the development of which is detailed in Chapters 3 – 5, are described here. The ability to modulate power to sectorized devices to achieve therapeutic temperatures  $>41^{\circ}\text{C}$  throughout the target heating volume is demonstrated in these treatments.

This chapter represents work that was presented at the International Symposium for Therapeutic Ultrasound (C. Diederich, J. Wootton, P. Prakash, V. Salgaonkar, T. Juang, S. Scott, et al. A Pilot Study of Catheter-Based Ultrasound Hyperthermia with HDR Brachytherapy for Treatment of Locally Advanced Cancer of the Prostate and Cervix. International Symposium on Therapeutic Ultrasound, Tokyo, Japan (2010)).

## 6.2 Introduction

Numerous randomized clinical trials have demonstrated improvements in tumor control and patient survival when heating at 40 – 45°C is combined with radiotherapy and/or chemotherapy [40-43, 46, 93]. The temperature effect is cumulative and thresholds of 6 – 10 equivalent minutes at 43°C (EM43°C) over the course of treatment have been identified for therapeutic enhancement of radiotherapy/chemotherapy by hyperthermia administration [50-52]. External microwave arrays used for deep hyperthermia in the pelvis have demonstrated positive results but typically produce tumor temperatures <40°C and thermal dose <1.5 EM43°C with similar temperatures in the rectum and bladder [46, 51, 95, 97]. Interstitial RF and microwave heating technology produces high temperatures (up to 60°C) at the device surface but heating falls off quickly in tissue and is sensitive to applicator orientation and phase [193, 195, 207]. Catheter-based ultrasound technology has been developed through theoretical study and *ex vivo* and *in vivo* experiment to deliver localized, 3-D conformal hyperthermia from within catheters used for HDR brachytherapy administration. These devices can produce therapeutic heating within tumors with good penetration and control of energy deposition to avoid over-heating of sensitive organs such as the rectum and bladder. A clinical pilot

study is underway at UCSF to investigate the feasibility of catheter-based ultrasound technology to deliver therapeutic levels of hyperthermia adjunct to HDR brachytherapy in the treatment of locally advanced cervical cancer. The endocervical ultrasound applicator developed as part of this dissertation has been incorporated in this trial. The results of two treatments using this device are reported here.

## **6.3 Methods**

### **6.3.1 Clinical Protocol**

A clinical pilot study is currently being conducted at UCSF to evaluate the feasibility and safety of catheter-based ultrasound hyperthermia integrated with HDR brachytherapy. Primary and recurrent cervical cancer (Stage IB2 – IVA) is considered ( $n = 12$ ). Each patient receives standard chemotherapy, radiation, and HDR brachytherapy. One hyperthermia session is given per implant, with typically two implants delivered one week apart. The thermal treatment goal is 40 – 45°C for 60 min. The clinical protocol is approved under NIH R01CA122276, FDA Investigational Device Exemption G040168, and UCSF Institutional Review Board approval H10778-32056-012. Two treatments in two different implants with the endocervical ultrasound device are analyzed.

### **6.3.2 Thermal Treatment Planning**

During HDR brachytherapy treatment planning and administration, a thermal treatment plan is generated similar to the methods described in Chapter 4. A physician has added organ contours to the CT images including rectum, bladder, and radiation

clinical target volume (CTV). In addition, a hyperthermia target volume (HTV) has been defined based on the tumor location. The HTV is the target of thermal delivery. Patient anatomical data are imported into the COMSOL/MATLAB treatment planning platform and reconstructed. Ultrasound applicator positions are selected based on catheters implanted for HDR brachytherapy. Initial values for applicator length, transducer sectoring, aiming direction, and power are set. Parameter selection and treatment strategies based on earlier work, including the study presented in Chapter 4, were employed in setting up the clinical treatment.

### **6.3.3 Catheter-Based Ultrasound Devices**

Two types of devices were used to administer catheter-based hyperthermia: 1) a directly implantable interstitial device and 2) an endocavity device for introduction into the uterine cavity (Fig. ). The interstitial device is comprised of 1.5 mm diameter transducers, housed within a 2.4 mm diameter Celcon catheter. The device has 3 transducers with 360° output and a total applicator length of 30 cm. The endocavity device, presented in Chapter 5, consists of 3.5 mm diameter transducers, housed within a 6 mm diameter polypropylene (PP) catheter (Liberty Medical). The device has 2 transducers with 2×180° output and a total applicator length of 40 cm. Applicators have an operating frequency of 6.5 – 8 MHz. Both devices have annular cooling water flow to couple energy between the transducers and catheter, enhance thermal penetration in tissue, and protect the endometrial lining. A hemostasis valve connects to the catheter for each applicator and seals cooling flow while allowing for rotation and translation of the



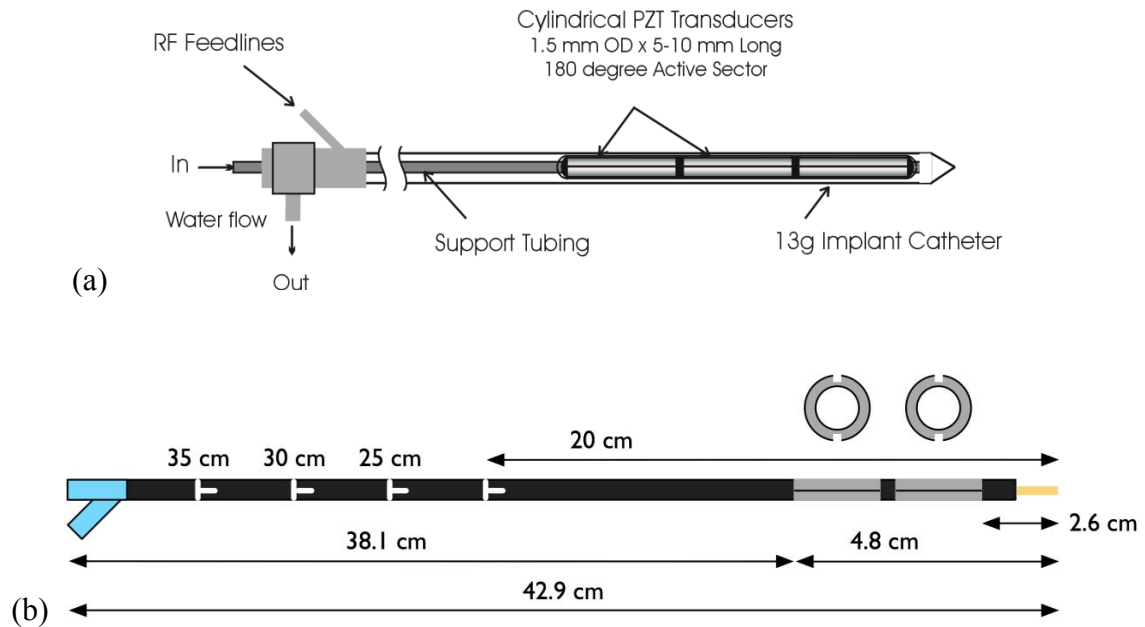


Fig. 6.1: (a) Interstitial and (b) endocavity applicator used in clinical hyperthermia delivery with  $360^\circ$  or  $2 \times 180^\circ$  output. The interstitial device is shown within a 13-gauge implant catheter with inflow and outflow ports conducting annular cooling water flow.

ultrasound device within the catheter. In both cases, the endocavity applicator is powered for some time before the interstitial applicator is powered.

Catheters implanted for HDR brachytherapy that are not used for radiation delivery can be used for thermometry. Constantan-manganin thermometry probes with 5 or 7 junctions that are spaced 10 mm apart are employed (Ella-CZ). A 48-channel data acquisition system (HP34970A) is used to collect temperature information. The positioning of thermometry probes and thermocouple junctions is planned using in house MATLAB software. Temperature distributions are monitored during hyperthermia delivery using a LabVIEW interface. The ultrasound devices are powered by a 32-

channel RF amplifier (Advanced Surgical Systems) with independent frequency and power control. Power is monitored and adjusted using a separate LabVIEW interface based on feedback thermometry. Power values applied to the applicators are converted from acoustic power values identified in treatment planning and converted to electrical power using the acoustic efficiency measured by the methods in Chapter 5 for each transducer or transducer sector.

## 6.4 Results

To date, 8 cervix implants have been performed with the catheter-based ultrasound system. 2 of these treatments involved the use of the endocavity device and will be described in depth. Both treatments proceeded >60 min with no adverse events or treatment-related toxicities, and therapeutic temperature >41.5°C was achieved throughout the target volume in both cases. Both treatments were delivered to the same patient one week apart, and involved the use of 1 endocavity device and 1 interstitial device, as shown in Fig. 6.2. The interstitial applicators are implanted lateral to the endocavity applicator. The cooling flow hubs for each device can be seen along with the thermometry probes used for temperature monitoring.

An anatomical reconstruction is shown in Fig. 6. along with the temperature elevation during the course of therapy for the first hyperthermia treatment. Initially the endocavity device receives power and the thermocouple junctions at 12 – 15 mm from the device are raised >42 – 43°C within ~10 minutes with thermometry points registering 40°C at 26 mm and registering 39°C at 35 – 37 mm (Fig. 6.a). The interstitial device is

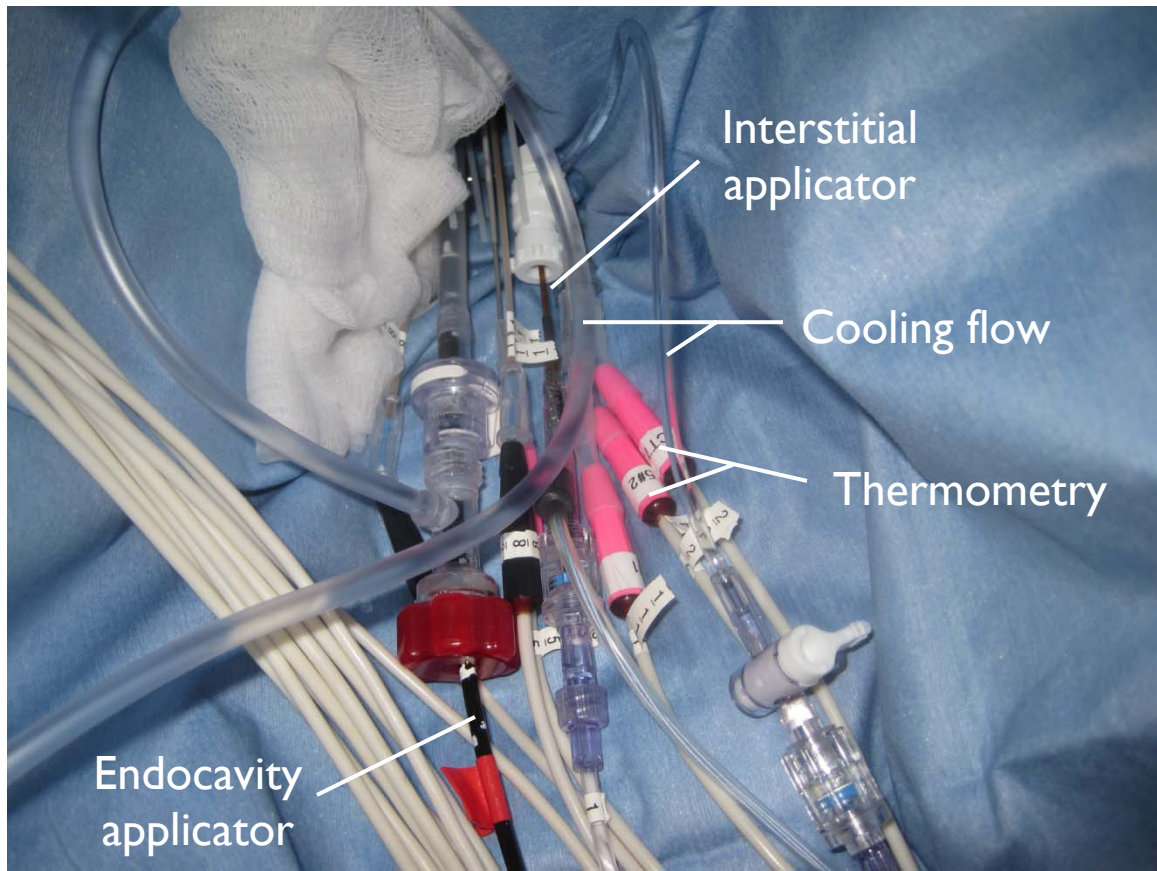


Fig. 6.2: Hyperthermia implant in cervix with endocavity and interstitial applicators. Cooling flow hubs and tubing can be seen, along with thermocouple probes for temperature monitoring during therapy.

then powered to extend thermal coverage  $>41^{\circ}\text{C}$  to the entire HTV (Fig. 6.b). Although maximum temperatures along each thermometry catheter are shown, the HTV is covered with temperatures  $>41^{\circ}\text{C}$  throughout the volume.

Temperature elevation for the second treatment is shown in Fig. 6.4. A high temperature of  $48.2^{\circ}\text{C}$  is achieved between the endocavity and interstitial applicator, although artifacts of  $1 - 2^{\circ}\text{C}$  can exist at these temperatures due to heating of the

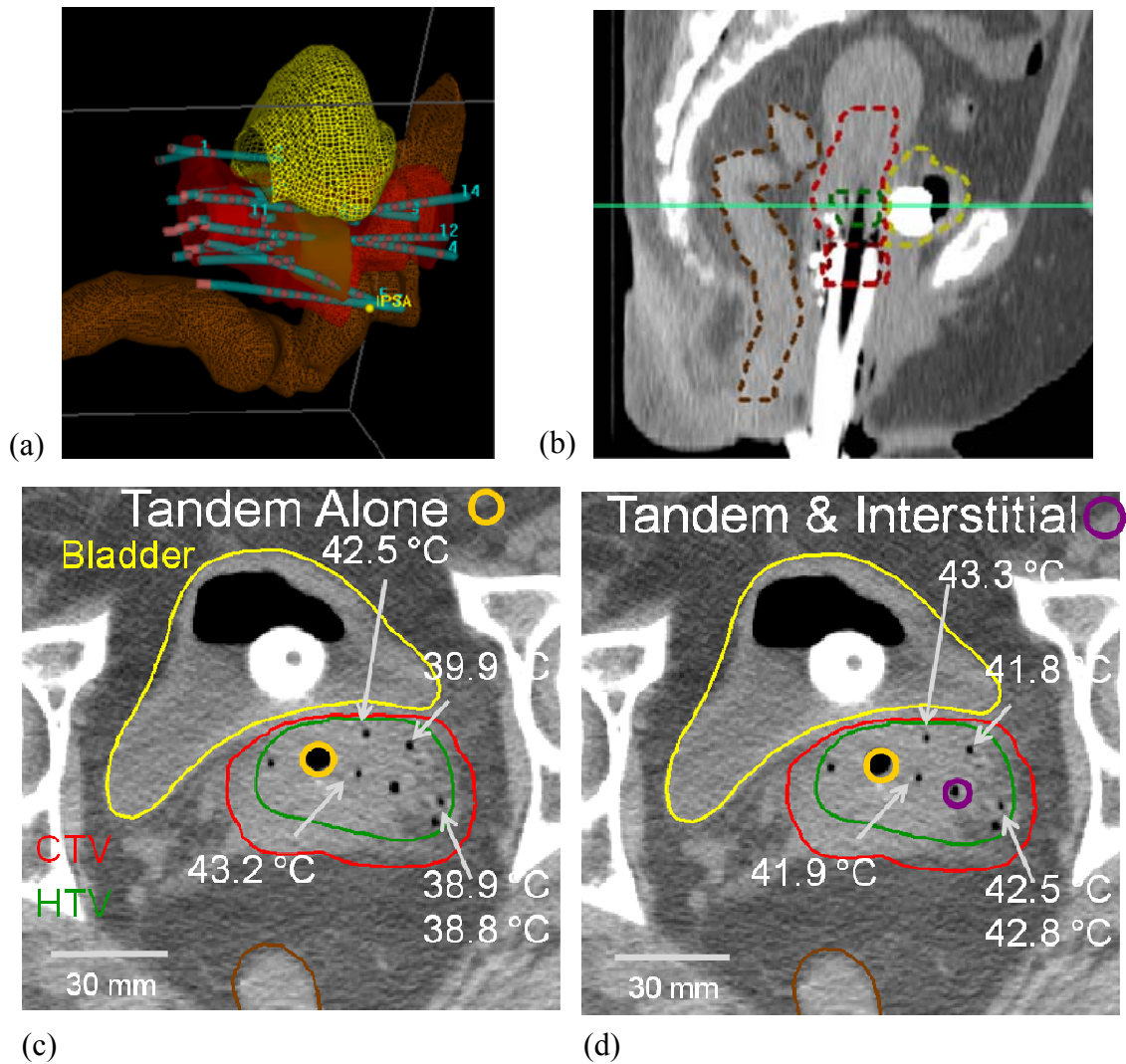


Fig. 6.3: (a,b) Cervix implant demonstrating the 3D reconstruction of the patient anatomy and catheter placement in HDR treatment planning. 2-D cross-section CT through cervix implant and resulting temperature profiles within the cervix and HTV in the first clinical treatment with (c) the 2×180° endocavity alone or (d) in combination with the 360° interstitial device. The endocavity device has sector 1 aimed to the patient's right and sector 2 to the patient's left. Temperatures given are the maximum along the length of the thermometry probe.

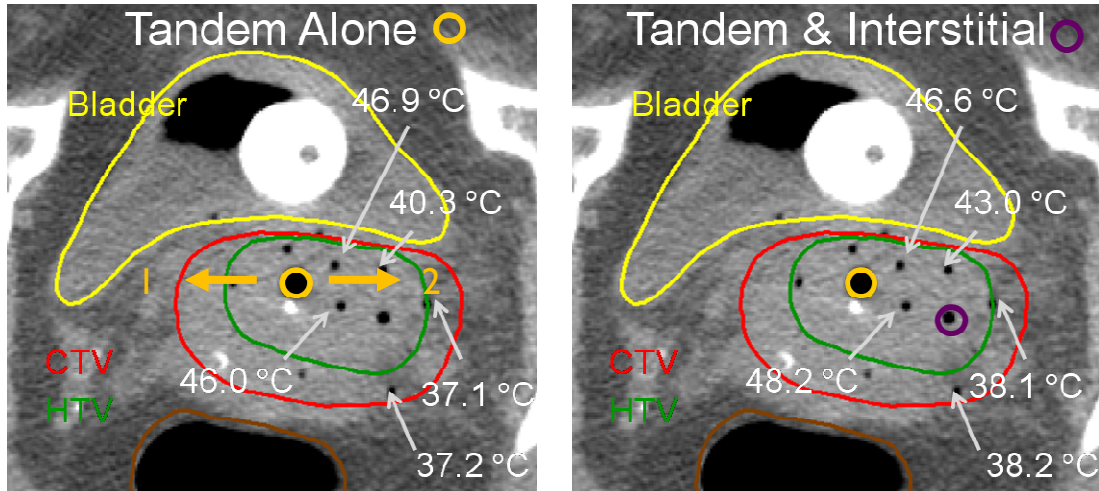


Fig. 6.4: CT cross-section images with temperature overlay for the second treatment with the  $2 \times 180^\circ$  tandem applicator alone (left) or in conjunction with a  $360^\circ$  interstitial applicator (right). The endocavity device has sector 1 aimed to the patient's right and sector 2 to the patient's left. Temperatures given are the maximum along the length of the thermometry probe.

thermometry probe by high ultrasound intensity levels. Temperature near the anterior-lateral HTV boundary is still  $43^\circ\text{C}$ . At the lateral boundary, temperatures of  $38^\circ\text{C}$  are measured, but this thermometry probe is likely deeper in tissue than the HTV due to alignment issues and patient movement.

Power levels for the endocavity device in the first treatment are initially set to  $1.5 - 3.5 \text{ W cm}^{-2}$  and then adjusted to  $2.8 - 3.2 \text{ W cm}^{-2}$  to achieve steady therapeutic temperatures (Fig. 6.5). In order to extend therapeutic heating laterally, the interstitial applicator are powered at  $3 \text{ W cm}^{-2}$  and maintained at  $3 - 3.5 \text{ W cm}^{-2}$  for the duration of treatment.

In the second treatment, power levels for the endocavity device ranged from  $2 - 4$

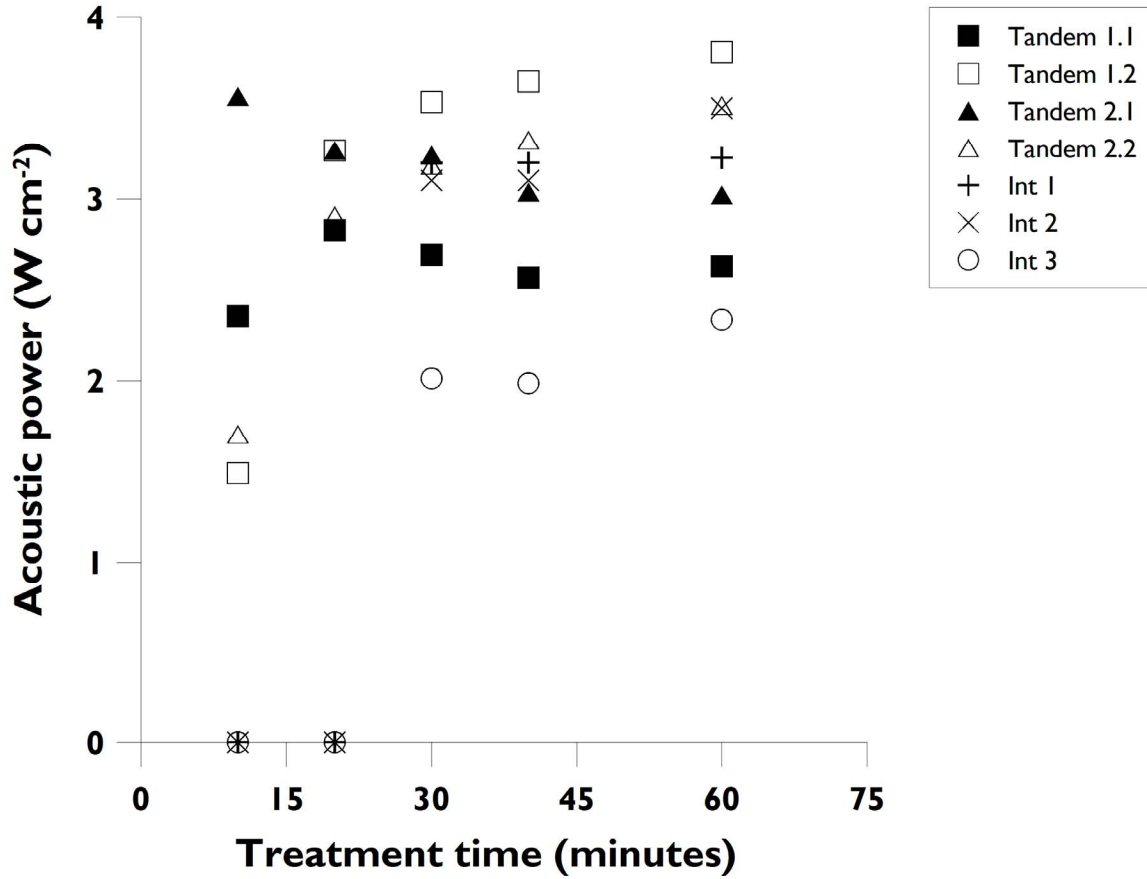


Fig. 6.5: Acoustic power values for the  $2 \times 180^\circ$  tandem and  $360^\circ$  interstitial device used in the first hyperthermia treatment

$\text{W cm}^{-2}$  acoustic in order to increase temperatures to therapeutic levels and maintain therapeutic temperature for  $>60$  min (Fig. 6.6). Sector 2 on each transducer on the tandem applicator is given higher power, as it is aimed towards the more extensive part of the HTV to the patient's left. Power values start at  $2 - 2.5 \text{ W cm}^{-2}$ , increasing to  $3 - 3.75 \text{ W cm}^{-2}$  by 30 minutes. Between 15 and 30 minutes the interstitial device receives power to  $\sim 2 \text{ W cm}^{-2}$ . When temperatures  $>47^\circ\text{C}$  are observed due to the combined heating of the tandem and interstitial devices, the power values are lowered to  $2 - 2.5 \text{ W cm}^{-2}$  for

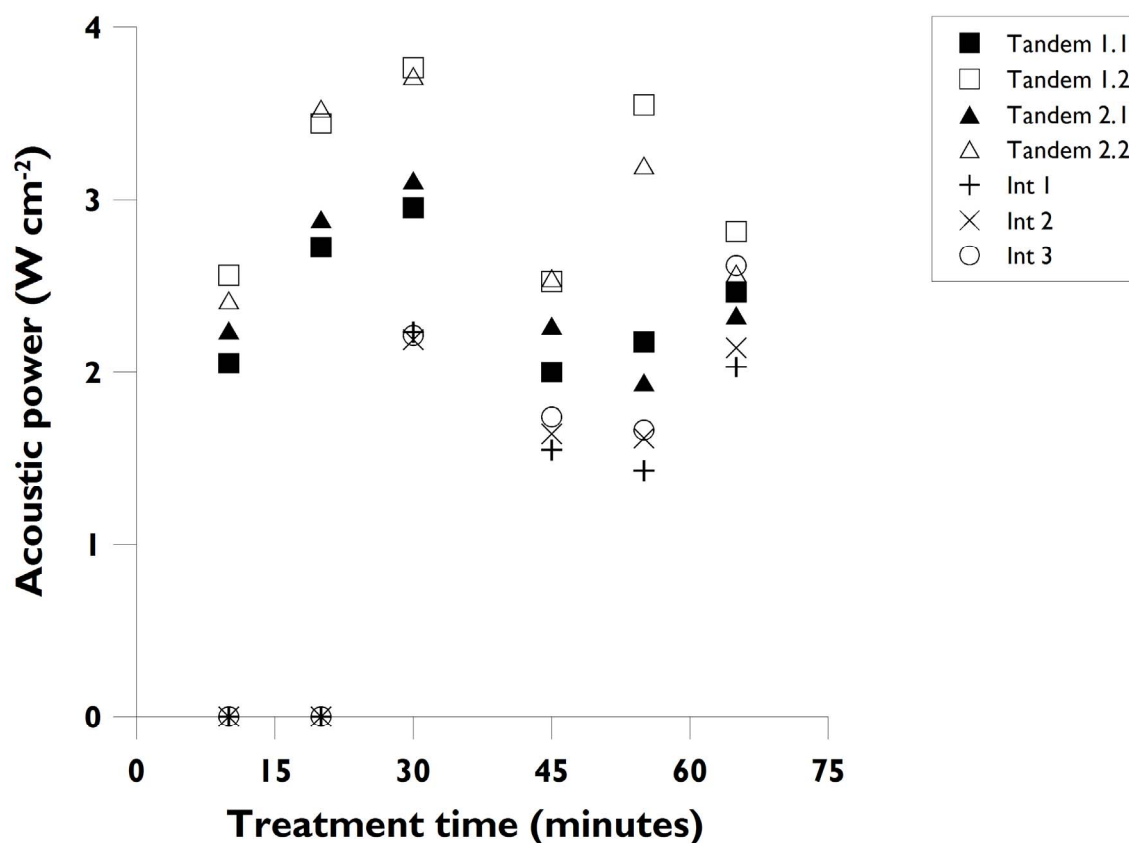


Fig. 6.6: Acoustic power values for the  $2 \times 180^\circ$  tandem and  $360^\circ$  interstitial device used in the second hyperthermia treatment

the tandem and  $1.5 - 1.75 \text{ W cm}^{-2}$  for the interstitial. As peak temperatures come down, power is increased to  $2.25 - 3.5 \text{ W cm}^{-2}$  for the tandem and  $2 - 2.5 \text{ W cm}^{-2}$  for the interstitial device until the completion of the hyperthermia session at  $\sim 75$  minutes.

## 6.5 Discussion/Conclusions

The initial feasibility of catheter-based endocervical and interstitial ultrasound hyperthermia integrated with HDR implant for treatment of cervical cancer has been demonstrated. Catheters implanted for HDR brachytherapy delivery were used for

ultrasound applicator introduction following radiotherapy. Additional catheters implanted in the treatment volume were used for introduction of thermometry probes and up to 36 temperature channels were monitored. Temperature feedback was important to guide power control of the endocavity and ultrasound devices, which varied from 1 – 4 W cm<sup>-2</sup> acoustic, to maintain therapeutic temperature >40 – 41°C without causing excessive temperature elevation in the tumor or in the rectum and bladder. The endocavity tandem applicator generated therapeutic temperatures greater than 2 cm diameter, and in good agreement with simulations. Power levels agreed well with the power levels from treatment planning simulations in Chapter 4. High temperatures >48°C were observed but may include an artifact of ~2°C. These artifacts are much smaller at lower temperatures due to lower incident ultrasound energy that causes self-heating of the thermometry probe. The extent of the artifact can be assessed by examining the temperature trace after power is turned off, although catheter and patient movement can confound this assessment. Despite temperatures >48°C measured, the patient treated in this study did not have any treatment-related complications, and after 4 months of follow-up was disease free. Although this is only one case, it demonstrates that catheter-based ultrasound thermal therapy can be feasible and effective.

Additional patients will be treated with the combination of endocavity and interstitial devices. Temperature distributions will be further analyzed to characterize volumetric thermal dose delivery, and temperature distributions achieved during clinical hyperthermia will be compared to thermal treatment plans to verify the model accuracy. Attempts are being made to speed up optimization methods so that it may be possible to



optimize planned thermal delivery within the timeframe of brachytherapy delivery rather than iteratively run forward plans.

## **Chapter 7**

# **Conclusions and Future Directions**

### **7.1 Research Summary**

The goals of this project were twofold: 1) to investigate the factors influencing thermal therapy delivery and devise treatment strategies with a focus on treating target volumes in the pelvis while limiting heating of non-targeted structures, and 2) to develop an endocavity ultrasound applicator based on theoretical and empirical analysis for locally targeted hyperthermia in the uterine cervix. Extensive studies using biothermal modeling deepened an understanding of ultrasound applicator parameters on temperature distributions in tissue, and will continue to contribute to future applicator design. Lessons learned from simulation work were put into practice in the design of a catheter-based, intrauterine ultrasound hyperthermia applicator capable of highly conformal heat delivery. Acoustic and thermal evaluation confirmed tailored heating capabilities. The feasibility of implementation in a clinical hyperthermia treatment was demonstrated in

one patient, in which therapeutic heating levels were delivered throughout the target volume in conjunction with HDR brachytherapy, and who was disease-free after 4 months of follow-up.

The study of transurethral ultrasound delivery and its influence on pelvic bone heating clearly has implications for prostate ablation treatments, but also for the use of any other ultrasound devices in close proximity to bone or other highly attenuating tissue. A variety of device types was considered in analyzing planar, curvilinear, and tubular transducers over a wide frequency range. Full acoustic field calculations were employed to improve temperature accuracy. Information about the extent of bone heating with the variety of parameters considered holds importance for avoiding toxicity during thermal therapy, but also has therapeutic implications for efforts to selectively treat bone metastases [208, 209]. Transducer shape and frequency selection affect thermal penetration in tissue, with influence on heating capabilities, toxicity, and treatment time. The frequency effect is not straightforward; although low frequency increases heating of bone at a distance, higher frequency may increase heating of bone in close proximity despite decreased thermal penetration. Since lower frequency decreases treatment time due to more rapid tissue coagulation in depth, thermal dose deposition in bone may be reduced despite higher bone temperatures. The complicated interaction of ultrasound transducer parameters will necessitate patient specific treatment planning for appropriate device selection. Tubular transducers are advantageous in their ability to coagulate large tissue volumes in a short amount of time with limited heating of non-targeted tissues beyond the treatment zone.

Development of the endocavity ultrasound device was warranted by an initial investigation into heating capabilities in relation to tumor volumes encountered in the clinic. Radiation clinical target volumes averaged 4 cm in diameter, and tumors that represent the true hyperthermia target are contained within these volumes. Therapeutic heating could be delivered by the endocavity ultrasound device to a 4 – 5 cm diameter with low maximum temperature ( $T_{\max} = 45^{\circ}\text{C}$ ) at moderate perfusion ( $1 \text{ kg m}^{-3} \text{ s}^{-1}$ ) through an implant catheter in biothermal simulations to cover tumor volumes. Multi-sectored transducers can be used to deliver heating to eccentric targets or dead zones between sectors oriented for thermal protection of organs at risk. The importance of thermal protection and power control is emphasized by the close proximity of the rectum and bladder to the cervix. It was presumed that interstitial catheters implanted for HDR brachytherapy delivery could be used for feedback thermometry to guide clinical hyperthermia treatments.

Further theoretical investigation into the feasibility of hyperthermia delivery by the endocervical ultrasound applicator was made using a 3-D, patient-specific treatment planning and optimization model. The heating performance of the endocervical device alone or in conjunction with interstitial devices in regular implant configurations and in the optimized treatment of actual patient target volumes with minimal heating of organs at risk was assessed. Therapeutic heating with  $T_{90} > 40^{\circ}\text{C}$  could be obtained in difficult to treat targets with  $T_{\max} = 47^{\circ}\text{C}$  and temperature elevation in rectum and bladder below levels linked to toxicity. The use of sectored interstitial and a multi-sectored endocavity device was critical to achieving therapeutic goals. Interstitial devices can effectively extend lateral penetration of the endocavity applicator into the parametrium to increase

the therapeutic heating volume without increasing heating in organs at risk. Blood perfusion has a prominent effect on temperature distributions, and thermal feedback will be highly important to guide power control in order to maintain therapeutic heating in the face of unpredictable and variable perfusion levels. The safest treatment strategy is to optimize powers with a low perfusion value, and then increase power under thermal guidance as necessary to improve thermal coverage of the target. Irregularly- and closely-spaced catheters for the brachytherapy implant in the target volume limited effective heating, and as many catheters as possible should be implanted spaced at 15 – 30 mm throughout the target volume to improve thermal coverage.

A family of endocavity ultrasound devices was fabricated with applicator parameters based on biothermal simulation results. These devices consisted of 1 – 3 unsectored or multi-sectored transducers. Given the utility of the inter-sector dead zones in providing thermal protection of rectum and bladder, the sectoring technique was modified over the course of device development to be able to control the size of the dead zone, with one cut for smaller dead zones and two cuts with variable spacing for larger dead zones. Imaging compatibility was verified with minimal MR artifact and moderate CT streaking artifact. Simultaneous hyperthermia and HDR brachytherapy using the endocavity ultrasound device has potential, if the 4 – 6 % radiation attenuation by the transducers can be accounted for in radiation treatment planning. Collimated acoustic output from electrically isolated sectors was observed in beam plots. Benchtop measurements of rotational temperature distributions in phantom have strong correlation with acoustic output assessed by beam plots and optical displacement. 3-D thermometry afforded by MR temperature imaging confirmed conformal heating capabilities with

power control to tailor thermal delivery along the device length and in angle. Thermal experimentation established the ability of the device to heat to a depth of several cm in phantom and *ex vivo* tissue.

Feasibility for clinical hyperthermia delivery by catheter-based ultrasound devices was supported by extensive theoretical work investigating heating profiles, planning thermal treatment of actual patient clinical volumes, and experimental analysis fully characterizing acoustic and thermal output of devices that demonstrated 3-D conformal, controllable thermal delivery. Clinical implementation of catheter-based ultrasound is further supported by numerous prior *in vivo* animal studies, primarily for prostate ablation, demonstrating safety and controllability of the technology. The biological and clinical justification for hyperthermia as an adjunct to HDR brachytherapy is well documented. The pilot trial at UCSF is intended to advance the use of catheter-based ultrasound in providing clinical hyperthermia for pelvic malignancies, with the aim of treating 12 patients for prostate cancer and 12 patients for cervical cancer. Interstitial ultrasound devices have been employed thus far for the treatment of 4 prostate and 8 cervix cases, with therapeutic heating longer than 60 minutes achieved in all cases with no adverse events reported. The details of one of the cervical cancer cases, which involved the use of the endocavity ultrasound device developed as part of this dissertation project, are presented in this report. 2 treatments were administered to the patient using the endocavity device along with an interstitial device. Temperatures  $>41^{\circ}\text{C}$  were achieved throughout the target volume for 65 – 75 minutes using power control guided by feedback from interstitial thermometry, and at 4 months the patient had no evidence of residual disease. Although this represents only one case, initial safety, feasibility, and

efficacy of clinical hyperthermia using the endocavity ultrasound device was demonstrated.

## **7.2 Future Directions**

The ability of sectored tubular transducers to rapidly coagulate portions of the prostate in a short period of time with limited bone heating was demonstrated. The 90° sectored tubular device in this work would have to be rotated to treat the entire prostate. Multi-sectored applicators can potentially treat the entire prostate gland without rotation, using tailored power levels to each sector to control the angular thermal profile. The influence of these devices on treatment time and bone heating should be investigated, particularly using a strategy involving alignment of sector cuts with bone, similar to alignment of sector cuts with rectum and bladder in cervical hyperthermia demonstrated in Chapters 3 & 4. Prostate gland volumes and pelvic bone positions from patient imaging data can be used to more accurately model bone heating in clinical treatments. An investigation into the use of more sophisticated power control strategies and effects on prostate treatment and bone heating is also warranted. Modeling of pelvic bone heating should be incorporated into the thermal treatment planning software described in Chapter 4 as a consideration in thermal delivery.

Modifications to the endocavity device can be made to improve its performance, particularly with regards to treatment monitoring. It may be possible to package thermometry probes based on nitinol wire that deploy when the applicator is implanted for additional thermometry information. Flat thermometry probes can also be integrated into the catheter to allow for temperature readings at the contact with tissue. This could

be important for ensuring that the endometrium does not overheat, which could lead to tissue sloughing and bleeding. Endometrial and additional catheter cooling can also be facilitated by the use of a cooling balloon on the outside of the catheter. This balloon would also aid in coupling the applicator to tissue in order to avoid air gaps. Additional cooling of the catheter would aid thermal penetration, as the maximum temperature would be pushed further into tissue. It may be possible to modify the applicator to treat larger volumes by adding additional ultrasound transducers, such as an annular transducer or multiple planar transducers along the surface of the ring portion of the tandem and ring brachytherapy applicator. This would supplement the lateral thermal coverage of the device, important for disease that has invaded the parametrium. Integration of imaging markers into the device would aid placement. The device could be made more sophisticated by the incorporation of ultrasound imaging transducers so that applicator placement could in part be verified from within the device.

Methods for applicator quality assurance continue to improve, which will aid in translating benchtop measurements of acoustic output into clinical device performance. The optical displacement measurement may provide a faster, more relevant indication of acoustic output as it translates to temperature distribution. Further correlation of acoustic output measured by rotational acoustic intensity mapping and optical displacement to temperature distributions in theory and experiment is merited. Additional characterization of the relationship between cut size, acoustic dead zone, and thermal dead zone will aid future applicator design.

Further investigation into the possibility for simultaneous thermoradiotherapy is warranted. Although initial testing has demonstrated a small but significant reduction in



radiation emission when a radioactive seed is within the ultrasound transducers, there has been no testing of the spatial variation in radiation dose profile. Radiation dose profiles can be computed using Monte Carlo simulation for an Ir<sup>192</sup> seed within the ultrasound device, and would provide more insight into the effects of radiation attenuation by the device on overall radiation dose distributions. It may be possible simply to increase dwell times of the seed to compensate for radiation attenuation by the ultrasound device, and this possibility should be further studied. Radiation dose delivery can also be visualized using radiographic film, which reacts to change brightness in proportion to the quantity of incident photons from the radioactive source. This would allow direct experimental determination of radiation dose falloff from a brachytherapy seed within the applicator.

The clinical trial will continue with the treatment of 6 additional cervix patients, although the number that will be treated with the endocavity device is unknown. Other applicators will be fabricated in addition to the 3-element, 360° device and 2-element, 2×180° device currently available to allow more versatility in treating lesions of various size and shape. The aim will be to encourage introduction of as many catheters as is feasible in order to improve thermal coverage of the target volume and increase the amount of thermal feedback during treatment.

The quality of hyperthermia delivery in patients treated so far, along with patients to be treated, has yet to be characterized in terms of cumulative thermal dose delivery to the target and to organs at risk. This will be important for determining not only the feasibility of delivering catheter-based ultrasound hyperthermia in the cervix, but verifying the ability to repeatedly deliver therapeutic levels of heating throughout the

target volume. Temperature and thermal dose characterization will also be important for validating the accuracy and utility of thermal treatment planning. So far, thermal treatment planning has been used as a base for setting initial power levels, but resulting temperature distributions in the clinic have not been directly compared to thermal models.

Optimal clinical hyperthermia would be delivered using automated feedback power control based on thermometry within the tumor. Development of control algorithms is a focal point of current research and will result in improved quality of hyperthermia. The most important factor that influences the ability to verify thermal delivery is the number of thermometry points in the tumor. The clinical experience thus far has been that there are occasions where limited catheters and thus limited thermometry is available, due to the desire of the physician to limit morbidity from the implantation of additional catheters. MR temperature imaging can get around limitations on implanted thermometry but is costly. Methods under development for CT- or ultrasound-based thermometry so far do not have temperature resolution sufficient for assessing heating in the hyperthermia range, but future development may make these methods more relevant for mild heating. Thermally-sensitive liposomes can possibly be used as contrast agents for imaging, where a rapid transition occurs at a particular temperature, so that the heating boundary can be visualized. Additional work is needed to fine-tune these agents to undergo transition at a particular temperature and within a narrow range.

The utility of the endocervical ultrasound device may go beyond hyperthermia in the cervix. The device can possibly be adapted for endocavity thermal treatment of other

sites such as the esophagus [210] and bile duct [211]. The targeted release of anti-oncogenic or anti-angiogenic drugs packaged in liposomes by the thermal and mechanical effects of ultrasound as an enhancement to therapy is possible. Non-oncologic indications of endocervical ultrasound may include thermal ablation of uterine fibroids or endometrial ablation for management of uterine bleeding, treatments that have been performed with radiofrequency and laser devices [212, 213].

It is my hope that the endocavity ultrasound device developed in this report, with safety and feasibility further demonstrated in the pilot trial at UCSF, will undergo more widespread clinical adoption for hyperthermia delivery. This applicator was developed through extensive parametric theoretical study and empirical characterization that drove iterative applicator design and refinement. A patient-specific focus with thorough analysis of potential target volumes from CT and MR imaging was introduced from the outset, maintained throughout the design process, and produced a device with expected performance based on prior analysis during clinical implementation. The extension of the catheter-based endocavity device to other therapeutic uses and other sites based on patient-specific analysis of the treatment site and thermal goals can further its overall adoption. As a result of this project, it is also my hope that the impact of bone in the treatment field becomes an important component of treatment planning for ultrasound thermal therapy, particularly in prostate treatment.

## Bibliography

- [1] M. Nikfarjam, V. Muralidharan, C. Christophi. Mechanisms of focal heat destruction of liver tumors. *J Surg Res*, 127(2), 208-23, 2005.
- [2] C. J. Diederich. Thermal ablation and high-temperature thermal therapy: overview of technology and clinical implementation. *Int J Hyperthermia*, 21(8), 745-53, 2005.
- [3] F. C. Henriques, Jr. Studies of thermal injury; the predictability and the significance of thermally induced rate processes leading to irreversible epidermal injury. *Arch Pathol (Chic)*, 43(5), 489-502, 1947.
- [4] F. C. Henriques, A. R. Moritz. Studies of Thermal Injury: I. The Conduction of Heat to and through Skin and the Temperatures Attained Therein. A Theoretical and an Experimental Investigation. *Am J Pathol*, 23(4), 530-49, 1947.
- [5] A. R. Moritz, F. C. Henriques. Studies of Thermal Injury: II. The Relative Importance of Time and Surface Temperature in the Causation of Cutaneous Burns. *Am J Pathol*, 23(5), 695-720, 1947.
- [6] A. R. Moritz. Studies of Thermal Injury: III. The Pathology and Pathogenesis of Cutaneous Burns. An Experimental Study. *Am J Pathol*, 23(6), 915-41, 1947.
- [7] W. C. Dewey. Arrhenius Relationships from the Molecule and Cell to the Clinic. *Int J Hyperthermia*, 10(4), 457-483, 1994.
- [8] S. A. Sapareto, W. C. Dewey. Thermal dose determination in cancer therapy. *Int J Radiat Oncol Biol Phys*, 10(6), 787-800, 1984.
- [9] W. C. Dewey, S. A. Sapareto. Concepts of Thermal Dose Calculation. *Strahlentherapie*, 159(6), 369-370, 1983.
- [10] M. W. Dewhirst, B. L. Viglianti, M. Lora-Michiels, M. Hanson, P. J. Hoopes. Basic principles of thermal dosimetry and thermal thresholds for tissue damage from hyperthermia. *Int J Hyperthermia*, 19(3), 267-94, 2003.
- [11] C. Damianou, K. Hynynen. Focal spacing and near-field heating during pulsed high temperature ultrasound therapy. *Ultrasound Med Biol*, 19(9), 777-87, 1993.
- [12] C. J. Diederich, R. J. Stafford, W. H. Nau, E. C. Burdette, R. E. Price, J. D. Hazle. Transurethral ultrasound applicators with directional heating patterns for prostate thermal therapy: in vivo evaluation using magnetic resonance thermometry. *Med Phys*, 31(2), 405-13, 2004.
- [13] R. D. Peters, E. Chan, J. Trachtenberg, S. Jothy, L. Kapusta, W. Kucharczyk, et al. Magnetic resonance thermometry for predicting thermal damage: an application

- of interstitial laser coagulation in an in vivo canine prostate model. *Magn Reson Med*, 44(6), 873-83, 2000.
- [14] M. Fujii, K. Sakamoto, Y. Toda, A. Negishi, H. Kanai. Study of the cause of the temperature rise at the muscle-bone interface during ultrasound hyperthermia. *IEEE Trans Biomed Eng*, 46(5), 494-504, 1999.
  - [15] J. Hand. Biophysics and technology of electromagnetic hyperthermia. In: Gautherie M, editor. *Methods of external hyperthermic heating*. Berlin: Springer-Verlag; 1990. p. 1-60.
  - [16] C. K. Chou. Therapeutic Heating Applications of Radio Frequency Energy. In: *Biological and Medical Aspects of Electromagnetic Fields*. null SV - null DO - doi:10.1201/9781420009460.ch12 ed: CRC Press; 2006.
  - [17] B. Quesson, J. A. de Zwart, C. T. Moonen. Magnetic resonance temperature imaging for guidance of thermotherapy. *J Magn Reson Imaging*, 12(4), 525-33, 2000.
  - [18] B. Denis de Senneville, B. Quesson, C. T. Moonen. Magnetic resonance temperature imaging. *Int J Hyperthermia*, 21(6), 515-31, 2005.
  - [19] R. J. Stafford, A. Shetty, A. M. Elliott, S. A. Klumpp, R. J. McNichols, A. Gowda, et al. Magnetic resonance guided, focal laser induced interstitial thermal therapy in a canine prostate model. *J Urol*, 184(4), 1514-20, 2010.
  - [20] D. Gianfelice, A. Khiat, Y. Boulanger, M. Amara, A. Belblidia. Feasibility of magnetic resonance imaging-guided focused ultrasound surgery as an adjunct to tamoxifen therapy in high-risk surgical patients with breast carcinoma. *J Vasc Interv Radiol*, 14(10), 1275-82, 2003.
  - [21] A. Carpentier, R. J. McNichols, R. J. Stafford, J. Itzcovitz, J. P. Guichard, D. Reizine, et al. Real-time magnetic resonance-guided laser thermal therapy for focal metastatic brain tumors. *Neurosurgery*, 63(1 Suppl 1), ONS21-8; discussion ONS28-9, 2008.
  - [22] C. M. Tempany, E. A. Stewart, N. McDannold, B. J. Quade, F. A. Jolesz, K. Hynynen. MR imaging-guided focused ultrasound surgery of uterine leiomyomas: a feasibility study. *Radiology*, 226(3), 897-905, 2003.
  - [23] S. N. Goldberg, D. E. Dupuy. Image-guided radiofrequency tumor ablation: challenges and opportunities--part I. *J Vasc Interv Radiol*, 12(9), 1021-32, 2001.
  - [24] E. Liapi, J. F. Geschwind. Transcatheter and ablative therapeutic approaches for solid malignancies. *J Clin Oncol*, 25(8), 978-86, 2007.
  - [25] C. Horkan, K. Dalal, J. A. Coderre, J. L. Kiger, D. E. Dupuy, S. Signoretti, et al. Reduced tumor growth with combined radiofrequency ablation and radiation therapy in a rat breast tumor model. *Radiology*, 235(1), 81-8, 2005.
  - [26] S. N. Goldberg, G. D. Girnan, A. N. Lukyanov, M. Ahmed, W. L. Monsky, G. S. Gazelle, et al. Percutaneous tumor ablation: Increased necrosis with combined radio-frequency ablation and intravenous liposomal doxorubicin in a rat breast tumor model. *Radiology*, 222(3), 797-804, 2002.
  - [27] B. Hildebrandt, P. Wust, O. Ahlers, A. Dieing, G. Sreenivasa, T. Kerner, et al. The cellular and molecular basis of hyperthermia. *Crit Rev Oncol Hematol*, 43(1), 33-56, 2002.
  - [28] M. W. Dewhirst, Z. Vujaskovic, E. Jones, D. Thrall. Re-setting the biologic rationale for thermal therapy. *Int J Hyperthermia*, 21(8), 779-90, 2005.

- [29] H. H. Kampinga, E. Dikomey. Hyperthermic radiosensitization: mode of action and clinical relevance. *Int J Radiat Biol*, 77(4), 399-408, 2001.
- [30] P. M. Corry, S. Robinson, S. Getz. Hyperthermic effects on DNA repair mechanisms. *Radiology*, 123(2), 475-82, 1977.
- [31] W. C. Dewey, S. A. Sapareto, D. A. Betten. Hyperthermic radiosensitization of synchronous Chinese hamster cells: relationship between lethality and chromosomal aberrations. *Radiat Res*, 76(1), 48-59, 1978.
- [32] E. Dikomey, H. Jung. Correlation between polymerase beta activity and thermal radiosensitization in Chinese hamster ovary cells. *Recent Results Cancer Res*, 109, 35-41, 1988.
- [33] G. Los, P. Sminia, J. Wondergem, P. H. Mutsaers, J. Havemen, D. ten Bokkel Huinink, et al. Optimisation of intraperitoneal cisplatin therapy with regional hyperthermia in rats. *Eur J Cancer*, 27(4), 472-7, 1991.
- [34] R. E. Meyn, P. M. Corry, S. E. Fletcher, M. Demetriades. Thermal enhancement of DNA damage in mammalian cells treated with cis-diamminedichloroplatinum(II). *Cancer Res*, 40(4), 1136-9, 1980.
- [35] S. H. Kim, J. H. Kim, E. W. Hahn. The radiosensitization of hypoxic tumor cells by hyperthermia. *Radiology*, 114(3), 727-8, 1975.
- [36] L. E. Gerweck, P. L. Kornblith, P. Burlett, J. Wang, S. Sweigert. Radiation sensitivity of cultured human glioblastoma cells. *Radiology*, 125(1), 231-4, 1977.
- [37] J. H. Kim, S. H. Kim, E. W. Hahn. Killing of glucose-deprived hypoxic cells with moderate hyperthermia. *Radiat Res*, 75(2), 448-51, 1978.
- [38] W. C. Dewey, A. Westra, H. H. Miller, H. Nagasawa. Heat-induced lethality and chromosomal damage in synchronized Chinese hamster cells treated with 5-bromodeoxyuridine. *Int J Radiat Biol Relat Stud Phys Chem Med*, 20(6), 505-20, 1971.
- [39] M. Hockel, K. Schlenger, B. Aral, M. Mitze, U. Schaffer, P. Vaupel. Association between tumor hypoxia and malignant progression in advanced cancer of the uterine cervix. *Cancer Res*, 56(19), 4509-15, 1996.
- [40] R. Valdagni, M. Amichetti. Report of long-term follow-up in a randomized trial comparing radiation therapy and radiation therapy plus hyperthermia to metastatic lymph nodes in stage IV head and neck patients. *Int J Radiat Oncol Biol Phys*, 28(1), 163-9, 1994.
- [41] C. C. Vernon, J. W. Hand, S. B. Field, D. Machin, J. B. Whaley, J. vanderZee, et al. Radiotherapy with or without hyperthermia in the treatment of superficial localized breast cancer: Results from five randomized controlled trials. *Int J Radiat Oncol Biol Phys*, 35(4), 731-744, 1996.
- [42] J. Overgaard, D. G. Gonzalez, M. C. C. M. Hulshof, G. Arcangeli, O. Dahl, O. Mella, et al. Randomized Trial of Hyperthermia as Adjuvant to Radiotherapy for Recurrent or Metastatic Malignant-Melanoma. *Lancet*, 345(8949), 540-543, 1995.
- [43] Y. Harima, K. Nagata, K. Harima, V. V. Ostapenko, Y. Tanaka, S. Sawada. A randomized clinical trial of radiation therapy versus thermoradiotherapy in stage IIIB cervical carcinoma. *Int J Hyperthermia*, 17(2), 97-105, 2001.
- [44] K. Sugimachi, H. Kuwano, H. Ide, T. Toge, M. Saku, Y. Oshiumi. Chemotherapy combined with or without hyperthermia for patients with oesophageal carcinoma: a prospective randomized trial. *Int J Hyperthermia*, 10(4), 485-93, 1994.

- [45] R. D. Issels, L. H. Lindner, J. Verweij, P. Wust, P. Reichardt, B. C. Schem, et al. Neo-adjuvant chemotherapy alone or with regional hyperthermia for localised high-risk soft-tissue sarcoma: a randomised phase 3 multicentre study. *Lancet Oncol*, 11(6), 561-70, 2010.
- [46] J. van der Zee, D. G. Gonzalez, G. C. van Rhoon, J. D. P. van Dijk, W. L. J. van Putten, A. A. M. Hart, et al. Comparison of radiotherapy alone with radiotherapy plus hyperthermia in locally advanced pelvic tumours: a prospective, randomised, multicentre trial. *Lancet*, 355(9210), 1119-1125, 2000.
- [47] S. Sharma, S. Singhal, A. P. Sandhu, S. Ghoshal, B. D. Gupta, N. S. Yadav. Local thermo-radiotherapy in carcinoma cervix: improved local control versus increased incidence of distant metastasis. *Asia Oceania J Obstet Gynaecol*, 17(1), 5-12, 1991.
- [48] B. Emami, C. Scott, C. A. Perez, S. Asbell, P. Swift, P. Grigsby, et al. Phase III study of interstitial thermoradiotherapy compared with interstitial radiotherapy alone in the treatment of recurrent or persistent human tumors. A prospectively controlled randomized study by the Radiation Therapy Group. *Int J Radiat Oncol Biol Phys*, 34(5), 1097-104, 1996.
- [49] A. Vasanthan, M. Mitsumori, J. H. Park, Z. Zhi-Fan, Z. Yu-Bin, P. Oliynychenko, et al. Regional hyperthermia combined with radiotherapy for uterine cervical cancers: a multi-institutional prospective randomized trial of the international atomic energy agency. *Int J Radiat Oncol Biol Phys*, 61(1), 145-53, 2005.
- [50] M. Sherar, F. F. Liu, M. Pintilie, W. Levin, J. Hunt, R. Hill, et al. Relationship between thermal dose and outcome in thermoradiotherapy treatments for superficial recurrences of breast cancer: Data from a phase III trial. *Int J Radiat Oncol Biol Phys*, 39(2), 371-380, 1997.
- [51] S. Dinges, C. Harder, R. Wurm, A. Buchali, J. Blohmer, J. Gellermann, et al. Combined treatment of inoperable carcinomas of the uterine cervix with radiotherapy and regional hyperthermia - Results of a phase II trial. *Strahlenther Onkol*, 174(10), 517-521, 1998.
- [52] E. L. Jones, J. R. Oleson, L. R. Prosnitz, T. V. Samulski, Z. Vujaskovic, D. Yu, et al. Randomized trial of hyperthermia and radiation for superficial tumors. *J Clin Oncol*, 23(13), 3079-85, 2005.
- [53] S. A. Sapareto, L. E. Hopwood, W. C. Dewey. Combined effects of X irradiation and hyperthermia on CHO cells for various temperatures and orders of application. *Radiat Res*, 73(2), 221-33, 1978.
- [54] R. Myers, S. B. Field. The response of the rat tail to combined heat and x rays. *Br J Radiol*, 50(596), 581-6, 1977.
- [55] M. D. Mills, R. E. Meyn. Hyperthermic potentiation of unrejoined DNA strand breaks following irradiation. *Radiat Res*, 95(2), 327-38, 1983.
- [56] J. Overgaard. Influence of sequence and interval on the biological response to combined hyperthermia and radiation. *Natl Cancer Inst Monogr*, 61, 325-32, 1982.
- [57] P. M. Corry, M. A. A. EP, E. G. Simultaneous hyperthermia and brachytherapy with remote afterloading. In: A M, Orton CG, RF M, editors. Brachytherapy HDR and LDR. Dearborn, MI: Nucletron; 1989. p. 193-204.
- [58] T. Juang, P. R. Stauffer, D. G. Neuman, J. L. Schlörff. Multilayer conformal applicator for microwave heating and brachytherapy treatment of superficial tissue disease. *Int J Hyperthermia*, 22(7), 527-44, 2006.

- [59] E. G. Moros, W. L. Straube, E. E. Klein, J. Maurath, R. J. Myerson. Clinical system for simultaneous external superficial microwave hyperthermia and cobalt-60 radiation. *Int J Hyperthermia*, 11(1), 11-26, 1995.
- [60] R. J. Myerson, W. L. Straube, E. G. Moros, B. N. Emami, H. K. Lee, C. A. Perez, et al. Simultaneous superficial hyperthermia and external radiotherapy: report of thermal dosimetry and tolerance to treatment. *Int J Hyperthermia*, 15(4), 251-66, 1999.
- [61] M. D. Hurwitz, I. D. Kaplan, J. L. Hansen, S. Prokopios-Davos, G. P. Topulos, K. Wishnow, et al. Hyperthermia combined with radiation in treatment of locally advanced prostate cancer is associated with a favourable toxicity profile. *Int J Hyperthermia*, 21(7), 649-56, 2005.
- [62] United States Cancer Statistics: 1999-2006 Incidence and Mortality Web-based Report. Atlanta: U.S. Department of Health and Human Services, Centers for Disease Control and Prevention and National Cancer Institute; 2010.
- [63] D. M. Parkin, F. Bray, J. Ferlay, P. Pisani. Global Cancer Statistics, 2002. *CA Cancer J Clin*, 55(2), 74-108, 2005.
- [64] A. Alcaraz, P. Hammerer, A. Tubaro, F. H. Schroder, R. Castro. Is there evidence of a relationship between benign prostatic hyperplasia and prostate cancer? Findings of a literature review. *Eur Urol*, 55(4), 864-73, 2009.
- [65] K. T. McVary. BPH: epidemiology and comorbidities. *Am J Manag Care*, 12(5 Suppl), S122-8, 2006.
- [66] J. T. Wei, E. Calhoun, S. J. Jacobsen. Urologic diseases in America project: benign prostatic hyperplasia. *J Urol*, 173(4), 1256-61, 2005.
- [67] R. M. Hoffman, M. Monga, S. P. Elliot, R. Macdonald, T. J. Wilt. Microwave thermotherapy for benign prostatic hyperplasia. *Cochrane Database Syst Rev*, (4), CD004135, 2007.
- [68] K. Shinohara. Thermal ablation of prostate diseases: advantages and limitations. *Int J Hyperthermia*, 20(7), 679-97, 2004.
- [69] M. D. Gillett, M. T. Gettman, H. Zincke, M. L. Blute. Tissue ablation technologies for localized prostate cancer. *Mayo Clin Proc*, 79(12), 1547-55, 2004.
- [70] T. R. Larson. Rationale and assessment of minimally invasive approaches to benign prostatic hyperplasia therapy. *Urology*, 59(2 Suppl 1), 12-6, 2002.
- [71] R. M. Hoffman, R. MacDonald, M. Monga, T. J. Wilt. Transurethral microwave thermotherapy vs transurethral resection for treating benign prostatic hyperplasia: a systematic review. *BJU Int*, 94(7), 1031-6, 2004.
- [72] S. Gravas, M. D. Melekos. Transurethral microwave thermotherapy: from evidence-based medicine to clinical practice. *Curr Opin Urol*, 17(1), 12-6, 2007.
- [73] S. Barmoshe, A. R. Zlotta. How do I treat and follow my TUNA patients. *World J Urol*, 24(4), 397-404, 2006.
- [74] M. D. Sherar, J. Trachtenberg, S. R. Davidson, M. R. Gertner. Interstitial microwave thermal therapy and its application to the treatment of recurrent prostate cancer. *Int J Hyperthermia*, 20(7), 757-68, 2004.
- [75] J. C. Rewcastle. High intensity focused ultrasound for prostate cancer: a review of the scientific foundation, technology and clinical outcomes. *Technol Cancer Res Treat*, 5(6), 619-25, 2006.



- [76] L. Poissonnier, J. Y. Chapelon, O. Rouviere, L. Curiel, R. Bouvier, X. Martin, et al. Control of prostate cancer by transrectal HIFU in 227 patients. *Eur Urol*, 51(2), 381-7, 2007.
- [77] C. Chaussy, S. Thuroff, T. Bergsdorf. [Local recurrence of prostate cancer after curative therapy. HIFU (Ablatherm) as a treatment option]. *Urologe A*, 45(10), 1271-5, 2006.
- [78] T. Uchida, N. T. Sanghvi, T. A. Gardner, M. O. Koch, D. Ishii, S. Minei, et al. Transrectal high-intensity focused ultrasound for treatment of patients with stage T1b-2n0m0 localized prostate cancer: a preliminary report. *Urology*, 59(3), 394-8; discussion 398-9, 2002.
- [79] F. A. Jolesz, N. McDannold. Current status and future potential of MRI-guided focused ultrasound surgery. *J Magn Reson Imaging*, 27(2), 391-9, 2008.
- [80] H. P. Beerlage, S. Thuroff, F. M. Debruyne, C. Chaussy, J. J. de la Rosette. Transrectal high-intensity focused ultrasound using the Ablatherm device in the treatment of localized prostate carcinoma. *Urology*, 54(2), 273-7, 1999.
- [81] G. Vallancien, D. Prapotnich, X. Cathelineau, H. Baumert, F. Rozet. Transrectal focused ultrasound combined with transurethral resection of the prostate for the treatment of localized prostate cancer: feasibility study. *J Urol*, 171(6 Pt 1), 2265-7, 2004.
- [82] O. Rouviere, D. Lyonnet, A. Raudrant, C. Colin-Pangaud, J. Y. Chapelon, R. Bouvier, et al. MRI appearance of prostate following transrectal HIFU ablation of localized cancer. *Eur Urol*, 40(3), 265-74, 2001.
- [83] M. Quinn, J. Benedet, F. Odicino, P. Maisonneuve, U. Beller, W. Creasman, et al. Carcinoma of the Cervix Uteri. FIGO 6th Annual Report on the Results of Treatment in Gynecological Cancer. *Int J Gynaecol Obstet*, 95(Supplement 1), S43-S103, 2006.
- [84] P. G. Rose. Stage IIB-IVA cancer of the cervix. *Cancer J*, 9(5), 404-14, 2003.
- [85] A. W. Fyles, M. Milosevic, R. Wong, M. C. Kavanagh, M. Pintilie, A. Sun, et al. Oxygenation predicts radiation response and survival in patients with cervix cancer. *Radiother Oncol*, 48(2), 149-156, 1998.
- [86] T. H. Knocke, H. D. Weitmann, H. J. Feldmann, E. Selzer, R. Potter. Intratumoral pO(2)-measurements as predictive assay in the treatment of carcinoma of the uterine cervix. *Radiother Oncol*, 53(2), 99-104, 1999.
- [87] C. A. Perez. Radiation therapy in the management of cancer of the cervix. *Oncology (Williston Park)*, 7(3), 61-9; discussion 70, 75-6, 1993.
- [88] M. Morris, P. J. Eifel, J. Lu, P. W. Grigsby, C. Levenback, R. E. Stevens, et al. Pelvic radiation with concurrent chemotherapy compared with pelvic and para-aortic radiation for high-risk cervical cancer. *N Engl J Med*, 340(15), 1137-43, 1999.
- [89] C. W. Whitney, W. Sause, B. N. Bundy, J. H. Malfetano, E. V. Hannigan, W. C. Fowler, Jr., et al. Randomized comparison of fluorouracil plus cisplatin versus hydroxyurea as an adjunct to radiation therapy in stage IIB-IVA carcinoma of the cervix with negative para-aortic lymph nodes: a Gynecologic Oncology Group and Southwest Oncology Group study. *J Clin Oncol*, 17(5), 1339-48, 1999.

- [90] P. G. Rose, B. N. Bundy, E. B. Watkins, J. T. Thigpen, G. Deppe, M. A. Maiman, et al. Concurrent cisplatin-based radiotherapy and chemotherapy for locally advanced cervical cancer. *N Engl J Med*, 340(15), 1144-53, 1999.
- [91] H. M. Keys, B. N. Bundy, F. B. Stehman, L. I. Muderspach, W. E. Chafe, C. L. Suggs, 3rd, et al. Cisplatin, radiation, and adjuvant hysterectomy compared with radiation and adjuvant hysterectomy for bulky stage IB cervical carcinoma. *N Engl J Med*, 340(15), 1154-61, 1999.
- [92] W. A. Peters, 3rd, P. Y. Liu, R. J. Barrett, 2nd, R. J. Stock, B. J. Monk, J. S. Berek, et al. Concurrent chemotherapy and pelvic radiation therapy compared with pelvic radiation therapy alone as adjuvant therapy after radical surgery in high-risk early-stage cancer of the cervix. *J Clin Oncol*, 18(8), 1606-13, 2000.
- [93] N. Datta, A. Bose, H. Kapoor. Thermoradiotherapy in the management of carcinoma of the cervix (IIIB): a controlled clinical study. *Ind Med Gaz*, 121, 68-71, 1987.
- [94] C. Hong-Wei, F. Jun-Jie, L. Wei. A randomized trial of hyperthermo-radiochemotherapy for uterine cervix cancer. *Chin J Clin Oncol*, 24, 249-51, 1997.
- [95] A. M. Westermann, E. L. Jones, B. C. Schem, E. M. van der Steen-Banasik, P. Koper, O. Mella, et al. First results of triple-modality treatment combining radiotherapy, chemotherapy, and hyperthermia for the treatment of patients with stage IIB, III, and IVA cervical carcinoma. *Cancer*, 104(4), 763-70, 2005.
- [96] E. L. Jones, Z. Vujaskovic, O. Craciunescu, L. R. Prosnitz, L. Havrilesky, A. Secord, et al. International Phase III Trial of Chemoradiotherapy  $\pm$  Hyperthermia for Locally Advanced Cervix Cancer: Interim Update on Toxicities. *Int J Radiat Oncol Biol Phys*, 69(3, Supplement 1), S392-S393, 2007.
- [97] D. Fatehi, J. van der Zee, A. Notenboom, G. C. van Rhoon. Comparison of Intratumor and Intraluminal Temperatures During Locoregional Deep Hyperthermia of Pelvic Tumors. *Strahlenther Onkol*, 183(9), 479-486, 2007.
- [98] G. Sreenivasa, J. Gellermann, B. Rau, J. Nadobny, P. Schlag, P. Deuflhard, et al. Clinical use of the hyperthermia treatment planning system HyperPlan to predict effectiveness and toxicity. *Int J Radiat Oncol Biol Phys*, 55(2), 407-19, 2003.
- [99] D. H. Wielheesen, P. A. Smitt, J. Haveman, D. Fatehi, G. C. Van Rhoon, J. Van Der Zee. Incidence of acute peripheral neurotoxicity after deep regional hyperthermia of the pelvis. *Int J Hyperthermia*, 24(4), 367-75, 2008.
- [100] D. Fatehi, J. van der Zee, M. de Bruijne, M. Franckena, G. C. van Rhoon. RF-power and temperature data analysis of 444 patients with primary cervical cancer: Deep hyperthermia using the Sigma-60 applicator is reproducible. *Int J Hyperthermia*, 23(8), 623 - 643, 2007.
- [101] J. Gellermann, J. Goke, R. Figiel, M. Weihrauch, C. H. Cho, V. Budach, et al. Simulation of different applicator positions for treatment of a presacral tumour. *Int J Hyperthermia*, 23(1), 37-47, 2007.
- [102] M. Zimmermann, J. Schorcht, W. Andree. Theoretical and experimental investigations of a newly developed intracavitary applicator system for the radiothermotherapy of gynaecological tumours. *Int J Hyperthermia*, 9(3), 463-77, 1993.
- [103] S. Sharma, F. D. Patel, A. P. Sandhu, B. D. Gupta, N. S. Yadav. A Prospective Randomized Study of Local Hyperthermia as a Supplement and Radiosensitizer in

- the Treatment of Carcinoma of the Cervix with Radiotherapy. *Endocurietherapy/Hyperthermia Oncol*, 5, 151-159, 1989.
- [104] Y. Hiraki, M. Nakajo, T. Takeshita, H. Churei. The position of the opposite flat applicator changes the SAR and thermal distributions of the RF capacitive intracavitary hyperthermia. *Int J Hyperthermia*, 16(3), 193-203, 2000.
  - [105] K. H. Hynynen. Biophysics and technology of ultrasound hyperthermia. In: Gautherie M, editor. *Methods of external hyperthermic heating*. Berlin: Springer-Verlag; 1990. p. 61-115.
  - [106] D. L. Deardorff, C. J. Diederich, W. H. Nau. Control of interstitial thermal coagulation: comparative evaluation of microwave and ultrasound applicators. *Med Phys*, 28(1), 104-17, 2001.
  - [107] C. J. Diederich. Ultrasound applicators with integrated catheter-cooling for interstitial hyperthermia: theory and preliminary experiments. *Int J Hyperthermia*, 12(2), 279-97; discussion 299-300, 1996.
  - [108] K. B. Pauly, C. J. Diederich, V. Rieke, D. Bouley, J. Chen, W. H. Nau, et al. Magnetic resonance-guided high-intensity ultrasound ablation of the prostate. *Top Magn Reson Imaging*, 17(3), 195-207, 2006.
  - [109] R. Chopra, M. Burtnyk, M. A. Haider, M. J. Bronskill. Method for MRI-guided conformal thermal therapy of prostate with planar transurethral ultrasound heating applicators. *Phys Med Biol*, 50(21), 4957-75, 2005.
  - [110] A. B. Ross, C. J. Diederich, W. H. Nau, H. Gill, D. M. Bouley, B. Daniel, et al. Highly directional transurethral ultrasound applicators with rotational control for MRI-guided prostatic thermal therapy. *Phys Med Biol*, 49(2), 189-204, 2004.
  - [111] A. B. Ross, C. J. Diederich, W. H. Nau, V. Rieke, R. K. Butts, G. Sommer, et al. Curvilinear transurethral ultrasound applicator for selective prostate thermal therapy. *Med Phys*, 32(6), 1555-65, 2005.
  - [112] C. J. Diederich, W. H. Nau, E. C. Burdette, I. S. Bustany, D. L. Deardorff, P. R. Stauffer. Combination of transurethral and interstitial ultrasound applicators for high-temperature prostate thermal therapy. *Int J Hyperthermia*, 16(5), 385-403, 2000.
  - [113] C. Lafon, L. Koszek, S. Chesnais, Y. Theillere, D. Cathignol. Feasibility of a transurethral ultrasound applicator for coagulation in prostate. *Ultrasound Med Biol*, 30(1), 113-22, 2004.
  - [114] W. H. Nau, C. J. Diederich, A. B. Ross, K. Butts, V. Rieke, D. M. Bouley, et al. MRI-guided interstitial ultrasound thermal therapy of the prostate: a feasibility study in the canine model. *Med Phys*, 32(3), 733-43, 2005.
  - [115] W. H. Nau, C. J. Diederich, P. R. Stauffer. Directional power deposition from direct-coupled and catheter-cooled interstitial ultrasound applicators. *Int J Hyperthermia*, 16(2), 129-44, 2000.
  - [116] A. M. Kinsey, C. J. Diederich, P. D. Tyreus, W. H. Nau, V. Rieke, K. B. Pauly. Multisectoral interstitial ultrasound applicators for dynamic angular control of thermal therapy. *Med Phys*, 33(5), 1352-63, 2006.
  - [117] J. H. Wootton, A. B. Ross, C. J. Diederich. Prostate thermal therapy with high intensity transurethral ultrasound: the impact of pelvic bone heating on treatment delivery. *Int J Hyperthermia*, 23(8), 609-22, 2007.

- [118] J. H. Wootton, I.-C. J. Hsu, C. Diederich. An endocervical ultrasound applicator for integrated hyperthermia and HDR brachytherapy in the treatment of locally advanced cervical carcinoma. *Med Phys*, 37(12), 2010 (in press).
- [119] J. H. Wootton, T. Juang, J. Pouliot, I.-C. J. Hsu, C. Diederich. An intrauterine ultrasound applicator for targeted delivery of thermal therapy in conjunction with HDR brachytherapy to the cervix. *Proc. SPIE*, 7181, 1-9, 2009.
- [120] C. Diederich, J. Wootton, P. Prakash, V. Salgaonkar, T. Juang, S. Scott, et al. A Pilot Study of Catheter-Based Ultrasound Hyperthermia with HDR Brachytherapy for Treatment of Locally Advanced Cancer of the Prostate and Cervix. In: International Symposium on Therapeutic Ultrasound; 2010; Tokyo, Japan; 2010.
- [121] C. J. Diederich, W. H. Nau, A. B. Ross, P. D. Tyreus, K. Butts, V. Rieke, et al. Catheter-based ultrasound applicators for selective thermal ablation: progress towards MRI-guided applications in prostate. *Int J Hyperthermia*, 20(7), 739-56, 2004.
- [122] C. J. Diederich, E. C. Burdette. Transurethral ultrasound array for prostate thermal therapy: initial studies. *IEEE Transactions on Ultrasonics, Ferroelectrics and Frequency Control*, 43(6), 1011-22, 1996.
- [123] R. Chopra, C. Luginbuhl, F. S. Foster, M. J. Bronskill. Multifrequency ultrasound transducers for conformal interstitial thermal therapy. *IEEE Trans Ultrason Ferroelectr Freq Control*, 50(7), 881-9, 2003.
- [124] F. Duck. Physical Properties of Tissue: A Comprehensive Reference Book. London: Academic Press Limited; 1990.
- [125] K. Hynynen, D. DeYoung. Temperature elevation at muscle-bone interface during scanned, focused ultrasound hyperthermia. *Int J Hyperthermia*, 4(3), 267-79, 1988.
- [126] N. B. Smith, J. M. Temkin, F. Shapiro, K. Hynynen. Thermal effects of focused ultrasound energy on bone tissue. *Ultrasound Med Biol*, 27(10), 1427-33, 2001.
- [127] E. G. Moros, X. Fan, W. L. Straube. Ultrasound power deposition model for the chest wall. *Ultrasound Med Biol*, 25(8), 1275-87, 1999.
- [128] C. W. Connor, K. Hynynen. Patterns of thermal deposition in the skull during transcranial focused ultrasound surgery. *IEEE Trans Biomed Eng*, 51(10), 1693-706, 2004.
- [129] K. Hynynen, F. A. Jolesz. Demonstration of potential noninvasive ultrasound brain therapy through an intact skull. *Ultrasound Med Biol*, 24(2), 275-83, 1998.
- [130] S. J. Tu, K. Hynynen, R. B. Roemer. Simulation of bidirectional ultrasound hyperthermia treatments of neck tumours. *Int J Hyperthermia*, 10(5), 707-22, 1994.
- [131] R. Catane, A. Beck, Y. Inbar, T. Rabin, N. Shabshin, S. Hengst, et al. MR-guided focused ultrasound surgery (MRgFUS) for the palliation of pain in patients with bone metastases--preliminary clinical experience. *Ann Oncol*, 2006.
- [132] R. Chopra, N. Baker, V. Choy, A. Boyes, K. Tang, S. Appu, et al. Targeted treatment of localized regions within the prostate gland using MRI-guided transurethral ultrasound therapy (<http://cds.ismrm.org/protected/07Presentations/0158>). In: Proc. Intl. Soc. Mag. Reson. Med. 15; 2007: p. 158.

- [133] A. B. Ross, C. J. Diederich, W. H. Nau, P. D. Tyreus, H. Gill, D. Bouley, et al. Biothermal modeling of transurethral ultrasound applicators for MR-guided prostate thermal therapy. *Proc. SPIE*, 5698, 220-7, 2005.
- [134] C. Ginestet, C. Malet, A. Cohen, F. Lafay, C. Carrie. Impact of tissues heterogeneities on monitor units calculation and ICRU dose point: Analysis of 30 cases of prostate cancer treated with 18-MV photons after three-dimensional planning. *Int J Radiat Oncol Biol Phys*, 48(2), 529-534, 2000.
- [135] A. Henderson, R. W. Laing, S. E. Langley. Identification of pubic arch interference in prostate brachytherapy: simplifying the transrectal ultrasound technique. *Brachytherapy*, 2(4), 240-5, 2003.
- [136] J. G. Strang, D. J. Rubens, R. A. Brasacchio, Y. Yu, E. M. Messing. Real-time US versus CT determination of pubic arch interference for brachytherapy. *Radiology*, 219(2), 387-393, 2001.
- [137] M. vanHerk, A. Bruce, A. P. G. Kroes, T. Shouman, A. Touw, J. V. Lebesque. Quantification of organ motion during conformal radiotherapy of the prostate by three dimensional image registration. *Int J Radiat Oncol Biol Phys*, 33(5), 1311-1320, 1995.
- [138] D. S. Shimm, K. H. Hynynen, D. P. Anhalt, R. B. Roemer, J. R. Cassady. Scanned focussed ultrasound hyperthermia: initial clinical results. *Int J Radiat Oncol Biol Phys*, 15(5), 1203-8, 1988.
- [139] P. M. Corry, B. Barlogie, E. J. Tilchen, E. P. Armour. Ultrasound-induced hyperthermia for the treatment of human superficial tumors. *Int J Radiat Oncol Biol Phys*, 8(7), 1225-9, 1982.
- [140] P. D. Tyreus, C. J. Diederich. Theoretical model of internally cooled interstitial ultrasound applicators for thermal therapy. *Phys Med Biol*, 47(7), 1073-89, 2002.
- [141] H. Pennes. Analysis of Tissue and Arterial Blood Temperatures in the Resting Human Forearm. *J Appl Physiol*, 1(2), 93-122, 1948.
- [142] K. B. Ocheltree, L. A. Frizzell. Sound Field Calculation for Rectangular Sources. *IEEE Trans Ultrason Ferroelectr Freq Control*, 36(2), 242-248, 1989.
- [143] S. A. Sapareto, W. C. Dewey. Thermal Dose Determination in Cancer-Therapy. *Int J Radiat Oncol Biol Phys*, 10(6), 787-800, 1984.
- [144] S. L. Brown, J. W. Hunt, R. P. Hill. Differential Thermal Sensitivity of Tumor and Normal Tissue Microvascular Response During Hyperthermia. *Int J Hyperthermia*, 8(4), 501-514, 1992.
- [145] H. Lyng, O. R. Monge, P. J. Bohler, E. K. Rofstad. Relationships between thermal dose and heat-induced tissue and vascular damage after thermoradiotherapy of locally advanced breast carcinoma. *Int J Hyperthermia*, 7(3), 403-15, 1991.
- [146] C. A. Damianou, N. T. Sanghvi, F. J. Fry, R. Maass-Moreno. Dependence of ultrasonic attenuation and absorption in dog soft tissues on temperature and thermal dose. *J Acoust Soc Am*, 102(1), 628-34, 1997.
- [147] M. R. Gertner, B. C. Wilson, M. D. Sherar. Ultrasound properties of liver tissue during heating. *Ultrasound Med Biol*, 23(9), 1395-403, 1997.
- [148] R. L. Clarke, N. L. Bush, G. R. Ter Haar. The changes in acoustic attenuation due to in vitro heating. *Ultrasound Med Biol*, 29(1), 127-35, 2003.

- [149] A. E. Worthington, J. Trachtenberg, M. D. Sherar. Ultrasound properties of human prostate tissue during heating. *Ultrasound Med Biol*, 28(10), 1311-1318, 2002.
- [150] P. D. Tyreus, C. Diederich. Two-dimensional acoustic attenuation mapping of high-temperature interstitial ultrasound lesions. *Phys Med Biol*, 49(4), 533-46, 2004.
- [151] Z. Liu, S. M. Lobo, S. Humphries, C. Horkan, S. A. Solazzo, A. U. Hines-Peralta, et al. Radiofrequency tumor ablation: insight into improved efficacy using computer modeling. *AJR Am J Roentgenol*, 184(4), 1347-52, 2005.
- [152] S. Biyikli, M. F. Modest, R. Tarr. Measurements of thermal properties for human femora. *J Biomed Mater Res*, 20(9), 1335-45, 1986.
- [153] W. L. Lin, C. T. Liauh, Y. Y. Chen, H. C. Liu, M. J. Shieh. Theoretical study of temperature elevation at muscle/bone interface during ultrasound hyperthermia. *Med Phys*, 27(5), 1131-40, 2000.
- [154] E. G. Moros, W. L. Straube, R. J. Myerson, X. Fan. The impact of ultrasonic parameters on chest wall hyperthermia. *Int J Hyperthermia*, 16(6), 523-38, 2000.
- [155] G. T. Clement, P. J. White, K. Hynynen. Enhanced ultrasound transmission through the human skull using shear mode conversion. *J Acoust Soc Am*, 115(3), 1356-64, 2004.
- [156] T. D. Mast, L. M. Hinkelman, L. A. Metlay, M. J. Orr, R. C. Waag. Simulation of ultrasonic pulse propagation, distortion, and attenuation in the human chest wall. *J Acoust Soc Am*, 106(6), 3665-77, 1999.
- [157] P. J. White, G. T. Clement, K. Hynynen. Longitudinal and shear mode ultrasound propagation in human skull bone. *Ultrasound Med Biol*, 32(7), 1085-96, 2006.
- [158] S. A. Goss, R. L. Johnston, F. Dunn. Comprehensive compilation of empirical ultrasonic properties of mammalian tissues. *Journal of Acoustical Society of America*, 64(2), 423-457, 1978.
- [159] S. J. Graham, L. Chen, M. Leitch, R. D. Peters, M. J. Bronskill, F. S. Foster, et al. Quantifying tissue damage due to focused ultrasound heating observed by MRI. *Magn Reson Med*, 41(2), 321-8, 1999.
- [160] Y. Y. Chen, W. L. Lin, H. L. Liou, J. Y. Yen, M. J. Shieh. Self-tuning fuzzy logic control for ultrasound hyperthermia with reference temperature based on objective functions. *Med Phys*, 26(5), 825-33, 1999.
- [161] R. Chopra, C. Luginbuhl, A. J. Weymouth, F. S. Foster, M. J. Bronskill. Interstitial ultrasound heating applicator for MR-guided thermal therapy. *Phys Med Biol*, 46(12), 3133-45, 2001.
- [162] H. L. Liu, Y. Y. Chen, J. Y. Yen, W. L. Lin. Pilot point temperature regulation for thermal lesion control during ultrasound thermal therapy. *Med Biol Eng Comput*, 42(2), 178-88, 2004.
- [163] R. Chopra, J. Wachsmuth, M. Burtnyk, M. A. Haider, M. J. Bronskill. Analysis of factors important for transurethral ultrasound prostate heating using MR temperature feedback. *Phys Med Biol*, 51(4), 827-44, 2006.
- [164] B. Y. Lu, W. L. Lin, Y. Y. Chen, R. S. Yang, T. S. Kuo, C. Y. Wang. A multifrequency driving system for ultrasound hyperthermia. *IEEE Eng Med Biol Mag*, 18(5), 106-11, 1999.

- [165] J. D. Hazle, C. J. Diederich, M. Kangasniemi, R. E. Price, L. E. Olsson, R. J. Stafford. MRI-guided thermal therapy of transplanted tumors in the canine prostate using a directional transurethral ultrasound applicator. *J Magn Reson Imaging*, 15(4), 409-17, 2002.
- [166] C. G. Nelson, E. C. Krishnan, J. R. Neff. Consideration of physical parameters to predict thermal necrosis in acrylic cement implants at the site of giant cell tumors of bone. *Med Phys*, 13(4), 462-8, 1986.
- [167] J. Lundskog. Heat and bone tissue. An experimental investigation of the thermal properties of bone and threshold levels for thermal injury. *Scand J Plast Reconstr Surg*, 9, 1-80, 1972.
- [168] W. Bonfield, C. H. Li. The temperature dependence of the deformation of bone. *J Biomech*, 1(4), 323-329, 1968.
- [169] R. A. Eriksson, T. Albrektsson. The effect of heat on bone regeneration: an experimental study in the rabbit using the bone growth chamber. *J Oral Maxillofac Surg*, 42(11), 705-11, 1984.
- [170] S. Willems, X. Chen, H. Kottkamp, G. Hindricks, W. Haverkamp, B. Rotman, et al. Temperature-controlled radiofrequency catheter ablation of manifest accessory pathways. *Eur Heart J*, 17(3), 445-52, 1996.
- [171] J. J. Langberg, H. Calkins, R. el-Atassi, M. Borganelli, A. Leon, S. J. Kalbfleisch, et al. Temperature monitoring during radiofrequency catheter ablation of accessory pathways. *Circulation*, 86(5), 1469-74, 1992.
- [172] W. W. Monafo, S. G. Eliasson. Sciatic nerve function following hindlimb thermal injury. *J Surg Res*, 43(4), 344-50, 1987.
- [173] R. J. McGough, M. L. Kessler, E. S. Ebbini, C. A. Cain. Treatment planning for hyperthermia with ultrasound phased arrays. *IEEE Trans Ultrason Ferroelectr Freq Control*, 43(6), 1074-1084, 1996.
- [174] E. G. Moros, P. Novak, W. L. Straube, P. Kolluri, D. A. Yablonskiy, R. J. Myerson. Thermal contribution of compact bone to intervening tissue-like media exposed to planar ultrasound. *Phys Med Biol*, 49(6), 869-86, 2004.
- [175] J. J. Lagendijk. Hyperthermia treatment planning. *Phys Med Biol*, 45(5), R61-76, 2000.
- [176] C. J. Diederich, K. Hynynen. Induction of hyperthermia using an intracavitary multielement ultrasonic applicator. *IEEE Trans Biomed Eng*, 36(4), 432-8, 1989.
- [177] T. A. Siddiqi, M. Miodovnik, R. A. Meyer, J. O'Brien, William D. In vivo ultrasonographic exposimetry: Human tissue-specific attenuation coefficients in the gynecologic examination, *Am J Obstet Gynecol*, 180(4), 866-874, 1999.
- [178] J. Olsrud, B. Friberg, M. Ahlgren, B. R. Persson. Thermal conductivity of uterine tissue in vitro. *Phys Med Biol*, 43(8), 2397-406, 1998.
- [179] S. A. Baldwin, A. Pelman, J. L. Bert. A heat transfer model of thermal balloon endometrial ablation. *Ann Biomed Eng*, 29(11), 1009-18, 2001.
- [180] H. Lyng, A. O. Vorren, K. Sundfor, I. Taksdal, H. H. Lien, O. Kaalhus, et al. Intra- and intertumor heterogeneity in blood perfusion of human cervical cancer before treatment and after radiotherapy. *Int J Cancer*, 96(3), 182-90, 2001.
- [181] W. L. Lin, R. B. Roemer, K. Hynynen. Theoretical and experimental evaluation of a temperature controller for scanned focused ultrasound hyperthermia. *Med Phys*, 17(4), 615-25, 1990.

- [182] P. E. Bloomfield, W. J. Lo, P. A. Lewin. Experimental study of the acoustical properties of polymers utilized to construct PVDF ultrasonic transducers and the acousto-electric properties of PVDF and P(VDF/TrFE) films. *IEEE Trans Ultrason Ferroelectr Freq Control*, 47(6), 1397-405, 2000.
- [183] B. N. Hung, A. Goldstein. Acoustic Parameters of Commercial Plastics. *IEEE Trans Sonics Ultrason*, 30(4), 249-254, 1983.
- [184] J. F. Guess, J. S. Campbell. Acoustic properties of some biocompatible polymers at body temperature. *Ultrasound Med Biol*, 21(2), 273-7, 1995.
- [185] G. W. C. a. L. Kaye, T.H. Tables of physical and chemical constants. 16 ed. London: Longman; 1995.
- [186] S. R. Davidson, M. D. Sherar. Theoretical modelling, experimental studies and clinical simulations of urethral cooling catheters for use during prostate thermal therapy. *Phys Med Biol*, 48(6), 729-44, 2003.
- [187] A. B. Ross. The design and evaluation of transurethral ultrasound applicators for precise MR-guided prostate ablation: University of California, San Francisco with the University of California, Berkeley; 2005.
- [188] J. W. Hand, D. Machin, C. C. Vernon, J. B. Whaley. Analysis of thermal parameters obtained during phase III trials of hyperthermia as an adjunct to radiotherapy in the treatment of breast carcinoma. *Int J Hyperthermia*, 13(4), 343-64, 1997.
- [189] P. Wust, H. Stahl, K. Dieckmann, S. Scheller, J. Loffel, H. Riess, et al. Local hyperthermia of N2/N3 cervical lymph node metastases: correlation of technical/thermal parameters and response. *Int J Radiat Oncol Biol Phys*, 34(3), 635-46, 1996.
- [190] C. W. Song. Effect of local hyperthermia on blood flow and microenvironment: a review. *Cancer Res*, 44(10 Suppl), 4721s-4730s, 1984.
- [191] Z. Vujaskovic, J. M. Poulson, A. A. Gaskin, D. E. Thrall, R. L. Page, H. C. Charles, et al. Temperature-dependent changes in physiologic parameters of spontaneous canine soft tissue sarcomas after combined radiotherapy and hyperthermia treatment. *Int J Radiat Oncol Biol Phys*, 46(1), 179-85, 2000.
- [192] X. Sun, L. Xing, C. C. Ling, G. C. Li. The effect of mild temperature hyperthermia on tumour hypoxia and blood perfusion: relevance for radiotherapy, vascular targeting and imaging. *Int J Hyperthermia*, 26(3), 224-31, 2010.
- [193] M. Van Vulpen, A. A. De Leeuw, B. W. Raaymakers, R. J. Van Moorselaar, P. Hofman, J. J. Lagendijk, et al. Radiotherapy and hyperthermia in the treatment of patients with locally advanced prostate cancer: preliminary results. *BJU Int*, 93(1), 36-41, 2004.
- [194] D. Fatehi, J. van der Zee, E. van der Wal, W. N. Van Wieringen, G. C. Van Rhoon. Temperature data analysis for 22 patients with advanced cervical carcinoma treated in Rotterdam using radiotherapy, hyperthermia and chemotherapy: a reference point is needed. *Int J Hyperthermia*, 22(4), 353-63, 2006.
- [195] D. S. Shimm, J. M. Kittelson, J. R. Oleson, S. A. Aristizabal, L. C. Barlow, T. C. Cetas. Interstitial thermoradiotherapy: thermal dosimetry and clinical results. *Int J Radiat Oncol Biol Phys*, 18(2), 383-7, 1990.



- [196] J. Schorcht, S. MH, M. Zimmermann. Thermoradiotherapy of uterine carcinoma. In: MH S, P F, Vernon C, editors. Thermoradiotherapy and Thermochemotherapy. Berlin: Springer-Verlag; 1996.
- [197] F. Gibbs. Thermoradiotherapy for genitourinary and gynecological tumors. In: MH S, P F, Vernon C, editors. Thermoradiotherapy and Thermochemotherapy. Berlin: Springer-Verlag; 1996.
- [198] X. Chen, C. J. Diederich, J. H. Wootton, J. Pouliot, I. C. Hsu. Optimisation-based thermal treatment planning for catheter-based ultrasound hyperthermia. *Int J Hyperthermia*, 26(1), 39-55, 2010.
- [199] W. H. Nau, C. J. Diederich, R. Shu. Feasibility of using interstitial ultrasound for intradiscal thermal therapy: a study in human cadaver lumbar discs. *Phys Med Biol*, 50(12), 2807-21, 2005.
- [200] D. T. Tompkins, R. Vanderby, S. A. Klein, W. A. Beckman, R. A. Steeves, D. M. Frye, et al. Temperature-dependent versus constant-rate blood perfusion modelling in ferromagnetic thermoseed hyperthermia: results with a model of the human prostate. *Int J Hyperthermia*, 10(4), 517-36, 1994.
- [201] P. Vaupel, F. Kallinowski, P. Okunieff. Blood flow, oxygen and nutrient supply, and metabolic microenvironment of human tumors: a review. *Cancer Res*, 49(23), 6449-65, 1989.
- [202] C. A. Van den Berg, J. B. Van de Kamer, A. A. De Leeuw, C. R. Jeukens, B. W. Raaymakers, M. van Vulpen, et al. Towards patient specific thermal modelling of the prostate. *Phys Med Biol*, 51(4), 809-25, 2006.
- [203] C. W. Song, A. Lokshina, J. G. Rhee, M. Patten, S. H. Levitt. Implication of blood flow in hyperthermic treatment of tumors. *IEEE Trans Biomed Eng*, 31(1), 9-16, 1984.
- [204] K. Hynynen. Acoustic power calibrations of cylindrical intracavitary ultrasound hyperthermia applicators. *Med Phys*, 20(1), 129-34, 1993.
- [205] R. L. King, B. A. Herman, S. Maruvada, K. A. Wear, G. R. Harris. Development of a HIFU phantom. In: 6th International Symposium on Therapeutic Ultrasound; 2007; 2007. p. 351.
- [206] M. Franckena, J. van der Zee. Use of combined radiation and hyperthermia for gynecological cancer. *Curr Opin Obstet Gynecol*, 22(1), 9-14, 2010.
- [207] B. W. Raaymakers, M. Van Vulpen, J. J. Lagendijk, A. A. De Leeuw, J. Crezee, J. J. Battermann. Determination and validation of the actual 3D temperature distribution during interstitial hyperthermia of prostate carcinoma. *Phys Med Biol*, 46(12), 3115-31, 2001.
- [208] D. Gianfelice, C. Gupta, W. Kucharczyk, P. Bret, D. Havill, M. Clemons. Palliative treatment of painful bone metastases with MR imaging-guided focused ultrasound. *Radiology*, 249(1), 355-363, 2008.
- [209] R. Catane, A. Beck, Y. Inbar, T. Rabin, N. Shabshin, S. Hengst, et al. MR-guided focused ultrasound surgery (MRgFUS) for the palliation of pain in patients with bone metastases - preliminary clinical experience. *Ann Oncol*, 18(1), 163-167, 2007.
- [210] D. Melodelima, C. Lafon, F. Prat, Y. Theillère, A. Arefiev, D. Cathignol. Transoesophageal ultrasound applicator for sector-based thermal ablation: first in vivo experiments. *Ultrasound Med Biol*, 29(2), 285-291, 2003.

- [211] K. Saito, K. Tsubouchi, M. Takahashi, K. Ito. Intracavitary Microwave Thermal Therapy for Bile Duct Carcinoma -Experimental Evaluations on Heating Performances of Antenna. International Workshop on Antenna Technology: "Small Antennas, Innovative Structures and Materials" (iWAT 2010), 4 -4,
- [212] A. E. Bent, D. R. Ostergard. Endometrial Ablation with the Neodymium - Yag Laser. *Obstet Gynecol*, 75(6), 923-925, 1990.
- [213] T. J. Clark, D. Mahajan, P. Sunder, J. K. Gupta. Hysteroscopic treatment of symptomatic submucous fibroids using a bipolar intrauterine system: a feasibility study. *European Journal of Obstetrics Gynecology and Reproductive Biology*, 100(2), 237-242, 2002.

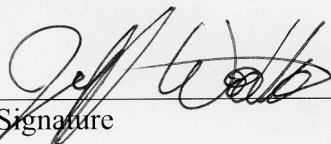
**Publishing Agreement**

*It is the policy of the University to encourage the distribution of all theses, dissertations, and manuscripts. Copies of all UCSF theses, dissertations, and manuscripts will be routed to the library via the Graduate Division. The library will make all theses, dissertations, and manuscripts accessible to the public and will preserve these to the best of their abilities, in perpetuity.*

***Please sign the following statement:***

*I hereby grant permission to the Graduate Division of the University of California, San Francisco to release copies of my thesis, dissertation, or manuscript to the Campus Library to provide access and preservation, in whole or in part, in perpetuity.*

\_\_\_\_\_  
Author Signature



\_\_\_\_\_  
Date

12/15/10